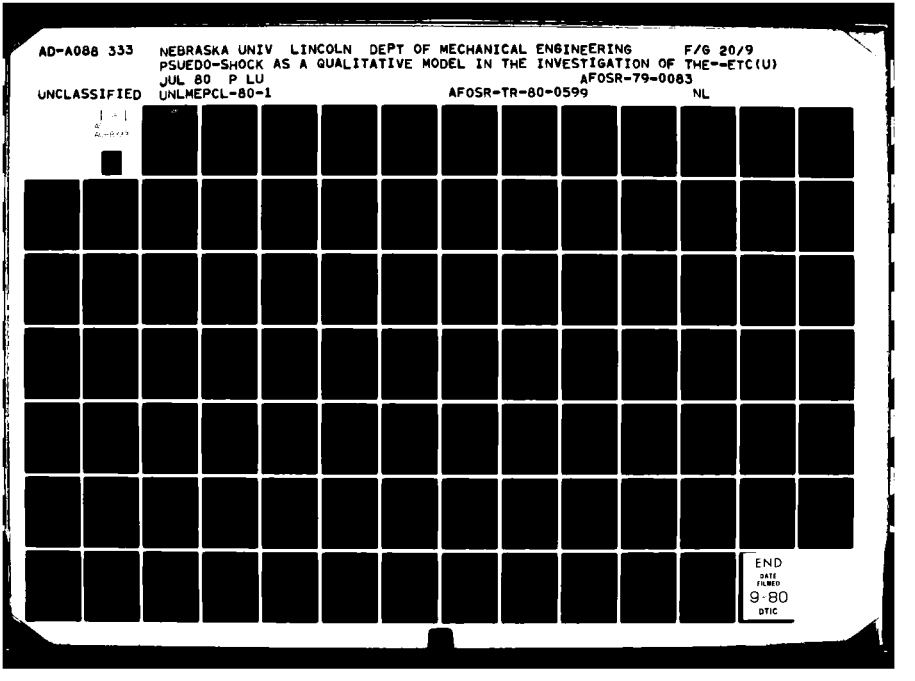
AD-A088 333
NEBRASKA UNIV LINCOLN DEPT OF MECHANICAL ENGINEERING F/G 20/9
PSUEDO-SHOCK AS A QUALITATIVE MODEL IN THE INVESTIGATION OF THE--ETC(U)
JUL 80 P LU
AFOSR-79-0083
UNCLASSIFIED
UNLMEPCL-80-1
AFOSR-TR-80-0599
NL
END
DATE FILMED
9-80
DTIC

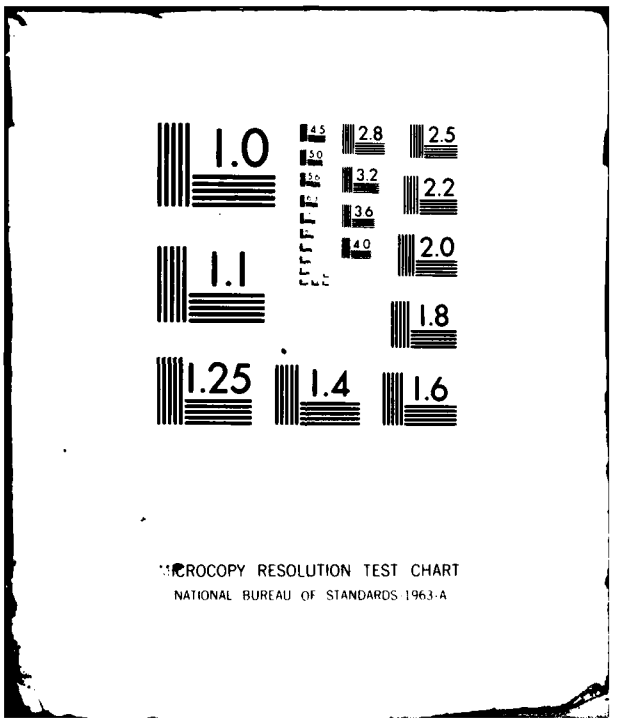
1.0
1.1
1.25
1.4
1.6
1.8
2.0
2.2
2.5
2.8
3.2
3.6
4.0
MICROCOPY RESOLUTION TEST CHART
NATIONAL BUREAU OF STANDARDS 1963-A

UNCLASSIFIED

SECURITY CLASSIFICATION OF THIS PAGE (When Data Entered)

LEVEL II

REPORT DOCUMENTATION PAGE

READ INSTRUCTIONS BEFORE COMPLETING FORM

1. REPORT NUMBER: AFOSR-TR-80-0599	2. GOVT ACCESSION NO.: AD-A088333
3. RECIPIENT'S CATALOG NUMBER	
4. TITLE (and Subtitle): PSEUDO-SHOCK AS A QUALITATIVE MODEL IN THE INVESTIGATION OF THE INFLUENCE OF WALL ROUGHNESS ON THE PERFORMANCE OF SUPERSONIC MHD GENERATORS.	5. TYPE OF REPORT & PERIOD COVERED: FINAL rept.
6. PERFORMING ORG. REPORT NUMBER: UNLMEPCL-80-1	
7. AUTHOR(s): PAU-CHANG LU	8. CONTRACT OR GRANT NUMBER(s): AFOSR-79-0083
9. PERFORMING ORGANIZATION NAME AND ADDRESS: THE UNIVERSITY OF NEBRASKA-LINCOLN, MECHANICAL ENGINEERING DEPARTMENT, LINCOLN, NEBRASKA 68588	10. PROGRAM ELEMENT, PROJECT, TASK AREA & WORK UNIT NUMBERS: 2308D9, 61102F
11. CONTROLLING OFFICE NAME AND ADDRESS: AIR FORCE OFFICE OF SCIENTIFIC RESEARCH/NA, BLDG 410, BOLLING AIR FORCE BASE, DC 20332	12. REPORT DATE: July 1980
	13. NUMBER OF PAGES: 89
14. MONITORING AGENCY NAME & ADDRESS (if different from Controlling Office)	15. SECURITY CLASS. (of this report): UNCLASSIFIED
	15a. DECLASSIFICATION/DOWNGRADING SCHEDULE

16. DISTRIBUTION STATEMENT (of this Report)

Approved for public release; distribution unlimited

17. DISTRIBUTION STATEMENT (of the abstract entered in Block 20, if different from Report)

DTIC ELECTE AUG 26 1980 S D E

18. SUPPLEMENTARY NOTES

19. KEY WORDS (Continue on reverse side if necessary and identify by block number)

MHD POWER GENERATION
HIGH-POWER DENSITY MHD GENERATORS
LOW TEMPERATURE PLASMADYNAMICS
OPEN CYCLE MHD GENERATORS
MHD PSEUDO-SHOCKS
MHD GENERATOR PRESSURE DISTRIBUTION
SHOCK-BOUNDARY LAYER INTERACTIONS

20. ABSTRACT (Continue on reverse side if necessary and identify by block number)

A preliminary study, based on an extension of Crocco's pseudo-shock model, has been carried out to explain and predict qualitatively the rather gradual pressure rise in a supersonic MHD generator, to account for the influence of wall roughness on the core flow. A system of non-linear ordinary differential equations is formulated for the wall layer and the core, with proper electromagnetic conditions enforced at the interface. Extensive numerical experiments are also presented, which demonstrate indeed the qualitative link between the theory of MHD pseudo-shock and the observed pressure ramp caused by rough walls.

DD FORM 1 JAN 73 1473 EDITION OF 1 NOV 65 IS OBSOLETE

UNCLASSIFIED 401106

AD A088333

FILE COPY

UNLMEPCL-80-1

FINAL SCIENTIFIC REPORT

for

Grant AFOSR 79-0083

(A Preliminary Investigation of the Influence of
Wall Roughness on the Core Flow in a
Supersonic MHD Generator)

PSEUDO-SHOCK AS A QUALITATIVE MODEL IN THE INVESTIGATION OF THE INFLUENCE OF WALL ROUGHNESS ON THE PERFORMANCE OF SUPERSONIC MHD GENERATORS

by

PAU-CHANG LU

Department of Mechanical Engineering
University of Nebraska - Lincoln

July, 1980

ABSTRACT

A preliminary study, based on an extension of Crocco's pseudo-shock model, has been carried out to explain and predict qualitatively the rather gradual pressure rise in a supersonic MHD generator, to account for the influence of wall roughness on the core flow. A system of non-linear ordinary differential equations is formulated for the wall layer and the core, with proper electromagnetic conditions enforced at the interface. Extensive numerical experiments are also presented, which demonstrate indeed the qualitative link between the theory of MHD pseudo-shock and the observed pressure ramp caused by rough walls.

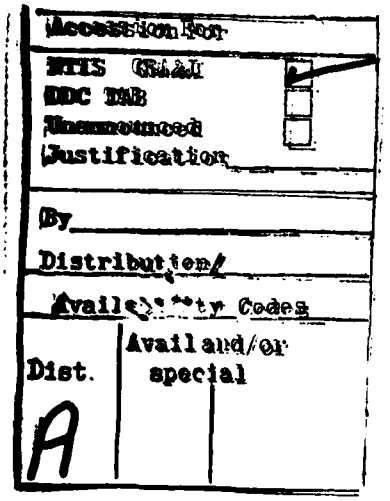

TABLE OF CONTENTS

CHAPTER 1 INTRODUCTION

1.1 INTRODUCTION

In the Air Force weapon-delivery and defense, advanced MHD electric power generators play an important role. In supersonic generatorsusing high magnetic field strength, designed for high power-density, the influence of the wall roughness is felt rather acutely in the core flow because of propagation of disturbances along shocks and Mach waves. When a generator is new, the (relatively small) roughness comes inherently from the unevenness between the segmented electrode surface and the adjacent insulation (Fig. 1.1); this roughness is periodic, and extends over the entire length of the channel. In test channels designed for the measurement of conductivity of a flowing plasma, it may be isolated in the middle of the channel (Fig. 1.2). After some extended use, the generator will show deeper and irregular wall roughness due to erosion, corrosion, burning-out, and inter-electrode sparks. As indicated schematically in Figs. 1.1 and 1.2, shocks and Mach waves appear in a supersonic flow, which interacts with the turbulent boundary layer; and their influence penetrates into the core flow. As a result, pressure rise in the flow direction is observed in actual MHD generators with supersonic inlet conditions [Ref. 12 and 13]. In the literature, there is insufficient understanding of phenomenon just described. An investigation is needed to establish, by steps of increasing sophistication, an analytical model that will provide additional understanding, add in the control or reduction of these effects, and contribute to the technology base required for development of more efficient generators.

As a preliminary endeavor in this direction, the present work explores the possible extension of Crocco's theory of pseudo-shocks [Ref. 3] so as (a) to devise a simple analytical model for the interaction near the wall and its influence

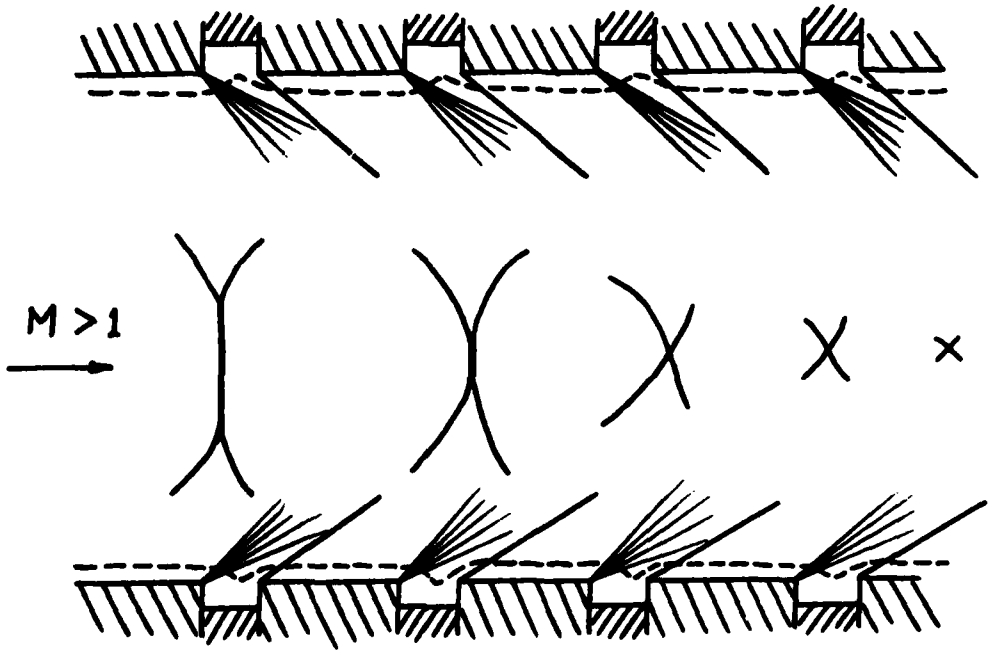

Fig. 1.1 Wall roughness and interaction of waves.

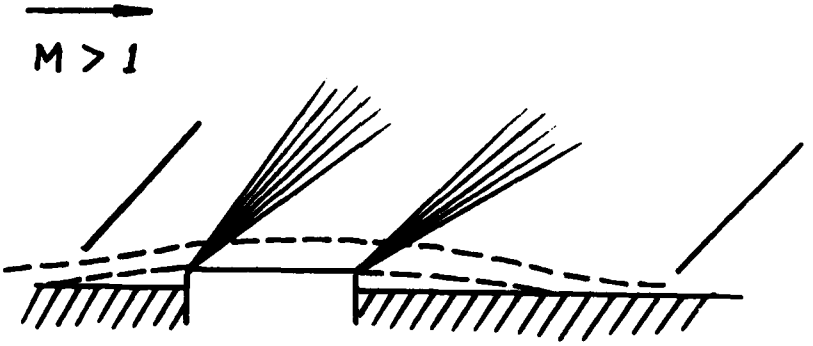

Fig. 1.2 A single element of roughness.

on the core flow through a supersonic (high power-density) generator, (b) to explain quantitatively (but on a rather primitive level) the possible pressure ramp in the flow direction as observed in actual generators, (c) to point out the kind of empirical data needed in completing or improving the analysis, and (d) to assess the role of the model in future studies. Crocco's theory is generalized to treat MHD pseudo-shocks as an exhibition of wave interaction; his control-volume analysis is enlarged to incorporate all the MHD aspects including load and Hall effects.

Extensive numerical experiments on the solution of the resulting system of nonlinear ordinary differential equations demonstrate actual qualitative link between pseudo-shocks and pressure ramps. Rough conclusions are also drawn as to the various roles played by the many parameters. The report closes with certain suggestions for future investigations.

1.2 CROCCO'S PSEUDO-SHOCK THEORY

In the literature, researchers in the field over-simplify the situation by attempting to explain the observed pressure rise by way of a single normal shock [Ref. 12 and 13] in the core of the generator. As a matter of fact, the solid curves in Fig. 1.3 would be exactly the pressure variations in the core, should a single normal shock appear in each case. The predicted variations are obviously too rough even when viewed qualitatively. The most outstanding feature of the measured pressure rise (Figs. 1.3 and 1.4) is that the increase toward a maximum is rather gradual, reflecting complicated interaction between different kinds of waves (which are oblique and hence comparatively weak) before they penetrate into the core region. This slow build-up is termed a pseudo-shock process in non-MHD gas dynamics (Fig. 1.5) by Crocco [Ref. 3]. The starting point of Crocco's work is a control-volume analysis which recognizes the non-

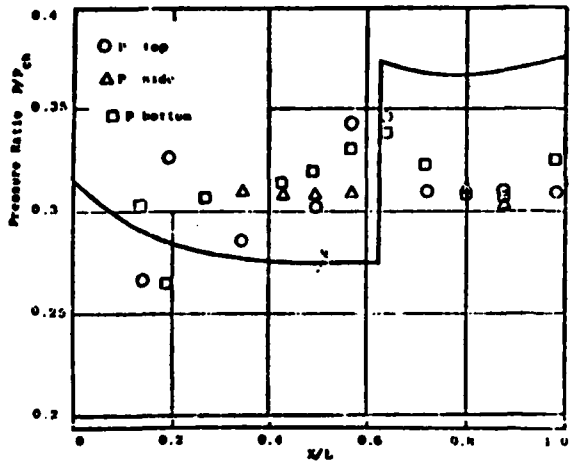

(B=2 Tesla, Power=11 KW, Load=10Ω).

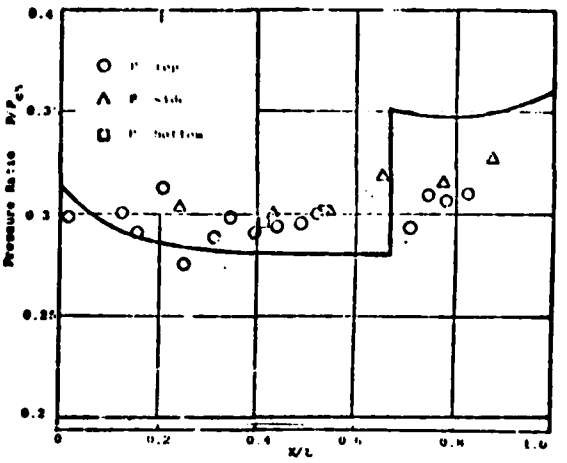

(B=2 Tesla, Power=22.3 kW, Load=2.5Ω)

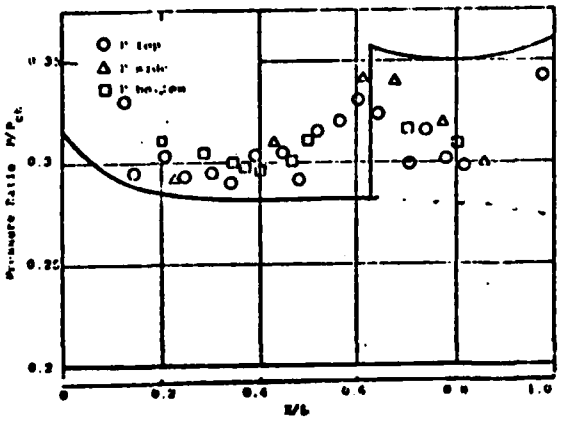

(B=2 Tesla, Power=26.4 kW, Load=4Ω)

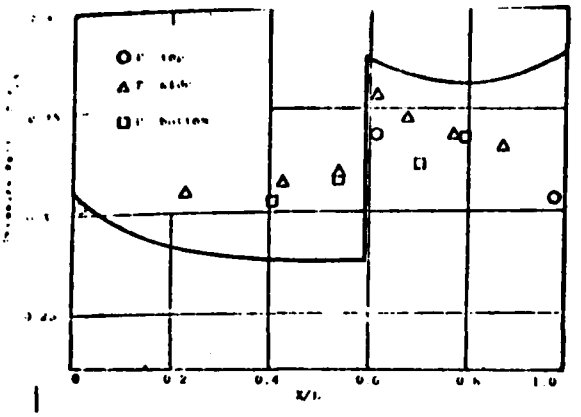

(B=2 Tesla, Power=31 kW, Load=15Ω).

Fig. 1.3 Pressure rise (measured) and attempted explanation via shock theory (Ref. 12).

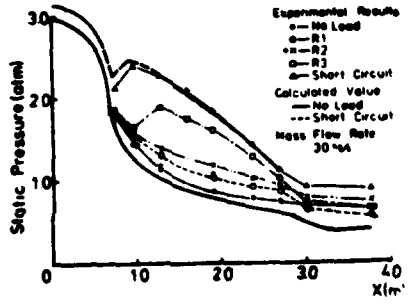

Fig. 1.4 Observed pressure rise at off-design conditions (Ref. 13).

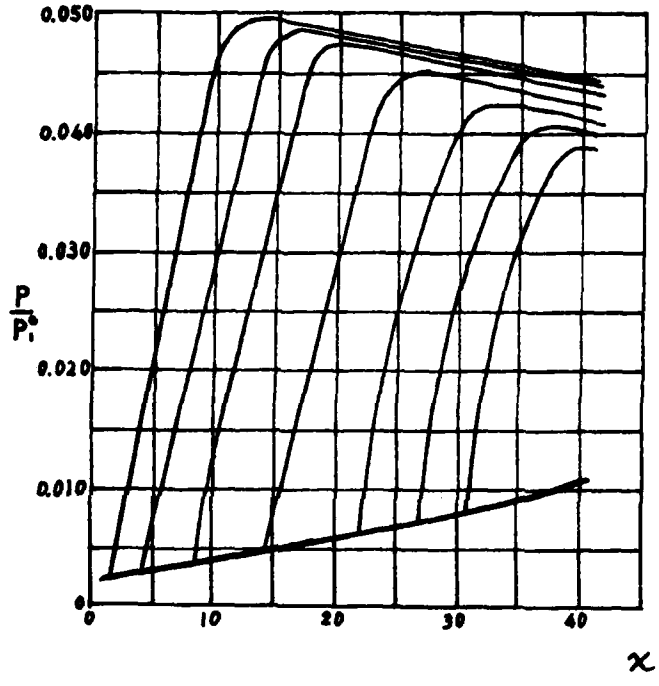

Fig. 1.5 Pressure rise through various pseudo-shocks (Crocco).

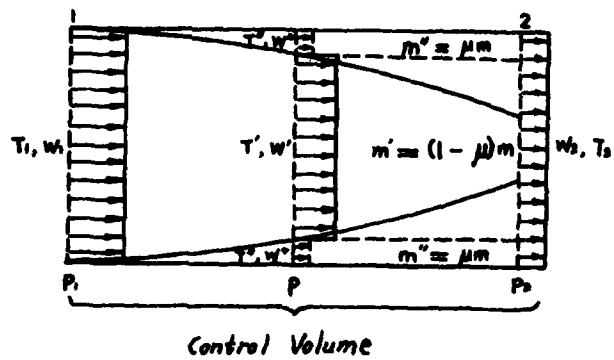

Fig. 1.6 Control volume across a pseudo-shock, non-MHD case (Crocco).

uniformity in going from the wall region to the core (Fig. 1.6). Some semi-empirical elements are then elaborated upon to make the analysis self-contained [Ref. 8, 14 and 15].

For the present investigation, the earlier and less elaborate (and hence not self-contained) phase of Crocco's theory [Ref. 3] is generalized to treat MHD pseudo-shocks. In this approach, emphasis is on the qualitative side. Crocco's control-volume analysis is enlarged under the usual MHD approximation that the magnetic field modifies the flow, yet the flow does not affect the field. In Chapter 2, mass, energy and momentum-force balances are performed. In Chapter 3, governing parameters are delineated; and in Chapter 4, numerical examples are displayed. It is to be emphasized that the approach inherently ignores the details of the wave interaction. From this stems the simplification (and power) of the analysis. But, at the same time one learns to expect certain lack of information.

In the rest of this section, we will summarize Crocco's non-MHD theory in preparation for our later generalization.

Referring* to Fig. 1.6, we have for mass balance

$$m = m' + m'' = m_1$$

and, for inviscid flow with common pressure in the two regions (boundary-layer- and jet-like),

$$\frac{d}{dx}\left(\rho' u'^2 A' + \rho'' u''^2 A''\right) = -\left(\frac{dp}{dx}\right)A$$

and, finally, the energy balance (neglecting wall heat-transfer and viscous energy dissipation)

$$\frac{d}{dx}\left[\rho' u' A'\left(h' + \frac{u'^2}{2}\right) + \rho'' u'' A''\left(h'' + \frac{u''^2}{2}\right)\right] = 0$$

*Please note that the symbols here, following [Ref. 3], are not in keeping with the LIST OF SYMBOLS.

The spatial coordinate x in the above can actually be ignored since the entire system can be rewritten in purely algebraic form [Ref. 3].

We may note also that there is no entropy production in the core region at all; and that, in the wall layer, the nonuniformity across the interface causes entropy to be produced. The solution of Crocco's system is a relatively simple matter; for details, the reader is referred to [Ref. 3]. (Incidentally, the formulation in Chapter 2, of course, contains Crocco's system as a special case.)

CHAPTER 2 FORMULATION OF PROBLEM

2.1 INTRODUCTION

This chapter contains a discussion of magnetohydrodynamic channel flow with a slowly varying cross-section area. The quasi-one-dimensional approximation will be used to study the phenomena of supersonic flow under the influence of channel wall roughness, in the presence of Lorentz force and Joule heating. In order to keep the discussion within reasonable bounds, we will consider only the steady and inviscid flow, with no heat transfer.

2.2 GENERAL RESTRICTIONS

Before we proceed, let us first limit the problem to its acceptable and reasonable range. In order to use the quasi-one-dimensional approach, the cross-section area of the channel must vary gradually so that the obliquity of the wall with reference to the axis is always small. Therefore, the velocity component which is perpendicular to the axis is negligible. We also neglect viscous stresses and the axial heat conduction.

Considering a channel as shown in Fig. 2.1. The channel wall is a combination of electrical insulators and conductors. The shaded portions are made of electrically conducting material, i.e., pairs of electrodes shorted diagonally. The rest of channel is made of electrically insulating material. The mode of operation is the so-called "single-load two-terminal generation" (see Fig. 2.2).

Further assumptions are introduced as follows:

(1) The temperature and pressure are approximately uniform over the channel cross-section.

(2) There is no wall friction.

(3) There is no heat transfer at the wall.

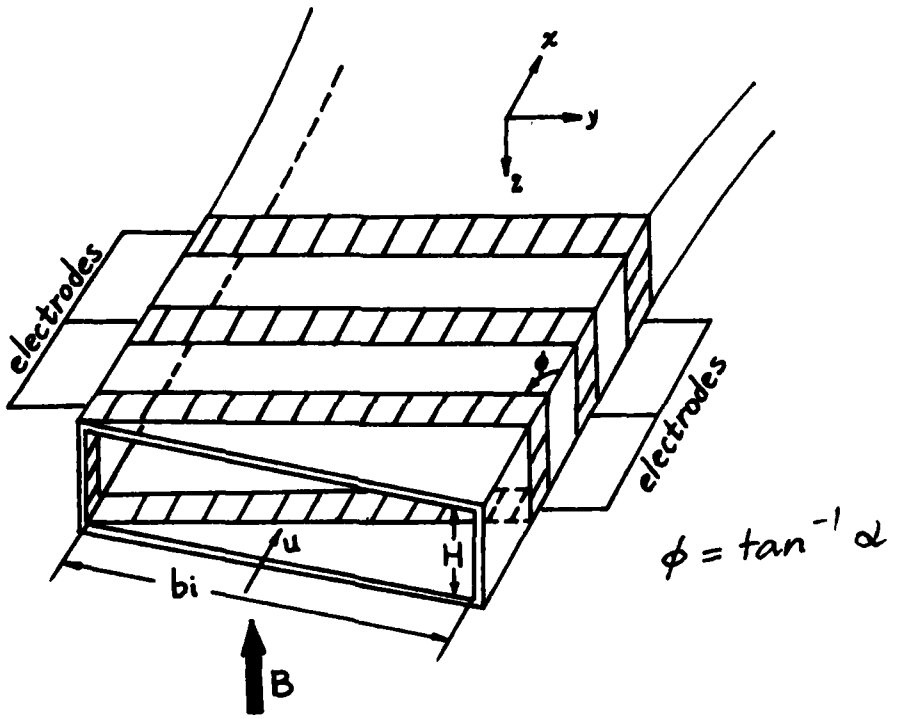

Fig. 2.1 A diagonal-wall MHD generator.

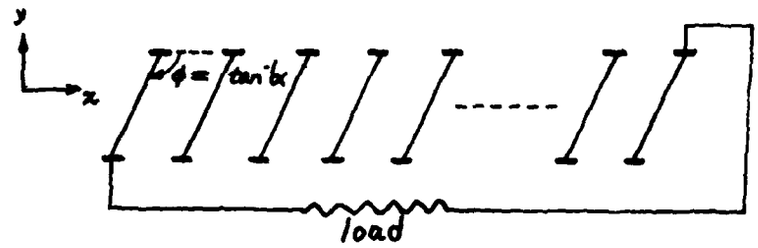

Fig. 2.2 Two-terminal operation.

2.3 SINGLE-REGION FLOW

Let us first consider the single-region MHD channel flow without bringing the wall roughness effect into the problem.

Mass Balance:

$$\rho u A = \rho_i u_i A_i = \text{constant } m \tag{2.1}$$

where subscript i denotes the initial condition, i.e., the quantities measured at the entrance of the channel.

Momentum Balance:

$$\rho u \frac{du}{dx} = - \frac{dp}{dx} + j_y B \tag{2.2}$$

where j_y = curent density in the y direction

B = applied magnetic field strength

Energy Balance:

$$\rho u \frac{dH}{dx} = j_y E_y + j_x E_x \tag{2.3}$$

where H = the total enthalpy, $c_p T + \frac{u^2}{2}$

j_x = current density in x-direction, or Hall current

E_x = electrical field strength in x-direction, or Hall field

E_y = electrical field strength in y-direction

Equation (2.3) can also be written in the following form

$$\rho u [c_p \frac{dT}{dx} + \frac{d}{dx} (\frac{u^2}{2})] = j_y E_y + j_x E_x \tag{2.4}$$

and $E_x = \alpha E_y$ (2.5)

where α = ratio of Hall field to Faraday field*

and $K = \frac{E_y}{uB}$ (2.6)

where K = loading factor.

---

*Please note that the angle of inclination ϕ in Figs. 2.1 and 2.2 is set to $\tan^{-1} \alpha$.

From the generalized Ohm's law [Ref. 2], we have two equations for j_x and j_y:

$$j_x = \frac{\sigma}{1 + \beta^2} [E_x - \beta(E_y - uB)] \tag{2.7}$$

$$j_y = \frac{\sigma}{1 + \beta^2} [E_y - uB + \beta E_x] \tag{2.8}$$

where σ = electrical conductivity

β = Hall parameter

From Eqns. (2.5) and (2.6), Eqns. (2.7) and (2.8) can be rewritten as

$$j_x = \frac{\sigma}{1 + \beta^2} [\alpha K - \beta(K - 1)](uB) \tag{2.9}$$

$$j_y = \frac{\sigma}{1 + \beta^2} [\alpha\beta K + (K - 1)](uB) \tag{2.10}$$

Substituting Eqn. (2.10) into Eqn. (2.2), we get:

$$\boxed{\rho u \frac{du}{dx} = - \frac{dp}{dx} + \left(\frac{\sigma}{1 + \beta^2}\right)[\alpha\beta K + (K - 1)](uB^2)} \tag{2.11}$$

Substituting Eqns. (2.5), (2.6), (2.9) and (2.10) into Eqn. (2.4), we have

$$\rho u\left[c_p \frac{dT}{dx} + u \frac{du}{dx}\right] = \left(\frac{\sigma}{1 + \beta^2}\right)[\alpha K - \beta(K - 1)](uB)\cdot\alpha K u B + \left(\frac{\sigma}{1 + \beta^2}\right)[\alpha\beta K + (K - 1)](uB)\cdot K u B \tag{2.12}$$

From the ideal gas law,

$$\rho = \frac{p}{RT} \quad \text{and} \quad c_p = \frac{\gamma R}{\gamma - 1} \tag{2.13}$$

where R = gas constant

γ = heat capacity ratio

Equations (2.11) and (2.13) then reduce Eqn. (2.12) to the following:

$$\boxed{\left(\frac{p}{RT}\right)\left(\frac{\gamma R}{\gamma - 1}\right)\frac{dT}{dx} = \frac{dp}{dx} + \left(\frac{\sigma}{1 + \beta^2}\right)[\alpha^2 K^2 + (K - 1)^2](uB^2)} \tag{2.14}$$

Equations (2.1), (2.11) and (2.14) are the so-called mass balance, momentum balance and energy balance equations for single-region MHD flows.

2.4 TWO-REGION FLOW

When a stream of high temperature plasma passes through nozzle and then enters the channel with high speed, it will form a layer near the wall because of the wall roughness. In that layer (which may be thick at off-design conditions), the velocity of the plasma is considerably slower because of the wall. We call such a layer the wall layer. We also call the main plasma flow in the central portion of the channel the core region. Thus, there are two regions in the MHD channel. For simplicity, we add now the following assumptions:

(1) Wall regions near anode and cathode sides are the same (or can be lumped together).

(2) No pressure change occurs across a section from region to region (as in unconfined jets, or boundary layers).

(3) There are no friction and heat transfer between regions.

(4) In the regions, no property changes in the z-direction.

(5) In keeping with general quasi-one-dimensionality, interfaces between regions are supposed to be rather flat so that its normal everywhere is almost in the y-direction.*

Now we can write down the equations which govern the two-region flows.

Mass Balance:

$$\rho_c u_c A_c + \rho_w u_w A_w = \rho_1 u_1 A_1 = \text{constant, } \dot{m} \qquad (2.15)$$

where subscripts c and w denote the core-region quantities and the wall-layer quantities individually.

*This assumption is needed in formulating electrical conditions at the interfaces.

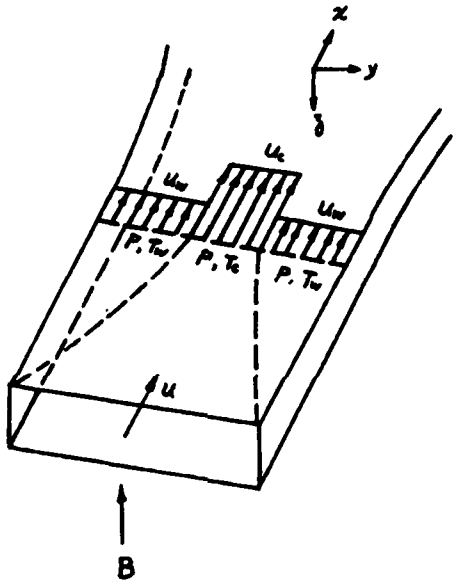

Fig. 2.3 Two-region model.

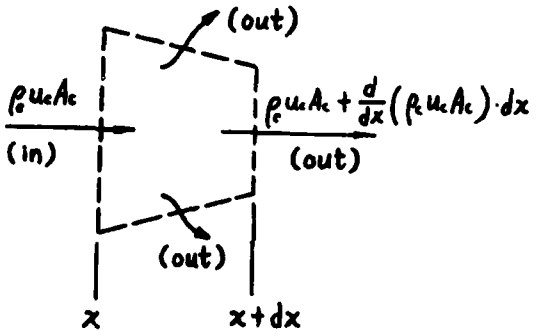

Fig. 2.4 Control-volume in the core.

Momentum Balance*:

$$\frac{d}{dx}(\rho_c u_c^2 A_c + \rho_w u_w^2 A_w) = -\frac{dp}{dx} A_c - \frac{dp}{dx} A_w + j_{yc} B + j_{yw} B \qquad (2.16)$$

where A_c = cross-section area of core-region

A_w = cross-section area of wall-layer

Let A be the total cross-section area of the channel flow. Then, $A = A_c + A_w$. Together with Eq. (2.10), Eq. (2.16) becomes:

$$\boxed{\begin{aligned}\frac{d}{dx}(\rho_f u_c^2 A_c + \rho_w u_w^2 A_w) = -\frac{dp}{dx} A + \left(\frac{\sigma_w}{1+\beta_w^2}\right)[\alpha_w \beta_w K_w + (K_w - 1)] u_w B^2 A_w \\ + \left(\frac{\sigma_c}{1+\beta_c^2}\right)[\alpha_c \beta_c K_c + (K_c - 1)] u_c B^2 A_c\end{aligned}} \qquad (2.17)$$

Similarly, for the Energy Balance, we have

$$\boxed{\begin{aligned}\frac{d}{dx}[\rho_c u_c A_c (h_c + \frac{u_c^2}{2}) + \rho_w u_w A_w (h_w + \frac{u_w^2}{2})] = (j_{xw} E_{xw} + j_{yw} E_{yw}) A_w \\ + (j_{xc} E_{xc} + j_{yc} E_{yc}) A_c\end{aligned}} \qquad (2.18)$$

Before we can go further to study this two-region problem, we have to find the key point which connects the core region and the wall layer. To achieve this goal, let us first examine the core region energy equation.

Core Energy Equation:

$$\boxed{\frac{d}{dx}(\rho_c u_c A_c (h_c + \frac{u_c^2}{2})] - (h_c + \frac{u_c^2}{2}) \frac{d}{dx}(\rho_c u_c A_c) = (j_{xc} E_{xc} + j_{yc} E_{yc}) A_c} \qquad (2.19)$$

where $\frac{d}{dx}(\rho_c u_c A_c) \leq 0$ for the core region is to be in force throughout the present investigation.

*For later use, we will also note here that the mass-rate out of the core across its lateral surface between x and x+dx is $\rho_c u_c A_c - [\rho_c u_c A_c + \frac{d}{dx}(\rho_c u_c A_c) \cdot dx] = -\frac{d}{dx}(\rho_c u_c A_c) \cdot dx$; that is, $-\frac{d}{dx}(\rho_c u_c A_c)$ per unit axial length (see Fig. 2.4).

It is important to realize the full implication of the above restriction, $\frac{d}{dx}(\rho_c u_c A_c) \leq 0$. Under this restriction, the fluid particles in the core region will keep on carrying energy out of it, and entering the wall layer. If $\frac{d}{dx}(\rho_c u_c A_c)$ were positive, energy would be carried into the core region from the wall layer. In that case, the contribution term (the second term on the lefthand side) of Eq. (2.19) would have to be replaced by $-(h_w + \frac{u_w^2}{2})\frac{d}{dx}(\rho_c u_c A_c)$, or $(h_w + \frac{u_w^2}{2})\frac{d}{dx}(\rho_w u_w A_w)$. This can be expressed by the following statement: ———

(Net energy carried out across sections at x and x+dx) + (Energy carried out of the core across the lateral surface) = (Electromagnetic work done on the plasma in the core between x and x+dx.)

Expanding Eq. (2.19), together with Eqs. (2.9) and (2.10), yields

$$(h_c + \frac{u_c^2}{2})\frac{d}{dx}(\rho_c u_c A_c) + \rho_c u_c A_c \frac{d}{dx}(h_c + \frac{u_c^2}{2}) - (h_c + \frac{u_c^2}{2})\frac{d}{dx}(\rho_c u_c A_c)$$

$$= \left\{(\frac{\sigma_c}{1+\beta_c^2})[\alpha_c K_c - \beta_c(K_c - 1)](u_c B)\cdot(\alpha_c K_c u_c B) + (\frac{\sigma_c}{1+\beta_c^2})[\alpha_c \beta_c K_c + (K_c - 1)](u_c B)\cdot(K_c u_c B)\right\}\cdot A_c$$

$$= (\frac{\sigma_c}{1+\beta_c^2})[\alpha_c^2 K_c^2 - \cancel{\alpha_c \beta_c K_c^2} + \alpha_c \beta_c K_c + \cancel{\alpha_c \beta_c K_c^2} + K_c^2 - K_c]u_c^2 B^2 A_c$$

i.e.,
$$\boxed{\frac{p}{T_c}\frac{\gamma}{\gamma-1}\frac{dT_c}{dx} = \frac{dp}{dx} + (\frac{\sigma_c}{1+\beta_c^2})[\alpha_c^2 K_c^2 + (K_c - 1)^2](u_c B^2)} \qquad (2.20)$$

where Eqs. (2.11) and (2.13) have been employed.

Similarly, we can derive the momentum equation of core region as follows:

$$\frac{d}{dx}(\rho_c u_c^2 A_c) - u_c \frac{d}{dx}(\rho_c u_c A_c) = -\frac{dp}{dx}A_c + (\frac{\sigma_c}{1+\beta_c^2})[\alpha_c \beta_c K_c + (K_c - 1)](u_c B)^2 \cdot A_c$$

Expanding the above equation, we get

$$u_c \frac{d}{dx}(\rho_c u_c A_c) + (\rho_c u_c A_c)\frac{du_c}{dx} - u_c \frac{d}{dx}(\rho_c u_c A_c) = -\frac{dp}{dx}A_c + \left(\frac{\sigma_c}{1+\beta_c^2}\right)[\alpha_c\beta_c K_c + (K_c - 1)](u_c B^2)A_c$$

or, using Eq. (2.13),

$$\boxed{\frac{p}{RT_c} u_c \frac{du_c}{dx} = -\frac{dp}{dx} + \left(\frac{\sigma_c}{1+\beta_c^2}\right)[\alpha_c\beta_c K_c + (K_c - 1)](u_c B^2)} \qquad (2.21)$$

Comparing Eqs. (2.21) and (2.20) to Eqs. (2.11) and (2.14), it is obvious that the core-region formulas are similar to the single-region ones. The wall-layer equations are not similar since the quantities carried into the wall-layer are $h_c + \frac{u_c^2}{2}$ and u_c, not $h_w + \frac{u_w^2}{2}$ and u_w.

For a two-region flow, the core region cannot be studied in a decoupled manner (independently of the wall layer) since α_c and K_c are related to wall-layer quantities through electrical conditions at the interface. We will make further discussion on this point later on.

Now that we have the equations governing the two regions combinedly and the core-region equations, we can then easily obtain the wall-layer equations by subtracting. For example, subtracting Eq. (2.20) from Eq. (2.18) will yield the energy equation of the wall layer:

$$\frac{d}{dx}\left[\rho_w u_w A_w \left(h_w + \frac{u_w^2}{2}\right)\right] + \left(h_c + \frac{u_c^2}{2}\right)\frac{d}{dx}(\rho_c u_c A_c) = (j_{xw}E_{xw} + j_{yw}E_{yw})A_w \qquad (2.22)$$

To continue our analysis, we need the assumed division of masses in the two regions in the spirit of Crocco [3]. Let us introduce the mass ratio μ such that

$$\begin{aligned} \rho_w u_w A_w &= \mu(x)m \\ \rho_c u_c A_c &= [1 - \mu(x)]m \end{aligned} \qquad (2.23)$$

where m = total mass flow rate

$$\mu(x) = \frac{\text{mass flow rate in wall layer}}{\text{total mass flow rate}}$$

Following our previous restriction, $\frac{d}{dx}(\rho_c u_c A_c) \leq 0$, we see that $\frac{d\mu(x)}{dx} \geq 0$.

An alternative approach would be to start with a division of flow cross-sectional areas in the two regions:

$$A_w = \nu(x) \cdot A$$
$$A_c = [1 - \nu(x)] \cdot A$$

where $\nu(x) = \frac{\mu(x) m}{\rho_w u_w A}$

It may appear superficially that $\nu(x)$ should be more directly measurable. But, to guarantee $\frac{d\mu}{dx} \geq 0$, it is safer to start with $\mu(x)$ given. And $\nu(x)$ can then be calculated as a part of the result.

In eq. (2.16), we have already employed the relation $A(x) = A_w + A_c$. Together with Eq. (2.23), this relation now yields

$$\frac{\mu(x)}{\rho_w u_w} + \frac{1 + \mu(x)}{\rho_c u_c} = \frac{A(x)}{m}$$

Introducing further the ideal gas law, we have

$$\boxed{\frac{A(x)}{m} \frac{p}{R} \frac{u_w}{T_w} \frac{u_c}{T_c} = \frac{u_w}{T_w} + \mu(x) \left[\frac{u_c}{T_c} - \frac{u_w}{T_w}\right]} \qquad (2.24)$$

From Eq. (2.22), we can write

$$h_w \frac{d}{dx}(\rho_w u_w A_w) + (\rho_w u_w A_w) \frac{dh_w}{dx} + (\rho_w u_w A_w) u_w \frac{du_w}{dx} + \frac{u_w^2}{2} \frac{d}{dx}(\rho_w u_w A_w)$$
$$+ (h_c + \frac{u_c^2}{2}) \frac{d}{dx}(m - \rho_w u_w A_w) = (j_{xw} E_{xw} + j_{yw} E_{yw}) A_w$$

But m is a constant, and

$$(h_c + \frac{u_c^2}{2}) \frac{d}{dx}(m - \rho_w u_w A_w) = -h_c \frac{d}{dx}(\rho_w u_w A_w) - \frac{u_c^2}{2} \frac{d}{dx}(\rho_w u_w A_w)$$

Therefore, $(\rho_w u_w A_w)\frac{dh_w}{dx} + (\rho_w u_w A_w)u_w \frac{du_w}{dx} + (h_w - h_c + \frac{u_w^2 - u_c^2}{2})\frac{d}{dx}(\rho_w u_w A_w) =$

$$A_w u_w \left\{ (\frac{\sigma_w}{1+\beta_w^2}) [\alpha_w^2 K_w^2 - \alpha_w \beta_w K_w^2 + \alpha_w \beta_w K_w + \alpha_w \beta_w K_w^2 + K_w^2 - K_w](u_w B^2) \right\}$$

or, $(\rho_w u_w A_w) \frac{dh_w}{dx} + (\rho_w u_w A_w)u_w \frac{du_w}{dx} + (h_w - h_c + \frac{u_w^2 - u_c^2}{2})\frac{d}{dx}(\rho_w u_w A_w) =$

$$A_w u_w \left\{ (\frac{\sigma_w}{1+\beta_w^2}) [\alpha_w^2 K_w^2 + \alpha_w \beta_w K_w + K_w^2 - K_w](u_w B^2) \right\} \qquad (2.25)$$

To derive the momentum equation for the wall-layer region, we subtract Eq. (2.21) from Eq. (2.17):

$$\frac{d}{dx}(\rho_w u_w^2 A_w) + u_c \frac{d}{dx}(\rho_c u_c A_c) = -\frac{dp}{dx} A_w + (\frac{\sigma_w}{1+\beta_w^2}[\alpha_w \beta_w K_w + (K_w - 1)](u_w B^2) A_w$$

But, $u_c \frac{d}{dx}(\rho_c u_c A_c) = u_c \frac{d}{dx}(m - \rho_w u_w A_w) = -u_c \frac{d}{dx}(\rho_w u_w A_w)$

So, the previous equation comes out the following form:

$$\rho_w u_w A_w \frac{du_w}{dx} + (u_w - u_c) \frac{d}{dx}(\rho_w u_w A_w) = -\frac{dp}{dx} A_w + (\frac{\sigma_w}{1+\beta_w^2})[\alpha_w \beta_w K_w + (K_w - 1)](u_w B^2) A_w \qquad (2.26)$$

We have now successfully derived the system of governing equations, Eqs. (2.20), (2.21), (2.24), (2.25) and (2.26). For simplicity, we will further transform Eqs. (2.25) and (2.26) to other forms. We first multiply Eq. (2.26) by u_w, and then subtract the product from eq. (2.25):

$$(\rho_w u_w A_w)\frac{dh_w}{dx} + \left[h_w - h_c - \frac{(u_c - u_w)^2}{2}\right]\frac{d}{dx}(\rho_w u_w A_w) = u_w A_w \frac{dp}{dx} +$$

$$\left(\frac{\sigma_w}{1+\beta_w^2}\right)[\alpha_w^2 K_w^2 + (K_w - 1)^2]u_w^2 B^2 A_w$$

that is, $$\rho_w u_w A_w \left(\frac{\gamma R}{\gamma - 1}\right)\frac{dT_w}{dx} + \left\{\frac{\gamma R}{\gamma - 1}(T_w - T_c) - \frac{(u_c - u_w)^2}{2}\right\}\frac{d}{dx}(\rho_w u_w A_w) =$$

$$A_w u_w \frac{dp}{dx} + A_w\left(\frac{\sigma_w}{1+\beta_w^2}\right)[\alpha_w^2 K_w^2 + (K_w - 1)^2]u_w^2 B^2$$

Finally, replacing $\rho_w u_w A_w$ by $\mu(x)\cdot m$ yields

$$\mu\frac{p}{T_w}\left(\frac{\gamma}{\gamma - 1}\right)\frac{dT_w}{dx} + \frac{p}{RT_w}\left\{\frac{\gamma}{\gamma - 1}(T_w - T_c) - \frac{1}{2}(u_c - u_w)^2\right\}\frac{d\mu}{dx} =$$

$$\mu\frac{dp}{dx} + \mu\left(\frac{\sigma_w}{1+\beta_w^2}\right)[\alpha_w^2 K_w^2 + (K_w - 1)^2](u_w B^2) \qquad (2.27)$$

Equation (2.26) can also be rewritten in terms of $\mu(x)$:

$$\mu\left(\frac{p}{RT_w}\right)u_w \frac{du_w}{dx} + \left(\frac{p}{RT_w}\right)u_w(u_w - u_c)\frac{d\mu}{dx} =$$

$$-\mu\frac{dp}{dx} + \mu\left(\frac{\sigma_w}{1+\beta_w^2}\right)[\alpha_w\beta_w K_w + (K_w - 1)](u_w B^2) \qquad (2.28)$$

Equations (2.20), (2.21), (2.24), (2.27) and (2.28) then govern the MHD two-region flow. Before we proceed, we must note carefully the dependent variables in the above five governing equations. Let us list all the dependent variables here:

$$p = p(x),\ u_c = u_c(x),\ u_w = u_w(x),\ T_c = T_c(x),\ T_w = T_w(x).$$

The auxiliary quantities,

$$\sigma_c = \text{fct. } (T_c, p)$$

$$\sigma_w = \text{fct. } (T_w, p)$$

β_c = fct. (T_c, p, B)

β_w = fct. (T_w, p, B)

are seen to be related to the other quantities via known functional forms (to be quoted later).

The given quantities of the problem are $A(x)$, $B(x)$, α_w, K_w, $\mu(x)$, and the initial values of p, u_w, u_c, T_w and T_c. (α_c and K_c will be related to α_w and K_w in Section 2.5.) In principle, $\alpha_w = \tan\phi$ (see Fig. 2.1) can be a general function of x; although a constant will be used throughout the present study.

It must be emphasized that μ as a given function of x reflects very clearly the qualitative nature of the present theory. The formulation yields a solution for a prescribed $\mu(x)$; but in a truly self-contained framework, $\mu(x)$ ought to come out as a part of the solution. As it stands, one will have to speculate about the functional form of $\mu(x)$ and calculate examples that are hopefully representative of actual cases in a qualitative manner. It is also not truly satisfying to view the theory as being semi-empirical (in the sense that, for every actually measured $\mu(x)$, one can predict a complete flow situation), simply because (1) it is impossible to measure locally the relative mass flow in the two regions, and (2) the quasi-one-dimensional approximation itself obliterates the true meaning of an interface*. Of course, such difficulties are already an integral part of Crocco's classical pseudo-shock theory [ref. 3]; we have only inherited Crocco's qualitative legacy in our attempted generalization.

2.5 ENTROPY PRODUCTION

Applying the perfect gas law and the general relation between entropy $\mathcal{S}$, internal energy U and volume V, one has

*This is quite similar to the fact that in the boundary layer approximation the "edge" of the boundary layer is a hazy concept.

$$d\mathcal{S} = \frac{dU}{T} + \frac{p\,dV}{T}$$

$$= c_p \frac{dT}{T} - R \frac{dp}{p}$$

where c_p = heat capacity at constant pressure $(= \frac{\gamma R}{\gamma - 1})$

Therefore,

$$d\mathcal{S} = \frac{\gamma R}{\gamma - 1} \frac{dT}{T} - R\frac{dp}{p} \tag{2.29}$$

or,

$$\frac{1}{R} \frac{d\mathcal{S}}{dx} = \left(\frac{\gamma}{\gamma - 1}\right) \frac{1}{T} \frac{dT}{dx} - \frac{1}{p} \frac{dp}{dx} \tag{2.30}$$

By comparing Eq. (2.30) with Eqs. (2.20) and (2.27), we may have the equations of entropy change in the core-region and the wall layer individually:

$$\frac{1}{R} \frac{d\mathcal{S}_c}{dx} = \frac{1}{p}\left(\frac{\sigma_c}{1 + \beta_c^2}\right)[\alpha_c^2 K_c^2 + (K_c - 1)^2](u_c B^2) \tag{2.31}$$

$$\frac{1}{R} \frac{d\mathcal{S}_w}{dx} = \frac{1}{p}\left(\frac{\sigma_w}{1 + \beta_w^2}\right)[\alpha_w^2 K_w^2 + (K_w - 1)^2](u_w B^2) +$$

$$\left(\frac{1}{\mu} \frac{d\mu}{dx}\right)\left(\frac{1}{RT_w}\right)\left[\left(\frac{\gamma R}{\gamma - 1}\right)(T_w - T_c) - \frac{1}{2}(u_c - u_w)^2\right] \tag{2.32}$$

where: subscript c denotes the quantities in the core-region,

subscript w denotes the quantities in the wall-layer.

It is thus seen that the entropy production in the core is due solely to the Joule heating (which is a form of energy dissipation). In the wall-layer, there are two sources of entropy production: Joule heating and non-uniform distributions of u and T in the two regions.

For the non-magnetic case [Ref. 3], the core flow is isentropic and the entropy production in the wall-layer is due only to the non-uniform distributions in the two regions.

2.6 ELECTRICAL CONDITIONS AT THE INTERFACE

In the previous discussion, we encountered several electrical quantities: j_y, j_x, E_y and E_x. To find the relationships which can link these electrical quantities all together is the key to the solution of our problem. According to Sec. 1.6 of [Ref. 4], we have (Fig. 2.5):

$$\langle \hat{n} \times \vec{E} \rangle = 0$$

$$\langle \hat{n} \cdot \vec{j} \rangle = 0$$

where < > stands for jumps across the interface:

$$E_{xc} = E_{xw} \tag{2.33}$$

$$j_{yc} = j_{yw} \tag{2.34}$$

(Note that $E_{yc} \neq E_{yw}$ and $j_{xc} \neq j_{xw}$.)

By using the interrelationships expressed in Eqs. (2.5), (2.6), (2.34) and (2.35), one has

$$\frac{\alpha_w}{\alpha_c} = \frac{E_{xw}/E_{yw}}{E_{xc}/E_{yc}} = \frac{E_{yc}}{E_{yw}} \tag{2.35}$$

$$\frac{K_w}{K_c} = \frac{E_{yw}/(u_w B)}{E_{yc}/(u_c B)} = \left(\frac{\alpha_c}{\alpha_w}\right)\left(\frac{u_c}{u_w}\right) \tag{2.36}$$

or,

$$K_w = \left(\frac{E_{yw}}{u_c B}\right)\left(\frac{u_c}{u_w}\right) = \mathcal{K}\left(\frac{u_c}{u_w}\right) \tag{2.37}$$

where $\mathcal{K} = \frac{E_{yw}}{u_c B}$ is a given quantity.*

Combining Eqs. (2.10), (2.36) and (2.34) will yield

$$\left(\frac{\sigma_c}{1+\beta_c^2}\right)[\alpha_c \beta_c K_c + (K_c - 1)](u_c B) = \left(\frac{\sigma_w}{1+\beta_w^2}\right)[\alpha_w \beta_w K_w + (K_w - 1)](u_w B)$$

*In usual designs, $\mathcal{K} = 0.5$ which is an optimizing value in some sense.

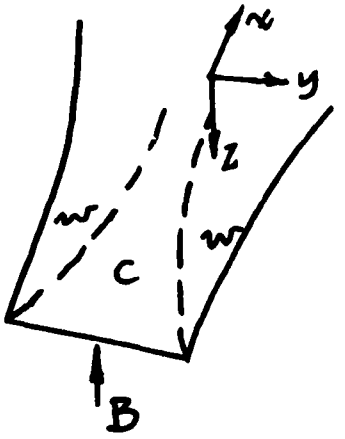

Fig. 2.5 Interface orientation.

which can also be written as follows:

$$\left(\frac{\sigma_c\beta_c}{1+\beta_c^2} - \frac{\sigma_w\beta_w}{1+\beta_w^2}\right)\alpha_c K_c u_c = \left(\frac{\sigma_w}{1+\beta_w^2}\right)(K_w - 1)u_w - \left(\frac{\sigma_c}{1+\beta_c^2}\right)(K_c - 1)u_c \qquad (2.38)$$

We also mention here as an addendum that, from the literature

$$\beta \propto B\sqrt{T}/P \qquad (2.39)$$

and

$$\sigma \propto T^m/P^n \qquad (2.40)$$

where m and n are universal constants (depending on the temperature range) for all plasmas.

CHAPTER 3 DIMENSIONLESS PARAMETERS

3.1 NONDIMENSIONALIZATION

Applying the process of dimensional analysis to the five governing equations, Eqs. (2.20), (2.21), (2.24), (2.27) and (2.28), we introduce the following representative quantities:

Density -- ρ_{ci}

Velocity -- u_{ci}

Area -- A_i

Generator Channel Width -- b_i, see Fig. 2.1

Magnetic Field Strength -- B_i

Pressure -- p_i

Temperature -- T_{ci}

Conductivity -- σ_{ci}

where subscript i denotes the initial conditions, i.e. the quantities at the entrance of MHD channel.

Then, define the following dimensionless variables:

$$x' = \frac{x}{b_i}, \quad u_c' = \frac{u_c}{u_{ci}}, \quad u_w' = \frac{u_w}{u_{ci}},$$

$$T_c' = \frac{T_c}{T_{ci}}, \quad T_w' = \frac{T_w}{T_{ci}}, \quad p' = \frac{p}{p_i},$$

$$B' = \frac{B}{B_i}, \quad \sigma_c' = \frac{\sigma_c}{\sigma_{ci}}, \quad \sigma_w' = \frac{\sigma_w}{\sigma_{ci}},$$

$$A' = \frac{A}{A_i}$$

where prime denotes dimensionless quantities.

Substituting the above dimensionless quantities into the governing equations derived in Chapter 2, we then have the new governing equations with dimensionless forms as follows:

(1) From Eq. (2.20),

$$\left(\frac{p_i p'}{T_{ci} T'_c}\right)\left(\frac{\gamma}{\gamma-1}\right)\frac{d(T_{ci}T'_c)}{d(b_i x')} = \frac{d(p_i p')}{d(b_i x')} + \left(\frac{\sigma_{ci}\sigma'_c}{1+\beta_c^2}\right)[\alpha_c^2 K_c^2 + (K_c-1)^2](u_{ci}u'_c B_i^2 B'^2)$$

After simplifying, we have

$$\left(\frac{p'}{T'_c}\right)\left(\frac{\gamma}{\gamma-1}\right)\frac{dT'_c}{dx'} = \frac{dp'}{dx'} + \left(\frac{b_i\sigma_{ci}u_{ci}B_i^2}{P_i}\right)\left(\frac{\sigma'_c}{1+\beta_c^2}\right)[\alpha_c^2 K_c^2 + (K_c-1)^2](u'_c B'^2) \qquad (3.1)$$

(2) From Eq. (2.21),

$$\left(\frac{p_i p' u_{ci} u'_c}{R T_{ci} T'_c}\right)\frac{d(u_{ci}u'_c)}{d(b_i x')} = -\frac{d(p_i p')}{d(b_i x')} + \left(\frac{\sigma_{ci}\sigma'_c}{1+\beta_c^2}\right)[\alpha_c\beta_c K_c + (K_c-1)](u_{ci}u'_c B_i^2 B'^2)$$

or

$$\left(\frac{u_{ci}^2}{R T_{ci}}\right)\left(\frac{p' u'_c}{T'_c}\right)\frac{du'_c}{dx'} = -\frac{dp'}{dx'} + \left(\frac{b_i\sigma_{ci}u_{ci}B_i^2}{P_i}\right)\left(\frac{\sigma'_c}{1+\beta_c^2}\right)[\alpha_c\beta_c K_c + (K_c-1)](u'_c B'^2)$$

Observing the above equation, let us multiply a quantity γ (the ratio of heat capacities) on both denominator and numerator in lefthand side and notice that

$$M_{ci} = \frac{u_{ci}}{\sqrt{\gamma R T_{ci}}}$$

is the Mach Number at the inlet of the channel in the core region.

Then, we have

$$(\gamma M_{ci}^2)\left(\frac{p' u'_c}{T'_c}\right)\frac{du'_c}{dx'} = -\frac{dp'}{dx'} + \left(\frac{b_i\sigma_{ci}u_{ci}B_i^2}{P_i}\right)\left(\frac{\sigma'_c}{1+\beta_c^2}\right)[\alpha_c\beta_c K_c + (K_c-1)](u'_c B'^2) \qquad (3.2)$$

(3) From Eq. (2.27),

$$\left(\frac{p_i p'}{\mu T_{ci} T'_w}\right)\left(\frac{\gamma}{\gamma-1}\right)\frac{d(T_{ci}T'_w)}{d(b_i x')} + \left(\frac{p_i p'}{R T_{ci} T'_w}\right)\left[\left(\frac{\gamma R}{\gamma-1}\right)T_{ci}(T'_w - T'_c) - \frac{u_{ci}^2}{2}(u'_c - u'_w)^2\right]\frac{d\mu}{d(b_i x')}$$

$$= \frac{d(p_i p')}{\mu\, d(b_i x')} + \mu\left(\frac{\sigma_{ci}\sigma'_w}{1+\beta_w^2}\right)[\alpha_w^2 K_w^2 + (K_w-1)^2](u_{ci}u'_w B_i^2 B'^2)$$

i.e.

$$\mu\left(\frac{p'}{T'_w}\right)\left(\frac{\gamma}{\gamma-1}\right)\frac{dT'_w}{dx'}+\left(\frac{p'}{T'_w}\right)\left[\left(\frac{\gamma}{\gamma-1}\right)(T'_w-T'_c)-\left(\frac{\gamma M^2_{c1}}{2}\right)(u'_c-u'_w)^2\right]\frac{du}{dx'}=$$

$$\mu\frac{dp'}{dx'}+\mu\left(\frac{b_1\sigma_{c1}u_{c1}B_1^2}{p_1}\right)\left(\frac{\sigma'_w}{1+\beta_w^2}\right)[\alpha_w^2K_w^2+(K_w-1)^2](u'_wB'^2) \qquad (3.3)$$

(4) From Eq. (2.28),

$$\mu\left(\frac{p_1p'}{RT_{c1}T'_w}\right)(u_{c1}u'_w)\frac{d(u_{c1}u'_w)}{d(b_1x')}+\left(\frac{p_1p'}{RT_{c1}T'_w}\right)(u^2_{c1}u'_w)(u'_w-u'_c)\frac{du}{d(b_1x')}=$$

$$-\mu\frac{d(p_1p')}{d(b_1x')}+\mu\left(\frac{\sigma_{c1}\sigma'_w}{1+\beta_w^2}\right)[\alpha_w\beta_wK_w+(K_w-1)](u_{c1}u'_wB_1^2B'^2)$$

or,

$$\mu(\gamma M^2_{c1})\left(\frac{p'u'_w}{T'_w}\right)\frac{du'_w}{dx'}+(\gamma M^2_{c1})\left(\frac{p'u'_w}{T'_w}\right)(u'_w-u'_c)\frac{du}{dx'}=$$

$$-\mu\frac{dp'}{dx'}+\mu\left(\frac{b_1\sigma_{c1}u_{c1}B_1^2}{p_1}\right)\left(\frac{\sigma'_w}{1+\beta_w^2}\right)[\alpha_w\beta_wK_w+(K_w-1)](u'_wB'^2) \qquad (3.4)$$

(5) From Eq. (2.24),

$$\left(\frac{A}{\rho_1u_{c1}A_1}\right)\left(\frac{p_1p'}{R}\right)\left(\frac{u_{c1}u'_w}{T_{c1}T'_w}\right)\left(\frac{u_{c1}u'_c}{T_{c1}T'_c}\right)=\left(\frac{u_{c1}u'_w}{T_{c1}T'_w}\right)+\mu\left(\frac{u_{c1}}{T_{c1}}\right)\left(\frac{u'_c}{T'_c}-\frac{u'_w}{T'_w}\right)$$

or,

$$p'=\frac{1}{A'}\left[\frac{T'_c}{u'_c}+\mu\left(\frac{T'_w}{u'_w}-\frac{T'_c}{u'_c}\right)\right] \qquad (3.5)$$

Here let us introduce a new parameter, $S_1=\frac{b_1\sigma_{c1}u_{c1}B_1^2}{p_1}$, called the Interaction Parameter. To summarize, now we have

$$\left(\frac{p'}{T'_c}\right)\left(\frac{\gamma}{\gamma-1}\right)\frac{dT'_c}{dx'}=\frac{dp'}{dx'}+S_1\left(\frac{\sigma'_c}{1+\beta_c^2}\right)[\alpha_c^2K_c^2+(K_c-1)^2](u'_cB'^2) \qquad (3.6)$$

$$(\gamma M^2_{c1})\left(\frac{p'u'_c}{T'_c}\right)\frac{du'_c}{dx'}=-\frac{dp'}{dx'}+S_1\left(\frac{\sigma'_c}{1+\beta_c^2}\right)[\alpha_c\beta_cK_c+(K_c-1)](u'_cB'^2) \qquad (3.7)$$

$$\mu\left(\frac{\rho'}{T'_w}\right)\left(\frac{\gamma}{\gamma-1}\right)\frac{dT'_w}{dx'}+\frac{\rho'}{T'_w}\left[\left(\frac{\gamma}{\gamma-1}\right)(T'_w-T'_c)-\left(\frac{\gamma M^2_{cf}}{2}\right)(u'_c-u'_w)^2\right]\frac{d\mu}{dx'}=$$

$$\mu\frac{d\rho'}{dx'}+\mu S_f\left(\frac{\sigma'_w}{1+\beta^2_w}\right)\left[\alpha^2_w K^2_w+(K_w-1)^2\right](u'_w B'^2) \qquad (3.8)$$

$$\mu(\gamma M^2_{cf})\left(\frac{\rho' u'_w}{T'_w}\right)\frac{du'_w}{dx'}+(\gamma M^2_{cf})\left(\frac{\rho' u'}{T'_w}\right)(u'_w-u'_c)\frac{d\mu}{dx'}=$$

$$-\mu\frac{d\rho'}{dx'}+\mu S_f\left(\frac{\sigma'_w}{1+\beta^2_w}\right)\left[\alpha_w\beta_w K_w+(K_w-1)\right](u'_w B'^2) \qquad (3.9)$$

$$\rho'=\left(\frac{1}{A' u'_c u'_w}\right)\left[T'_c u'_w+\mu(T'_w u'_c-T'_c u'_w)\right] \qquad (3.10)$$

If we take the natural logarithm on both sides of Eq. (3.10), it will yield

$$\ell n\rho'=\ell n\left[T'_c u'_w+\mu(T'_w u'_c-T'_c u'_w)\right]-\ell n(A' u'_c u'_w)$$

Then, differentiating the above equation with respect to x', we have

$$\frac{1}{\rho'}\frac{d\rho'}{dx'}=\left\{\left[\left(T'_c\frac{du'_w}{dx'}+u'_w\frac{dT'_c}{dx'}\right)+\mu\left(T'_w\frac{du'_c}{dx'}+u'_c\frac{dT'_w}{dx'}-T'_c\frac{du'_w}{dx'}-u'_w\frac{dT'_c}{dx'}\right)\right]\Big/\right.$$

$$\left.\Big/\left[T'_c u'_w+\mu(T'_w u'_c-T'_c u'_w)\right]\right\}-\frac{1}{A'}\frac{dA'}{dx'}-\frac{1}{u'_c}\frac{du'_c}{dx'}-\frac{1}{u'_w}\frac{du'_w}{dx'} \qquad (3.11)$$

Eqs. (3.6) through (3.9) together with Eq. (3.11) form a system of non-linear differential equations, which can be solved numerically.

3.2 DIMENSIONLESS FORMS OF AUXILIARY EQUATIONS AND CONDITIONS

Referring to Sec. 2.6 and introducing the dimensionless quantities defined in previous section, we can get the following relationships which connect the loading factor K, the velocity of plasma u and α (the ratio of Hall to Faraday field):

$$K_w=K\left(\frac{u'_c}{u'_w}\right) \qquad (3.12)$$

$$K_c=K_w\left(\frac{\alpha_w}{\alpha_c}\right)\left(\frac{u'_w}{u'_c}\right)=K\left(\frac{\alpha_w}{\alpha_c}\right)$$

or, $$\alpha_c = \alpha_w(\frac{K}{K_c}) \tag{3.13}$$

Substituting Eq. (3.13) into Eq. (2.39) and nondimensionalizing will yield

$$(\frac{\sigma_{ci}\sigma'_c\beta_c}{1+\beta_c^2} - \frac{\sigma_{ci}\sigma'_w\beta_w}{1+\beta_w^2})(\frac{K}{K_c})(\alpha_w K_c u_{ci} u'_c) =$$

$$(\frac{\sigma_{ci}\sigma'_w}{1+\beta_w^2})(K_w - 1)(u_{ci}u'_w) - (\frac{\sigma_{ci}\sigma'_c}{1+\beta_c^2})(K_c - 1)(u_{ci}u'_c)$$

i.e.,

$$K_c = (\frac{1+\beta_c^2}{\sigma'_c})(\frac{\sigma'_w}{1+\beta_w^2})(\alpha_w\beta_w K + K - \frac{u'_w}{u'_c}) + 1 - \alpha_w\beta_c K \tag{3.14}$$

In Eq. (3.14), there are two quantities which vary with respect to x', i.e., β and σ'. As mentioned in Sec. 2.6, is related to the mth power of temperature and the nth power of pressure. And from the literature, the values of m and n are respectively 10 and 0.5. Introducing these values to Eq. (2.41) and rewriting Eqs. (2.40) and (2.41) in dimensionless forms, one has

$$\frac{\beta}{\beta_{ci}} = (\frac{B}{B_i})(\sqrt{\frac{T}{T_{ci}}} \Big/ (\frac{p}{p_i}) \tag{3.15}$$

$$\frac{\sigma}{\sigma_{ci}} = (\frac{T}{T_{ci}})^{10} \Big/ (\frac{p}{p_i})^{0.5} \tag{3.16}$$

In later calculations, we will let β_{ci} equal to 1*. Then, the above equations become the following forms:

$$\beta = \frac{B'\sqrt{T'}}{p'} \tag{3.17}$$

$$\sigma' = \frac{(T')^{10}}{\sqrt{p'}} \tag{3.18}$$

*In existing diagonal-wall generators, β_{ci} is always close to 1; there is also rational ground for $\beta_{ci} = 1$ in good designs, see [Ref. 7].

We also change the electrical quantities to dimensionless forms by the following steps:

$$j_{yw} = \frac{\sigma_{cf}\sigma'_w}{1+\beta_w^2}[\alpha_w\beta_w K_w + (K_w - 1)](u_{cf}u'_w B_f B')$$

$$= (\sigma_{cf}u_{cf}B_f)(\frac{\sigma'_w}{1+\beta_w^2})[\alpha_w\beta_w K_w + (K_w - 1)](u'_w B') \qquad (3.19)$$

$$j_{xc} = \frac{\sigma_{cf}\sigma'_c}{1+\beta_c^2}[\alpha_c K_c - \beta_c(K_c - 1)](u_{cf}u'_c B_f B')$$

$$= (\sigma_{cf}u_{cf}B_f)(\frac{\sigma'_c}{1+\beta_c^2})[\alpha_c K_c - \beta_c(K_c - 1)](u'_c B') \qquad (3.20)$$

Similarly,
$$j_{xw} = (\sigma_{cf}u_{cf}B_f)(\frac{\sigma'_w}{1+\beta_w^2})[\alpha_w K_w - \beta_w(K_w - 1)](u'_w B') \qquad (3.21)$$

From Eqs. (2.6) and (2.5), let us rewrite the electrical field strength as follows:

In the y direction, we have

$$E_{yc} = K_c u_{cf}u'_c B_f B' = (u_{cf}B_f)(K_c u'_c B') \qquad (3.22)$$

$$E_{yw} = (u_{cf}B_f)(K_w u'_w B') \qquad (3.23)$$

In the x direction, $E_{xc} = E_{xw}$

$$E_{xc} = \alpha_c E_{yc} = (u_{cf}B_f)(\alpha_c K_c u'_c B') \qquad (3.24)$$

Now let us define the following dimensionless electrical quantities:

$$j'_{yw} = \frac{j_{yw}}{\sigma_{cf}u_{cf}B_f}, \quad j'_{xc} = \frac{j_{xc}}{\sigma_{cf}u_{cf}B_f}, \quad j'_{xw} = \frac{j_{xw}}{\sigma_{cf}u_{cf}B_f},$$

$$E'_{yc} = \frac{E_{yc}}{u_{cf}B_f}, \quad E'_{yw} = \frac{E_{yw}}{u_{cf}B_f}, \quad E'_{xc} = \frac{E_{xc}}{u_{cf}B_f}$$

And from Eqs. (2.34) and (2.35), $j'_{yw} = j'_{yc}$, $E'_{xc} = E'_{xw}$. From above definitions, Eqs. (3.19) through (3.24) become

$$j'_{yw}(= j'_{yc}) = \left(\frac{\sigma'_w}{1+\beta_w^2}\right)[\alpha_w\beta_w K_w + (K_w - 1)](u'_w B') \tag{3.25}$$

$$j'_{xc} = \left(\frac{\sigma'_c}{1+\beta_c^2}\right)[\alpha_c K_c - \beta_c(K_c - 1)](u'_c B') \tag{3.26}$$

$$j'_{xw} = \left(\frac{\sigma'_w}{1+\beta_w^2}\right)[\alpha_w K_w - \beta_w(K_w - 1)](u'_w B') \tag{3.27}$$

$$E'_{yc} = K_c u'_c B' \tag{3.28}$$

$$E'_{yw} = K_w u'_w B' \tag{3.29}$$

$$E'_{xc}(= E'_{xw}) = \alpha_c E'_{yc} \tag{3.30}$$

With these dimensionless electrical quantities on hand , we can find the trend of these variables in a two-region MHD channel flow problem.

Another object which we are interested in is the area variation. In order to develop the area ratio, we combine Eq. (2.15) and Eq. (2.23) and get

$$\rho_w u_w A_w = \mu \rho_1 u_{c1} A_1$$

Simply by mathematical manipulation, we have

$$A'_w = \mu\left(\frac{T'_w}{u'_w p'}\right) \tag{3.31}$$

where A'_w = the ratio of wall-layer cross-section area to the cross-section area at entrance, i.e., A_w/A_1

Similarly,

$$A'_c = (1 - \mu)\left(\frac{T'_c}{u'_c p'}\right) \tag{3.32}$$

or,

$$A'_c = A' - A'_w \tag{3.33}$$

From Eqs. (3.31) and (3.32), we see that the cross-section area of wall-layer is proportional to temperature and mass ratio, and inverse to velocity and pressure.

3.3 PHYSICAL SIGNIFICANCE OF GOVERNING PARAMETERS M_{ci} AND S_i

In Sec. 3.1, there are two parameters which appeare in governing equations, Eqs. (3.6) through (3.9), that play very important roles in the two-region MHD channel flow. These two parameters are the Mach Number at the inlet (M_{ci}) and the Interaction Parameter (S_i). Since M_{ci} and S_i almost appeare in each equation, we can predict that these two governing parameters will influence strongly the behavior of plasma in the generator. For example, in Eq. (3.7), we have in the x direction and on an elementary plasma cell:

(Inertial Force) = (Pressure Force) + (Lorentz Force)

Thus,

$$\frac{\text{Lorentz Force}}{\text{Inertial Force}} \propto \frac{S_i}{M_{ci}^2}$$

$$\frac{\text{Lorentz Force}}{\text{Pressure Force}} \propto S_i$$

which means that the larger the interaction parameter S_i, the larger the Lorentz Force while the smaller the Inertial Force and the Pressure Force. On the other hand, the larger the Mach number, the smaller the Lorentz Force while the larger the Inertial Force.

Also, in Eq. (3.6),

(Change in Internal Energy) = (Work Done) + (Joule Heating)

i.e.,

$$\frac{\text{Joule Heating}}{\text{Energy Change}} \propto S_i$$

$$\frac{\text{Joule Heating}}{\text{Work}} \propto S_i$$

which means that large value of S_i will produce strong effect of Joule Heating and vice versa.

For this problem, since plasma which comes out from nozzle enters the channel with supersonic speed, the Mach Number M_{ci} is always greater than 1.

To estimate representative value of S_i, let us use some ranges of data gathered from existing literature:

σ_i -- 25 to 60 mho/m

p_i -- 1 to 3 atm

b_i -- around 0.15 m

B_i -- 2 to 6 Tesla

u_{ci} -- around 750 m/sec

T_i -- 3000 to 4000 °K

Therefore, S_i is approximately in the range from 0.3 to 2.0. As a result we will use $S_i = 0.3 \sim 0.5$ in our calculations, to keep to the lower (and more realistic) end of the range.

CHAPTER 4 RESULTS AND DISCUSSION

4.1 NUMERICAL EXAMPLES

Several examples* are worked for a plasma with $\gamma = 1.1$, to display certain trends. Figure 4.2 to 4.14 show plots of various quantities for the case where

$$A' = 1 + 0.2x'$$

$$\mu = 0.0003 + 0.12x', \ \mu < 0.3$$

$$= 0.3, \ \mu \geq 0.3$$

$$u'_{ci} = 1, \ u'_{wi} = 0.008$$

$$T'_{ci} = 1, \ T'_{wi} = 1$$

$$p'_i = 1$$

$$S_i = 0.4$$

$$K = 0.5$$

$$\alpha_w = -1$$

The curves marked with crosses are for $M_{ci} = 1.4$, and those with small squares, $M_{ci} = 1.5$.

For comparison, Fig. 4.1 shows the pressure variation for the single-region model where A', S_i, K, p'_i are kept the same; $\alpha = -1$, $u'_i = 1$, $T'_i = 1$; and $M_i = 1.4$ (1.5) for the curve marked with crosses (squares). It is seen that the plasma pressure decreases monotonously in the flow direction. This, no doubt, would be indicative of the case where there is no appreciable wall roughness. In contrast, Fig. 4.2 shows that the plasma rises in its pressure rather gradually in the flow direction, exhibiting a (MHD) pseudo-shock when a two-region model is adopted. This lends credence to the qualitative rationale behind an explanation of the observed pressure ramp by way of a two-region pseudo-shock. This highlight

*All with $B'(x) = 1 + 0.5x'$, for $x' \leq 1$; and $1.5\ (1 - 0.1x')$, for $x' > 1$.

of the present investigation, however, does not shine too much quantitatively, since the ratio of the mass flow in the wall layer, $\mu(x')$, has to be conjectured for the calculation. Furthermore, there does not seem to be any practical means that could yield actual data leading to $\mu(x')$ for a given run of a real generator. Thus, it would be futile to hope for a close comparison between a calculation and data recorded for an actual run; yet, it is perhaps possible to gain some understanding of the underlying mechanism, and the general trend by examining the numerical plots.

Figure 4.3 shows the local Mach number in the core; and Fig. 4.4, that in the wall layer. M_c is seen to decrease monotonously; M_w, first increases and then decreases. Sharing the same trend is the velocity in the core (Fig. 4.5); and that in the wall layer (Fig. 4.6). Thus, as the wall layer grows its velocity is first promoted by the core flow (at the expense of the core velocity); but later decelerates, probably due to the Lorentz force accompanying the generation of electricity. The core temperature, as shown in Fig. 4.7, increases monotonously (but only by about 10%). The wall-layer temperature (Fig. 4.8) takes a rather sudden jump near the entrance, and then increases more gradually until 15 or 30% higher than the initial value. The reason for the jump in wall-layer temperature at the entrance is not clear; but an educated guess is that it is brought on by the specific $\mu(x')$ we used (either its initial value or initial slope). It probably has no realistic counterpart in actual cases.

Figures 4.9 to 4.14 show various electrical quantities. Since the situation we are investigating is patently off the design condition, we will refrain from commenting on these plots as they serve no practical purpose, except to be complete and to display rather wild off-design variations.

Similarly, Figs. 4.15 to 4.23 show plots for the case with

$$A' = 1 + 0.061x'$$

$$S_i = 0.3$$

and $M_{ci} = 1.5$ (curves marked with triangles), 1.6 (circles), 1.7 (crosses); all the other parameters are the same as in the previous case. These figures show the same trend as before.

Another set of results is given in Figs. 4.24-4.35. Here, $S_i = 0.4$, $M_i = 1.7$; everything else is the same as for the previous case. In addition, Fig. 4.36 also shows the relative cross-sectional area of the wall layer (as fraction of the total area) for this case. It is seen that the wall layer thickens quickly near the entrance; and eventually fills more than 80% of the duct for this particular case.

Finally, in Figs. 4.36-4.38, influences on the pressure variation, due to changes in inlet Mach number, maximum μ-value, and degree of duct divergence are (respectively) plotted. In all these, $S_i = 0.4$; and u_{ci}, u_{wi}, etc., are all the same as before.

In Fig. 4.36,

$$A' = 1 + 0.061x'$$

$$\mu = 0.0003 + 0.12x'$$

$$= 0.3 \text{ when the calculated } \mu \geq 0.3$$

The curve marked with triangles is the case with $M_{ci} = 1.5$; that with circles, 1.6; and that with crosses, 1.7. Thus, the "strength" of the pseudo-shock increases with M_{ci}.

In Fig. 4.37, $M_{ci} = 1.5$, $A'(x')$ is the same as for Fig. 4.36.

$$\mu = 0.0003 + 0.1x', \quad x' < 1$$

$$= 0.1003 + 0.12(x' - 1), \quad x' \geq 1$$

$$= \mu_{max} \text{ when the calculated } \mu \geq \mu_{max}$$

The curve marked with triangles represents the case with $\mu_{max} = 0.2$; that with crossed circles, 0.3; that with squares, 0.4; and that with crosses, 0.5. The trend of larger μ_{max} is seen to make the pressure ramp flatter.

Figure 4.38 shares with Fig. 4.36 the same $\mu(x')$; and with FIg. 4.37, the same M_{cf}. For the curve marked with triangles, we have:

$$A' = 1 + 0.061x'$$

that with crossed circles:

$$A' = 1 + 0.1x'$$

that with squares:

$$A' = 1 + 0.2x'$$

and that with crosses,

$$A' = 1 + 0.3x'$$

There is no clear trend discernible. However, it is noted that the pressure variation is very sensitive to the duct divergence.

4.2 CONCLUSIONS

Under the present Grant, we have successfully demonstrated the feasibility of extending Crocco's pseudo-shock model to explain qualitatively the observed pressure rise in a rather extended portion of supersonic MHD generators, with rough walls and at off-design conditions.

For future refinement, we may list a number of ways by which (singly or combinedly) the formulation may be improved:

(1) Heat transfer and friction at the wall can be introduced through additional coefficients.

(2) Heat transfer and friction at the interface can be accounted for.

(3) The formulation can be coupled with a boundary layer analysis (using Kármán-Pohlhausen technique) at the wall.

(4) The wall layers at the cathode and anode can be distinguished, and the formulation extended to a three-region model.

(5) Cases with $d\mu/dx < 0$ can be tested (with due modification of the governing equations).

However, the major drawback in our analysis (also in Crocco's), i.e., the empirical assignment of a $\mu(x)$ to start the calculation will always be with us.

It may also be interesting to apply the two-region model to flow apparata other than power generators.

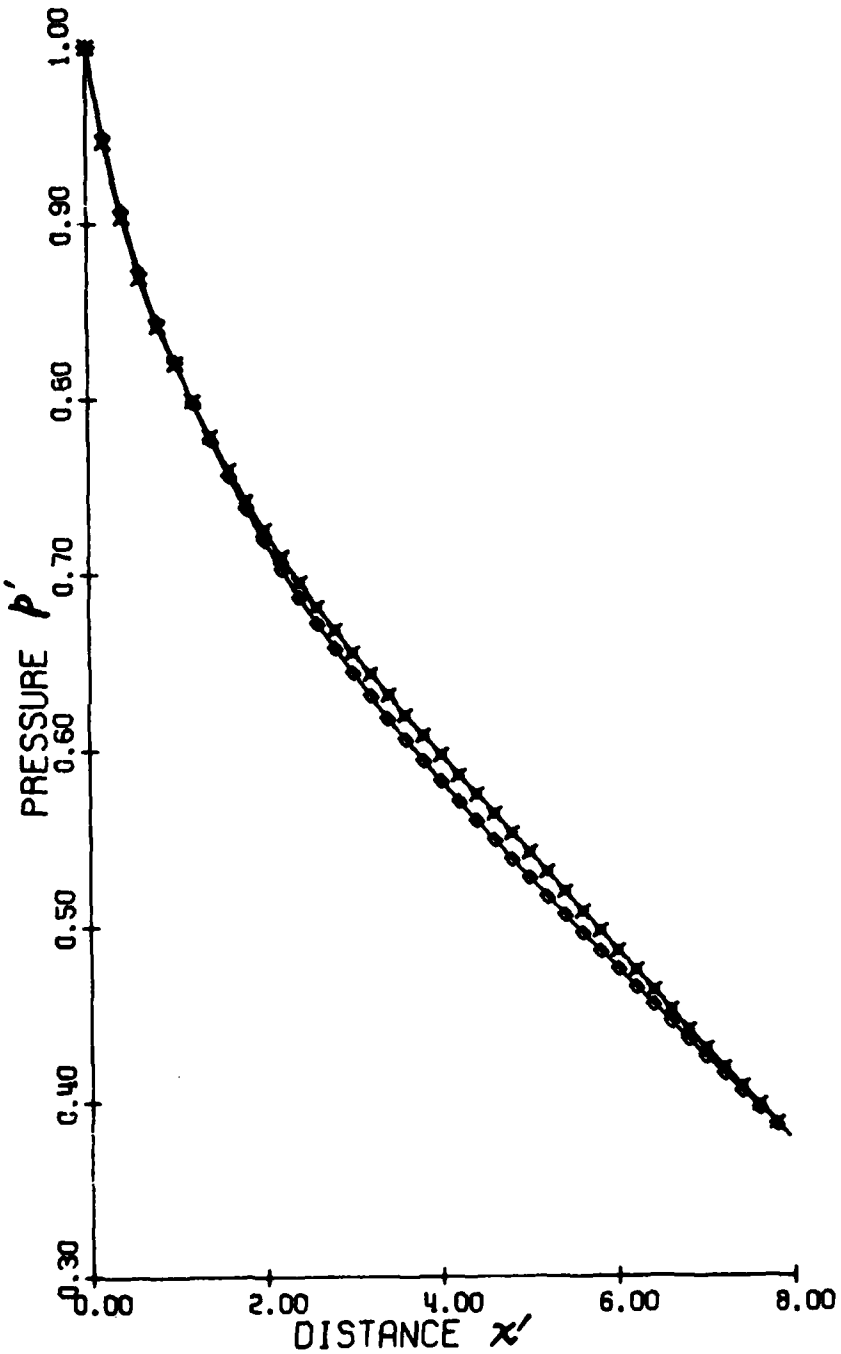
1.00
0.90
0.80
0.70
0.60
0.50
0.40
0.30
PRESSURE P'
0.00
2.00
4.00
6.00
8.00
DISTANCE x'

Fig. 4.1

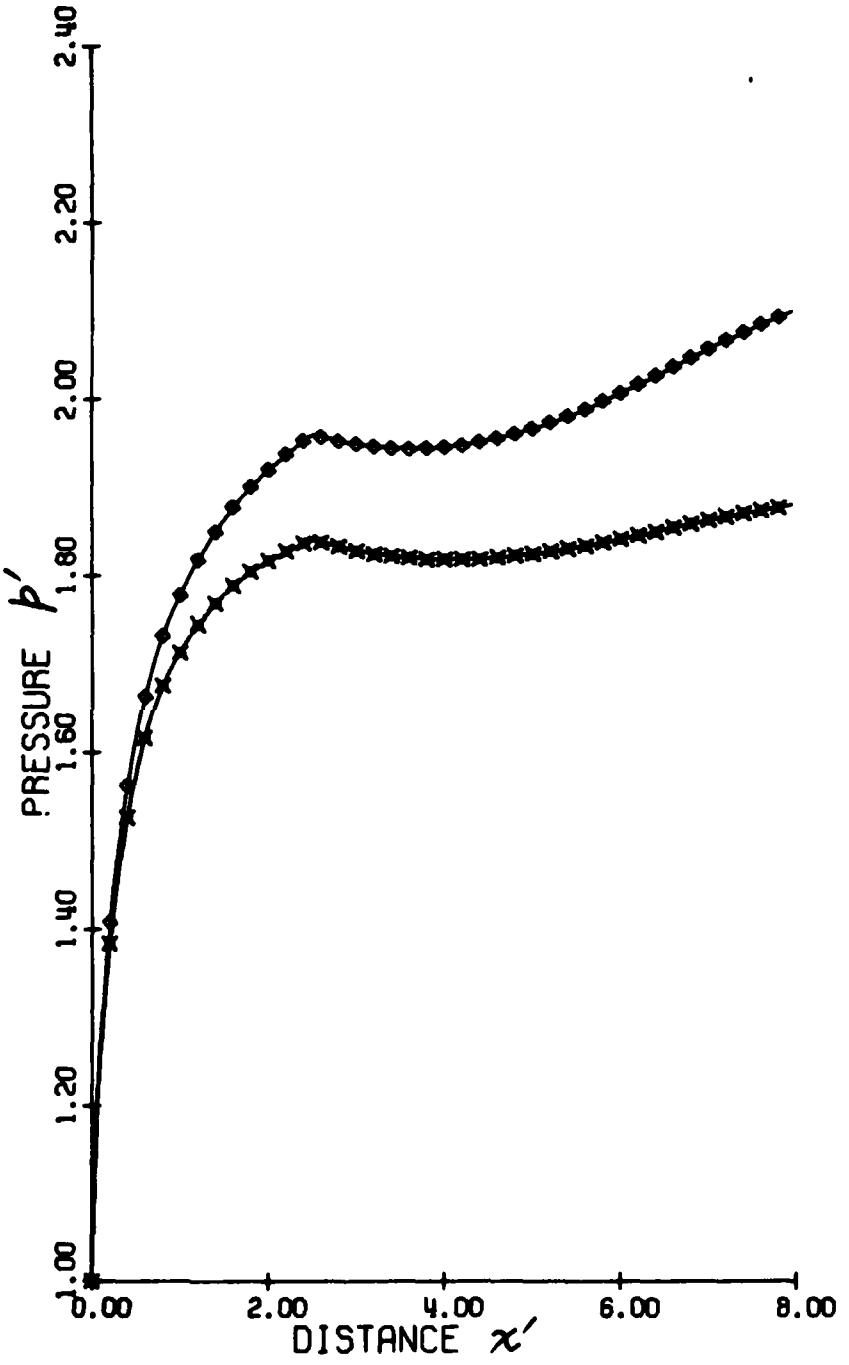
PRESSURE p'
1.00
1.20
1.40
1.60
1.80
2.00
2.20
2.40
0.00
2.00
4.00
6.00
8.00
DISTANCE x'

Fig. 4.2

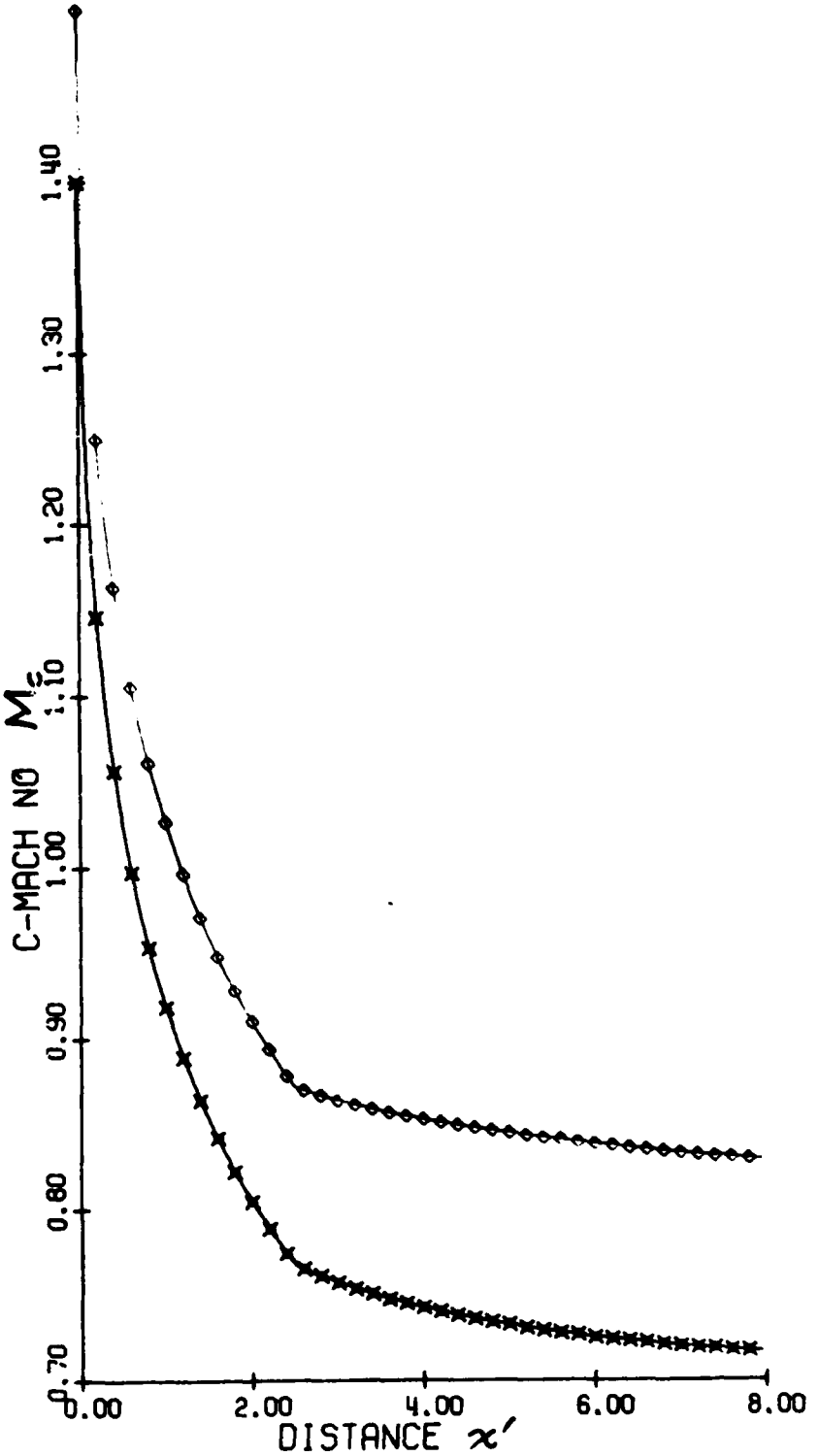
C-MACH NO M_c
1.40
1.30
1.20
1.10
1.00
0.90
0.80
0.70
0.00
2.00
4.00
6.00
8.00
DISTANCE x'

Fig. 4.3

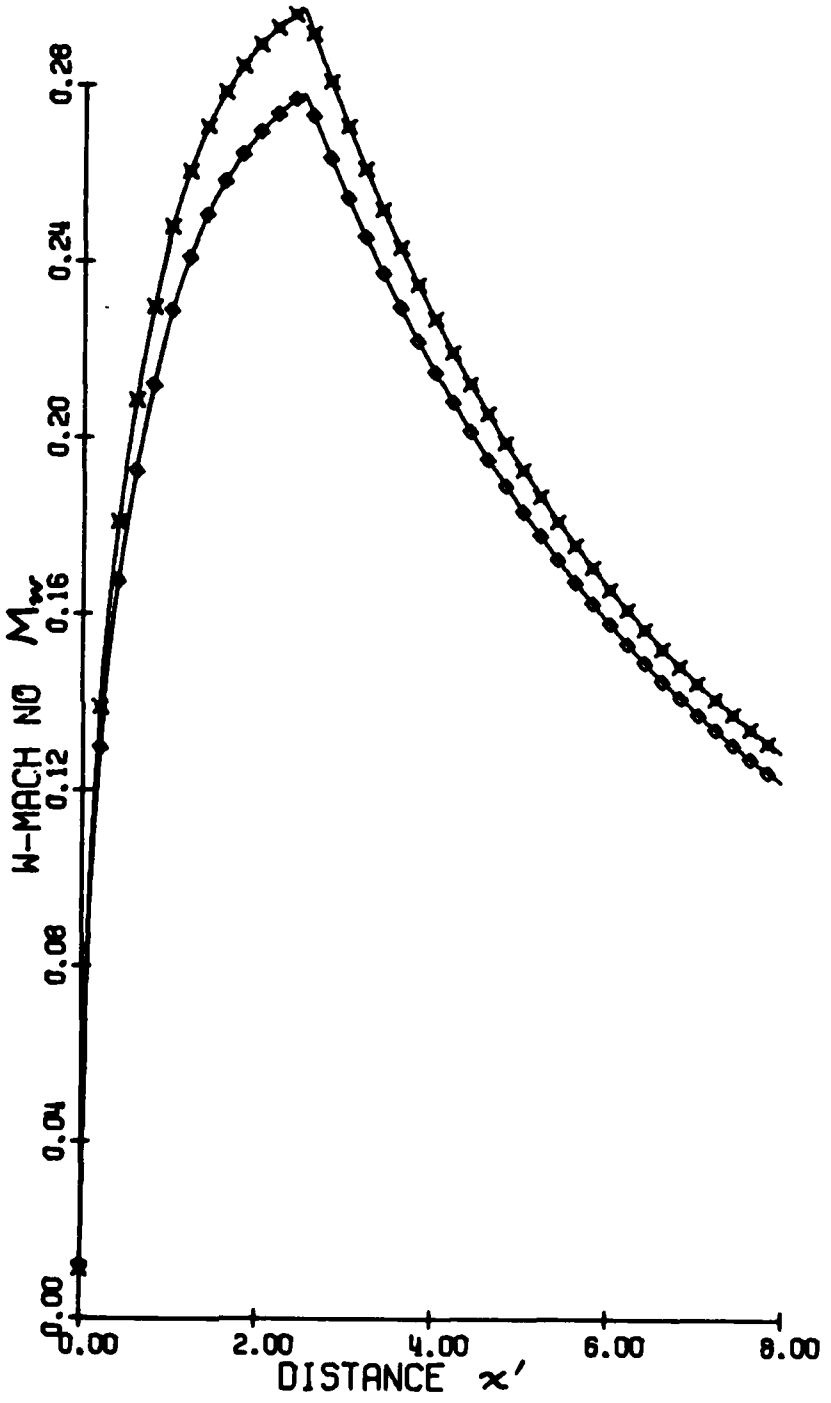
W-MACH NO M_w
0.00
0.04
0.08
0.12
0.16
0.20
0.24
0.28
0.00
2.00
4.00
6.00
8.00
DISTANCE x'

Fig. 4.4

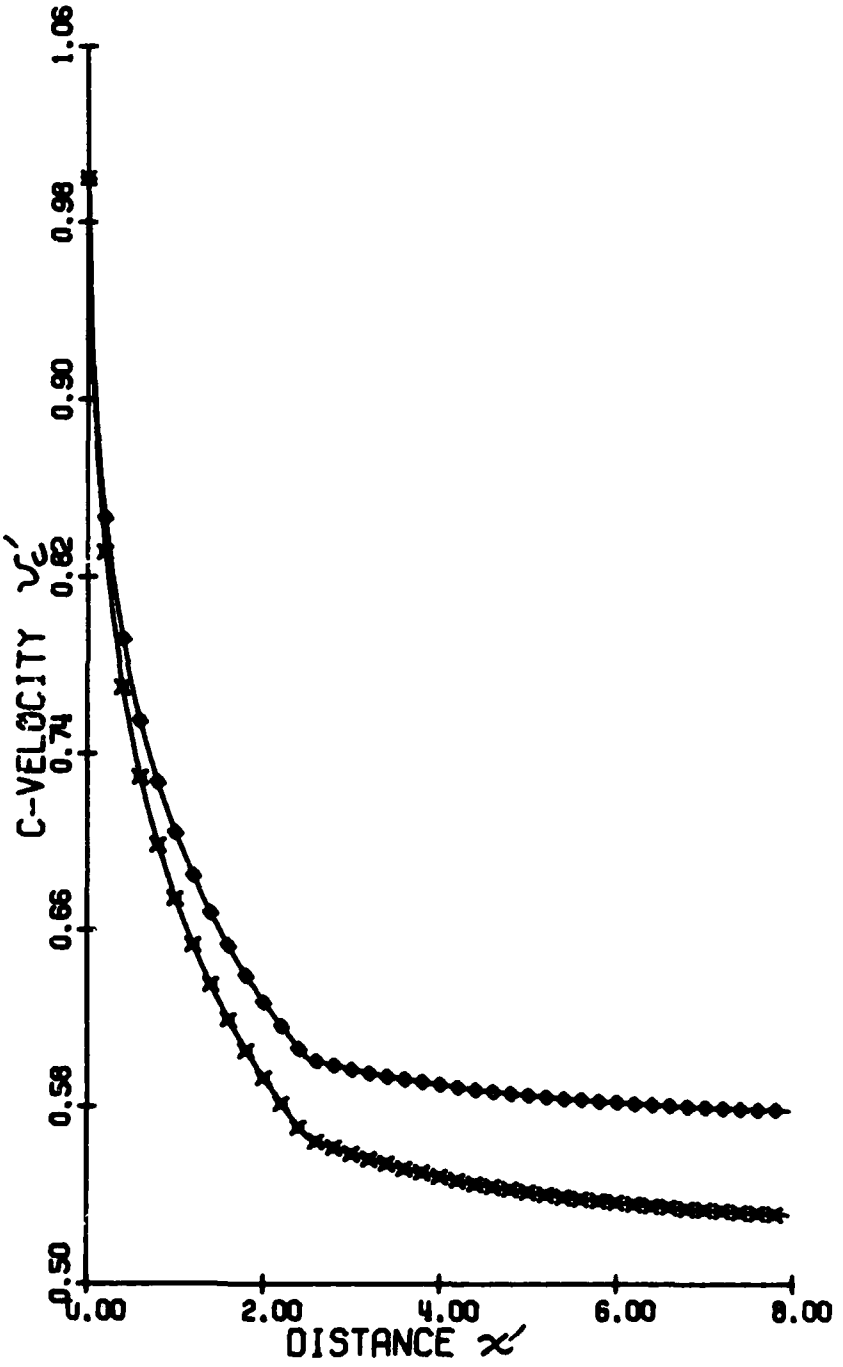
C-VELOCITY v_c'
1.06
0.98
0.90
0.82
0.74
0.66
0.58
0.50
0.00
2.00
4.00
6.00
8.00
DISTANCE x'

Fig. 4.5

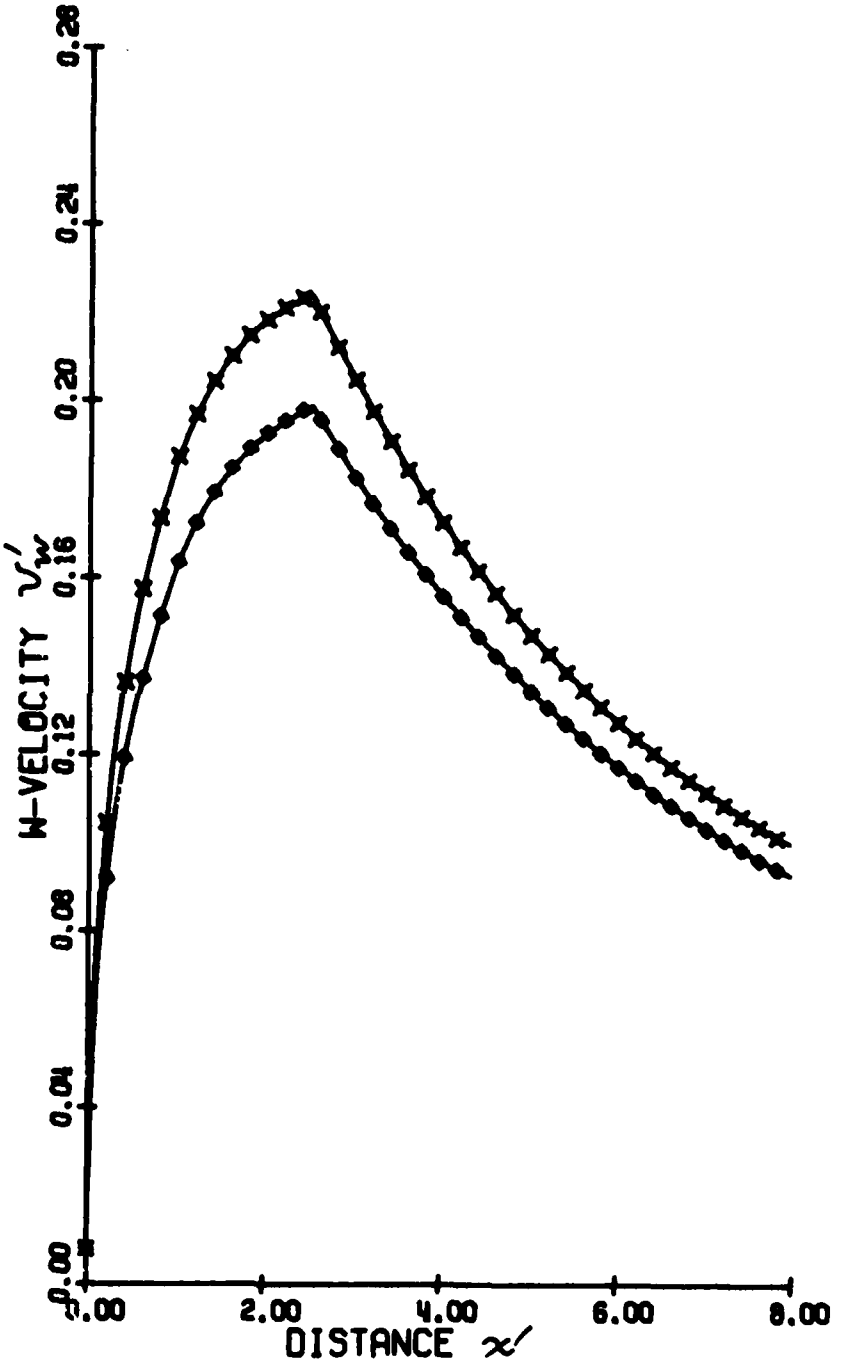
W-VELOCITY v'_w
0.00
0.04
0.08
0.12
0.16
0.20
0.24
0.28
0.00
2.00
4.00
6.00
8.00
DISTANCE x'

Fig. 4.6

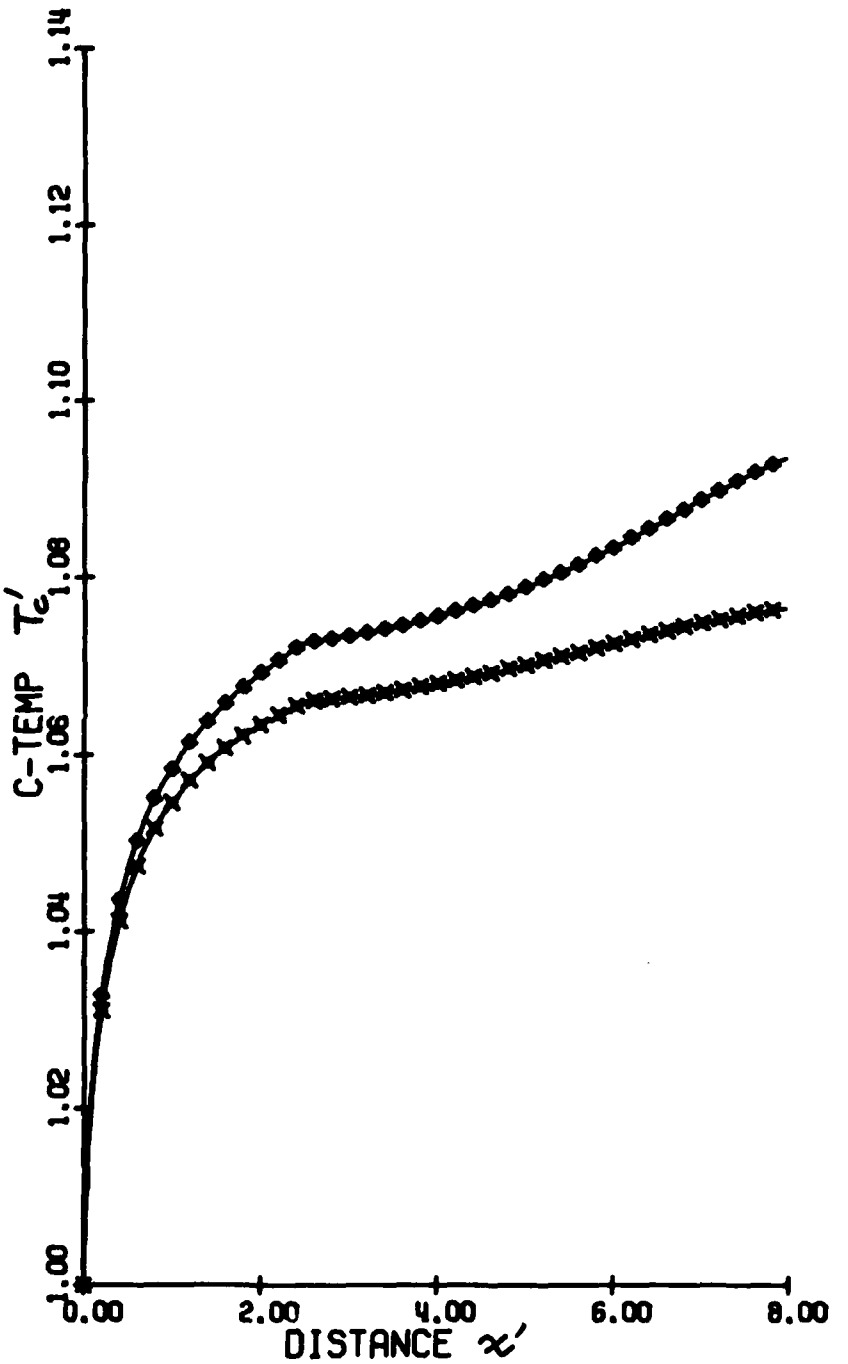
C-TEMP T_c'
1.00
1.02
1.04
1.06
1.08
1.10
1.12
1.14
0.00
2.00
4.00
6.00
8.00
DISTANCE x'

Fig. 4.7

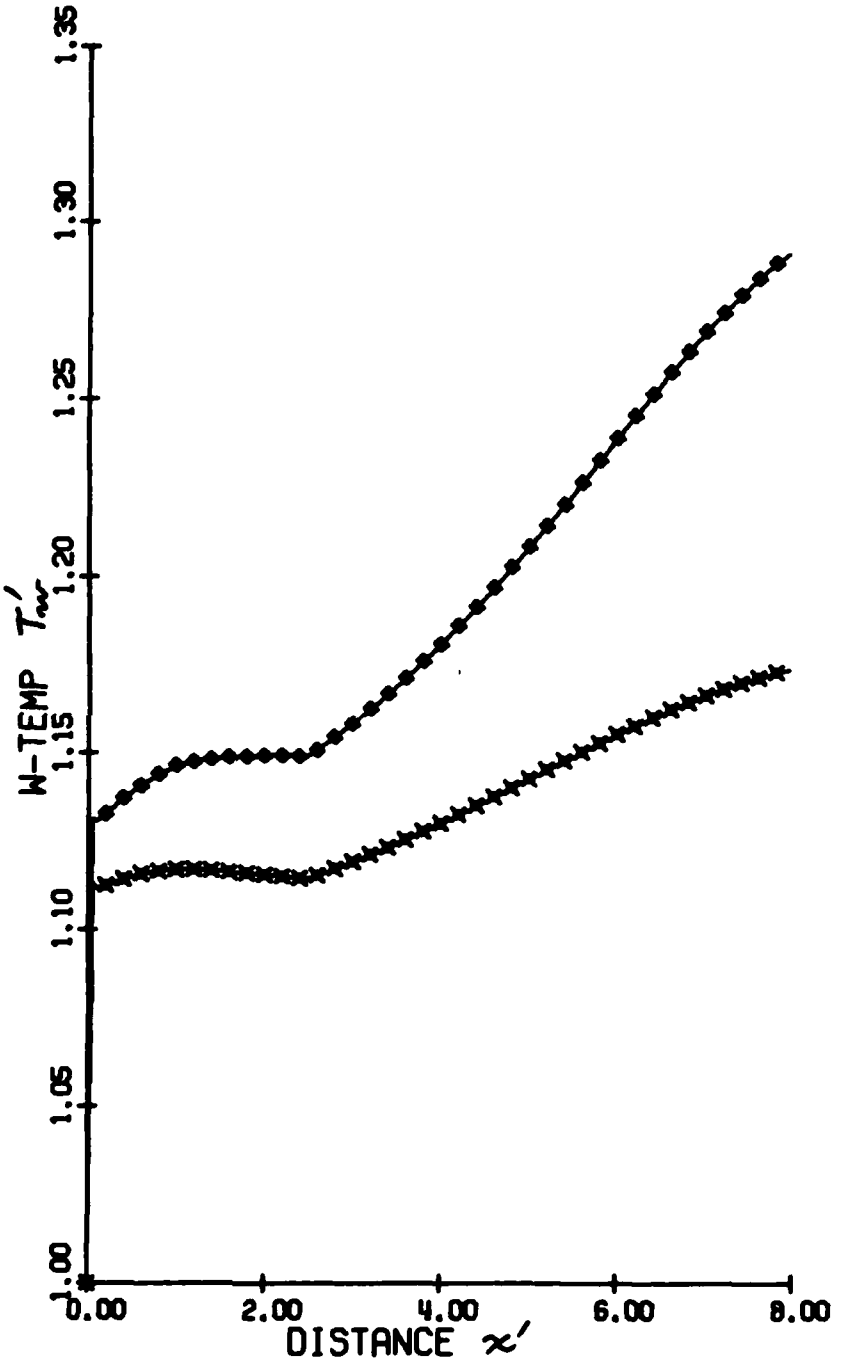
W-TEMP T_w'
1.00
1.05
1.10
1.15
1.20
1.25
1.30
1.35
0.00
2.00
4.00
6.00
8.00
DISTANCE x'

Fig. 4.8

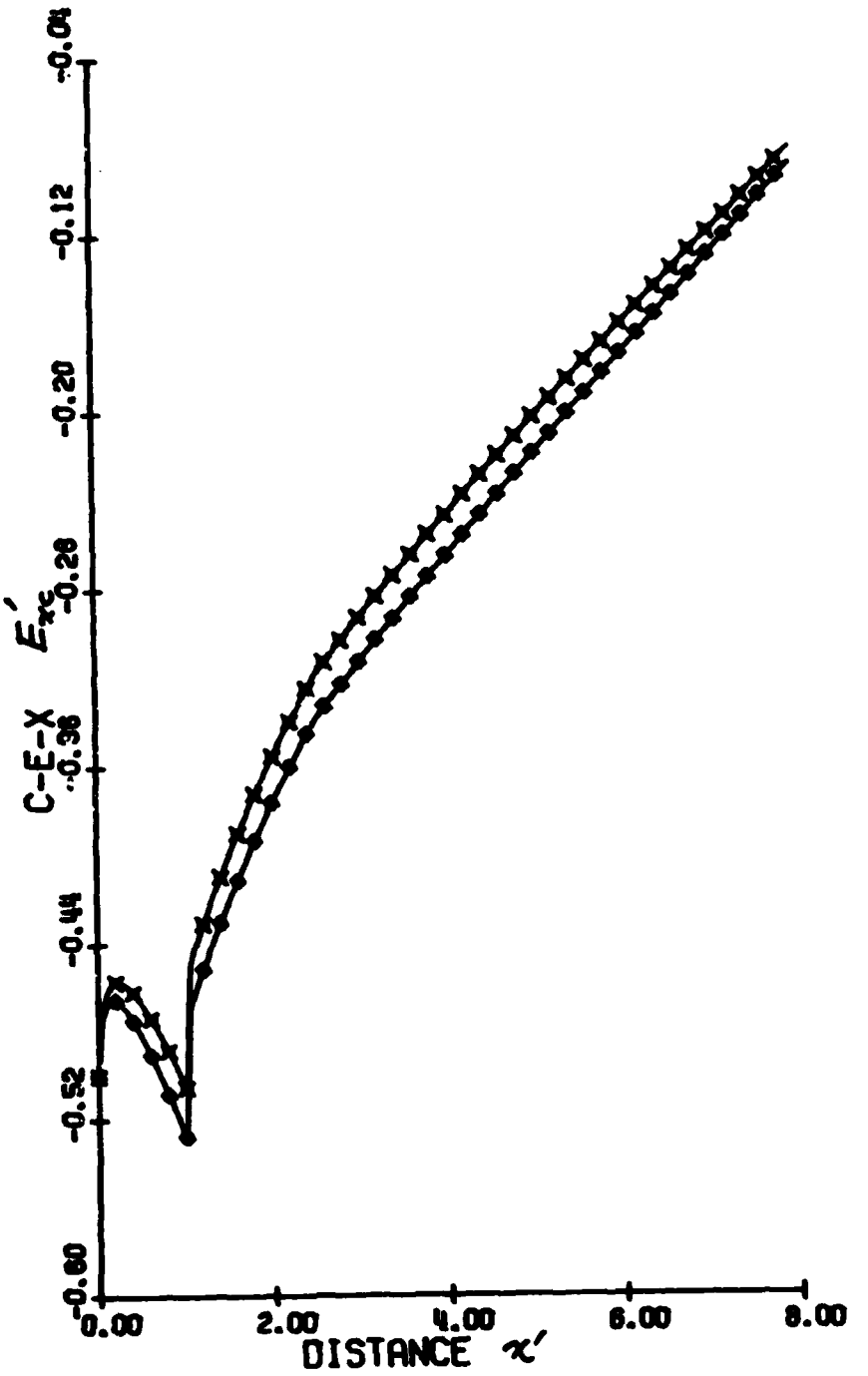
C-E-X E'_{xc}
-0.04
-0.12
-0.20
-0.28
-0.36
-0.44
-0.52
-0.60
0.00
2.00
4.00
6.00
8.00
DISTANCE x'

Fig. 4.9

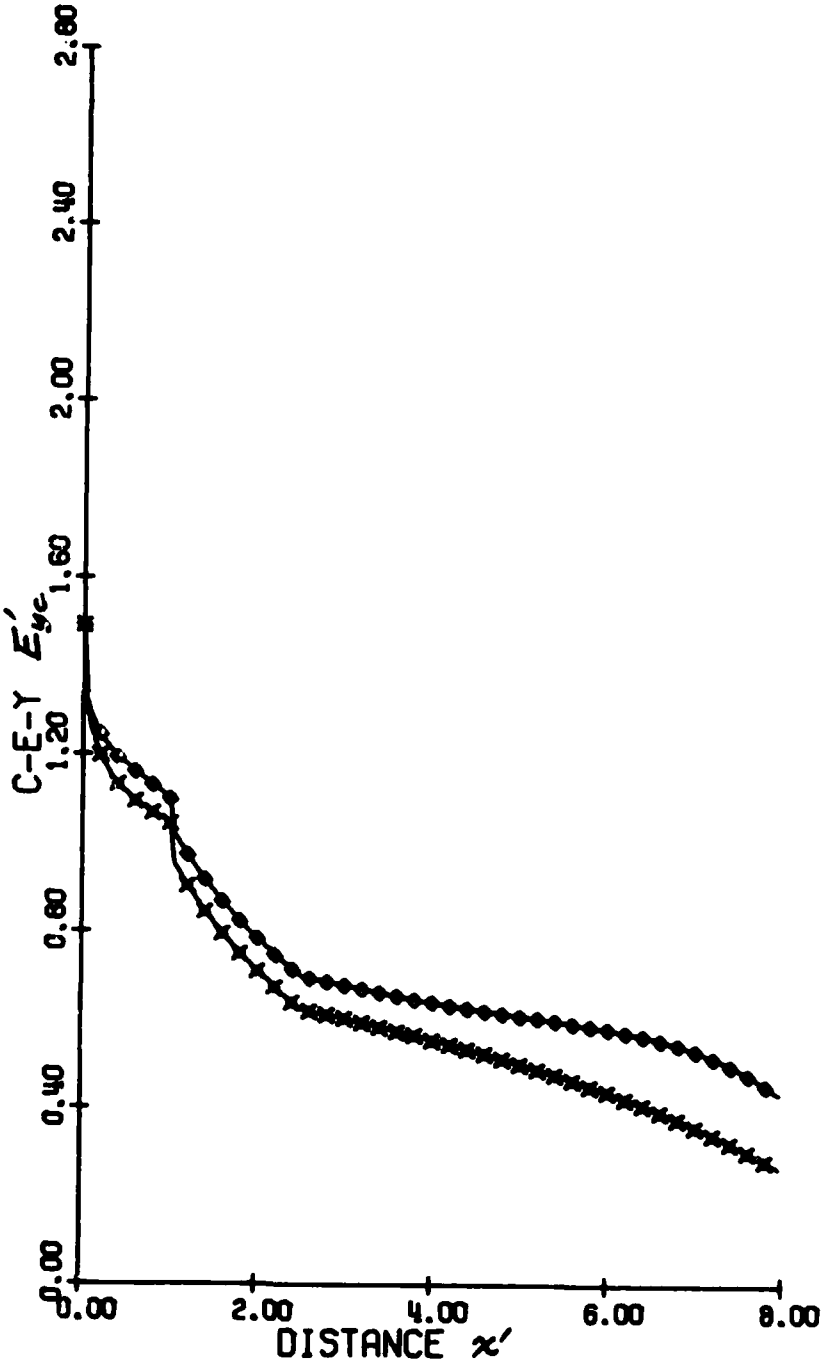
C-E-Y E'_{ye}
2.80
2.40
2.00
1.60
1.20
0.80
0.40
0.00
0.00
2.00
4.00
6.00
8.00
DISTANCE x'

Fig. 4.10

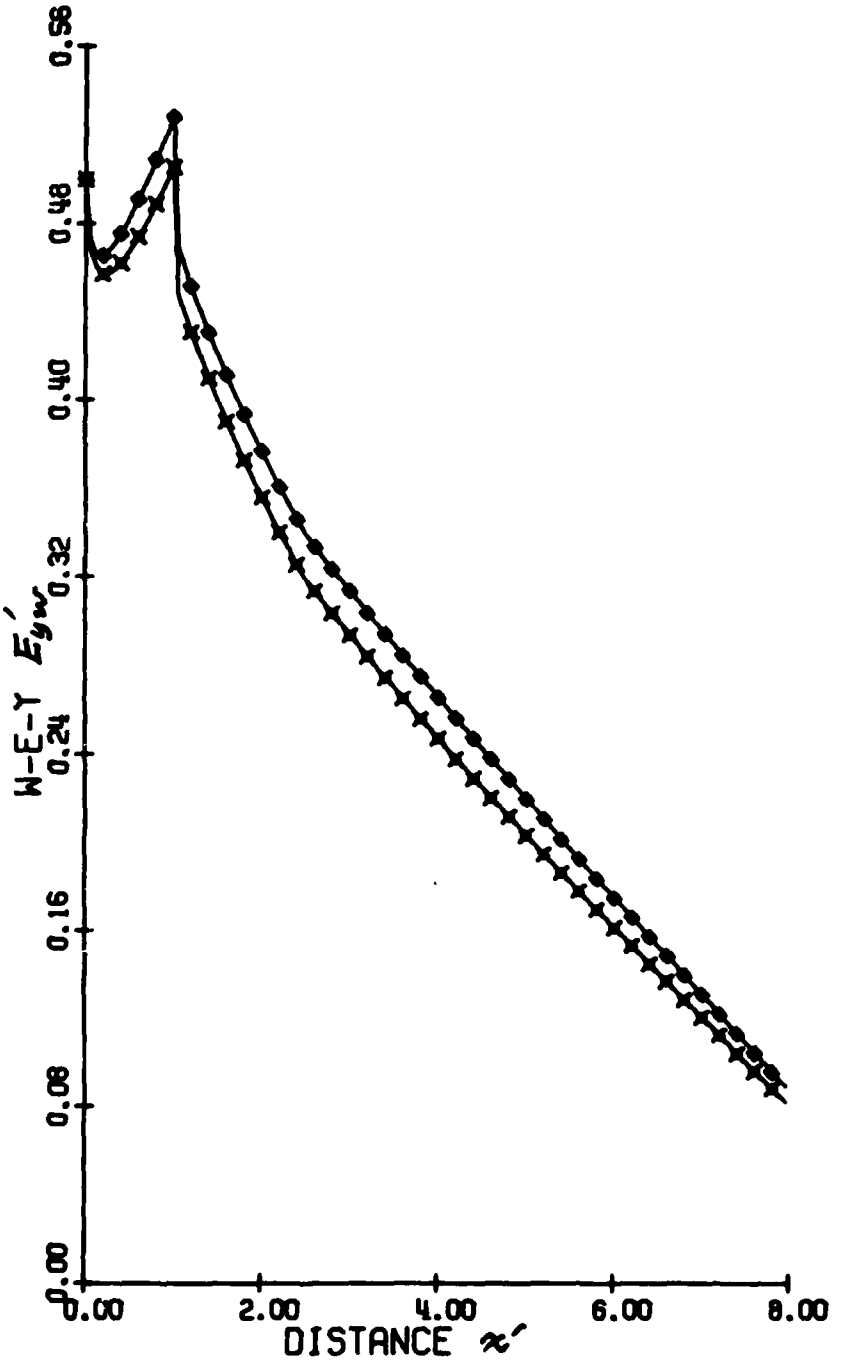
0.56
0.48
0.40
0.32
0.24
0.16
0.08
0.00
W-E-Y E'_{yw}
0.00
2.00
4.00
6.00
8.00
DISTANCE x'

Fig. 4.11

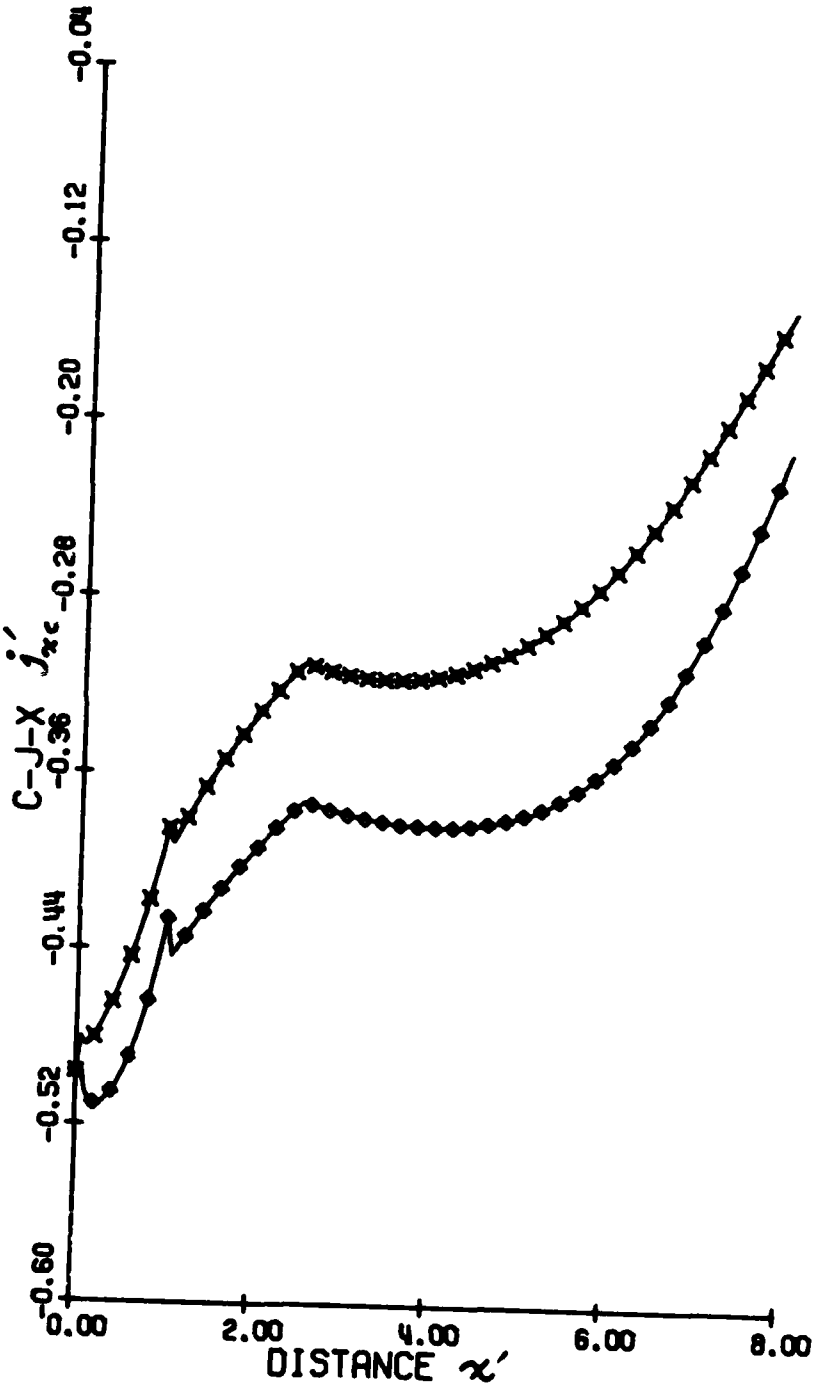
-0.04
-0.12
-0.20
-0.28
-0.36
-0.44
-0.52
-0.60
C-J-X j'_{xc}
0.00
2.00
4.00
6.00
8.00
DISTANCE x'

Fig. 4.12

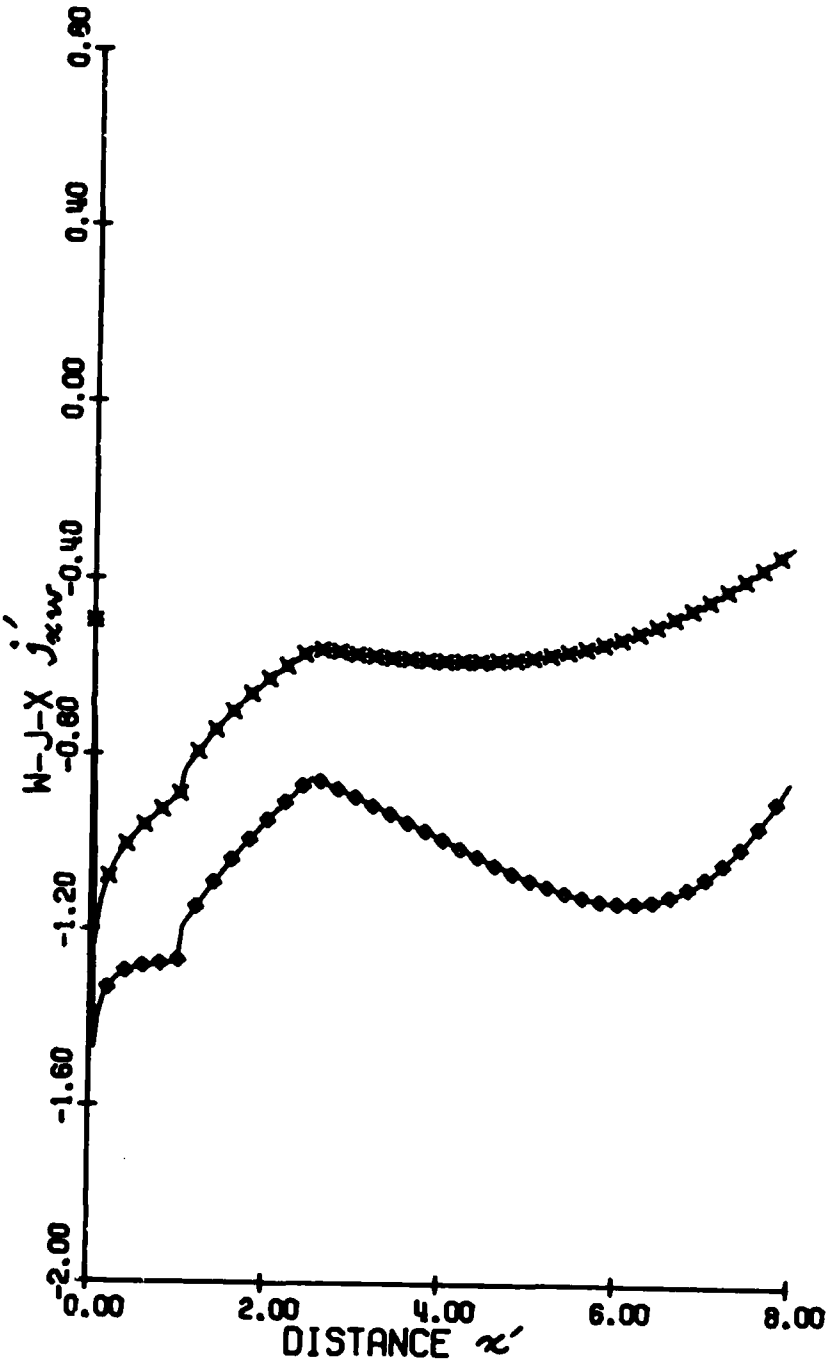
0.80
0.40
0.00
-0.40
-0.80
-1.20
-1.60
-2.00
W-J-X j'_{xw}
0.00
2.00
4.00
6.00
8.00
DISTANCE x'

Fig. 4.13

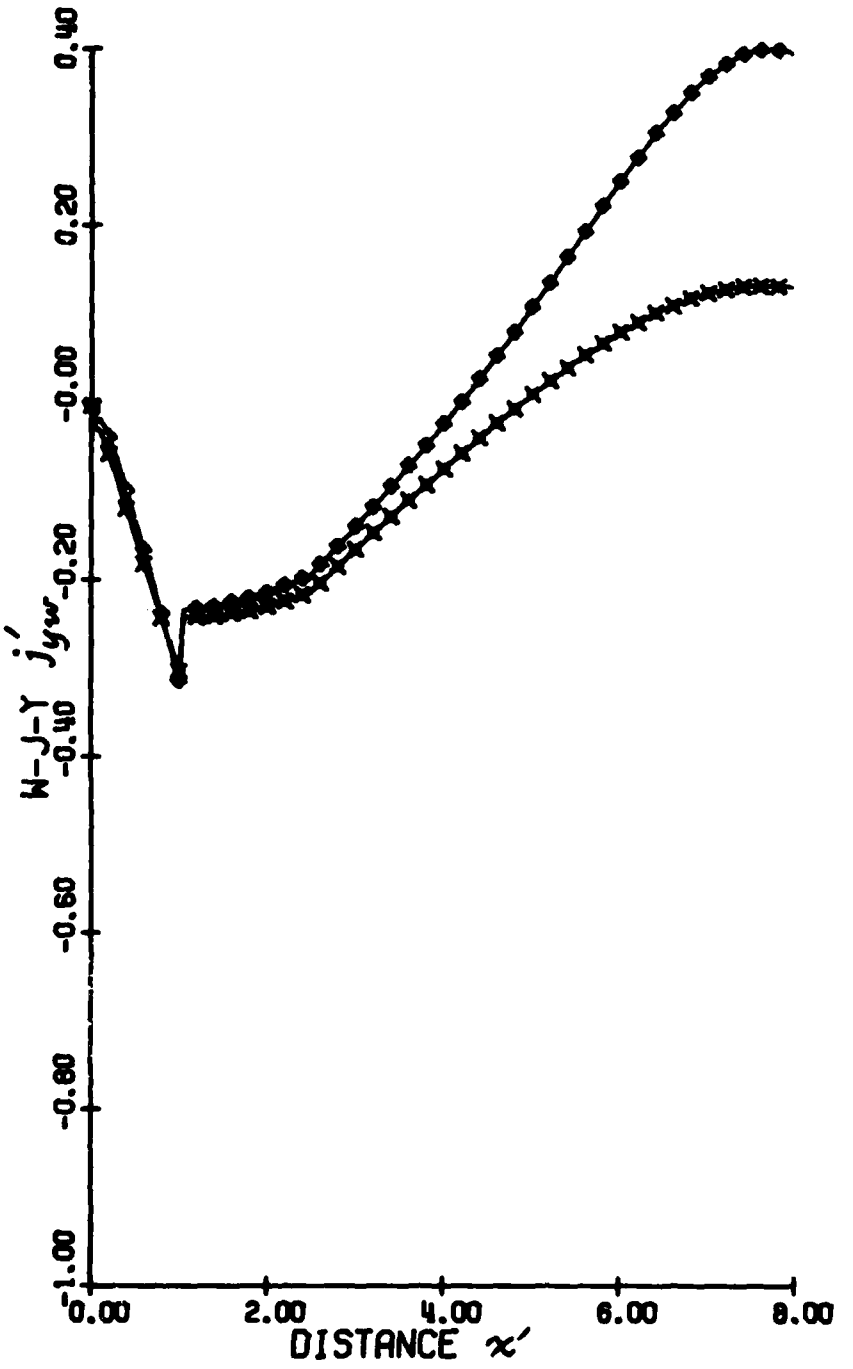
0.40
0.20
-0.00
-0.20
-0.40
-0.60
-0.80
-1.00
W-J-Y j'_{yw}
0.00
2.00
4.00
6.00
8.00
DISTANCE x'

Fig. 4.14

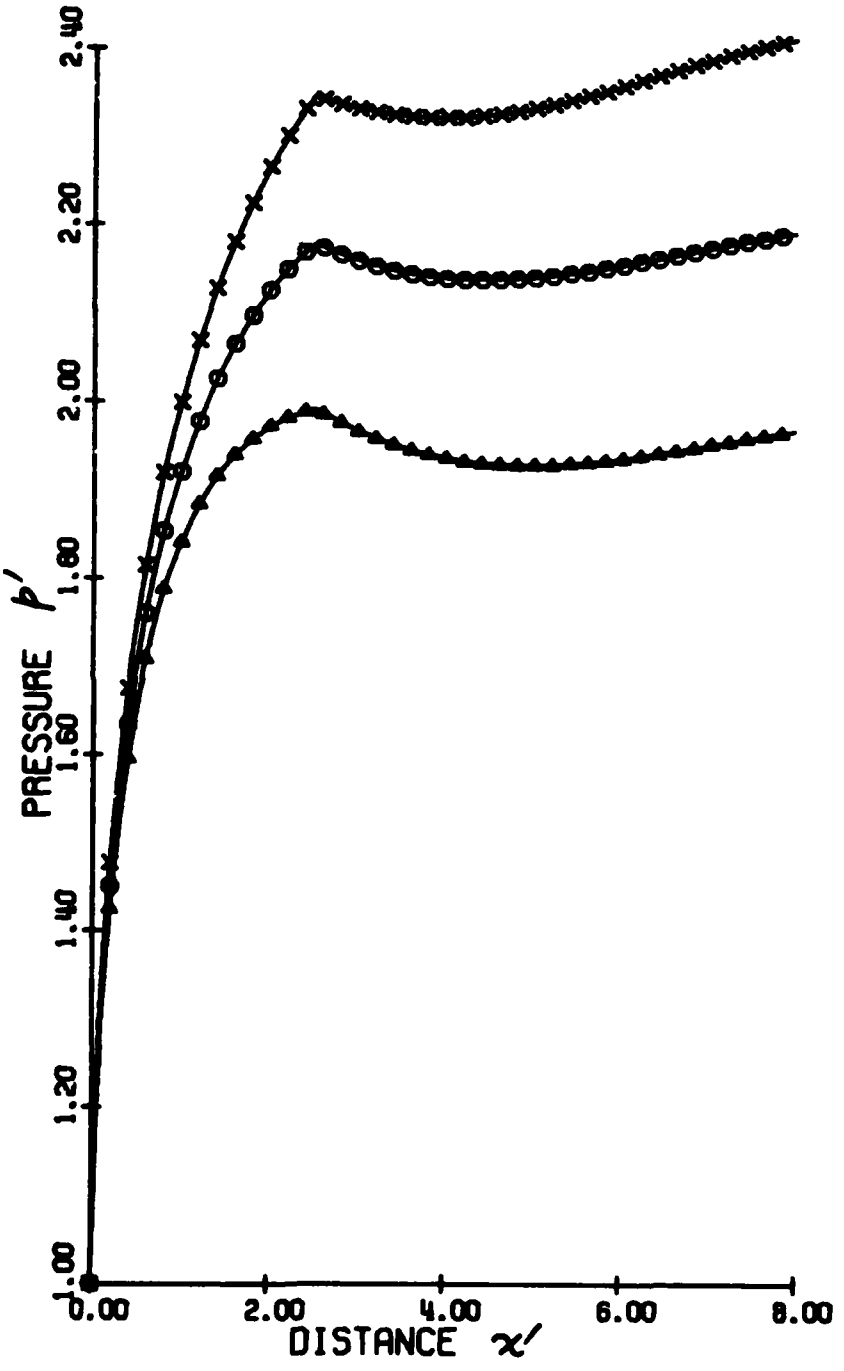
PRESSURE p'
1.00
1.20
1.40
1.60
1.80
2.00
2.20
2.40
0.00
2.00
4.00
6.00
8.00
DISTANCE x'

Fig. 4.15

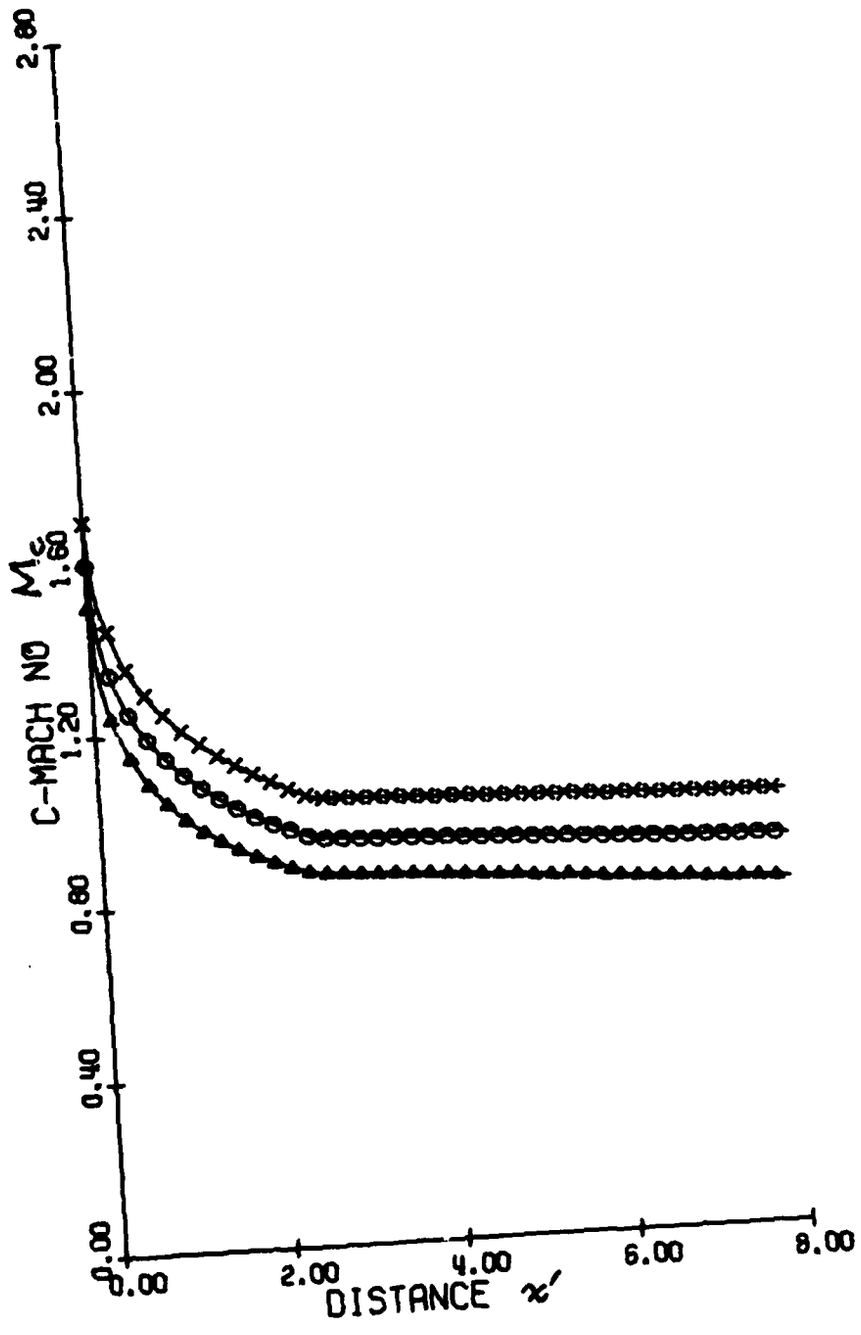
C-MACH NO M_e
2.80
2.40
2.00
1.80
1.20
0.80
0.40
0.00
0.00
2.00
4.00
6.00
8.00
DISTANCE x'

Fig. 4.16

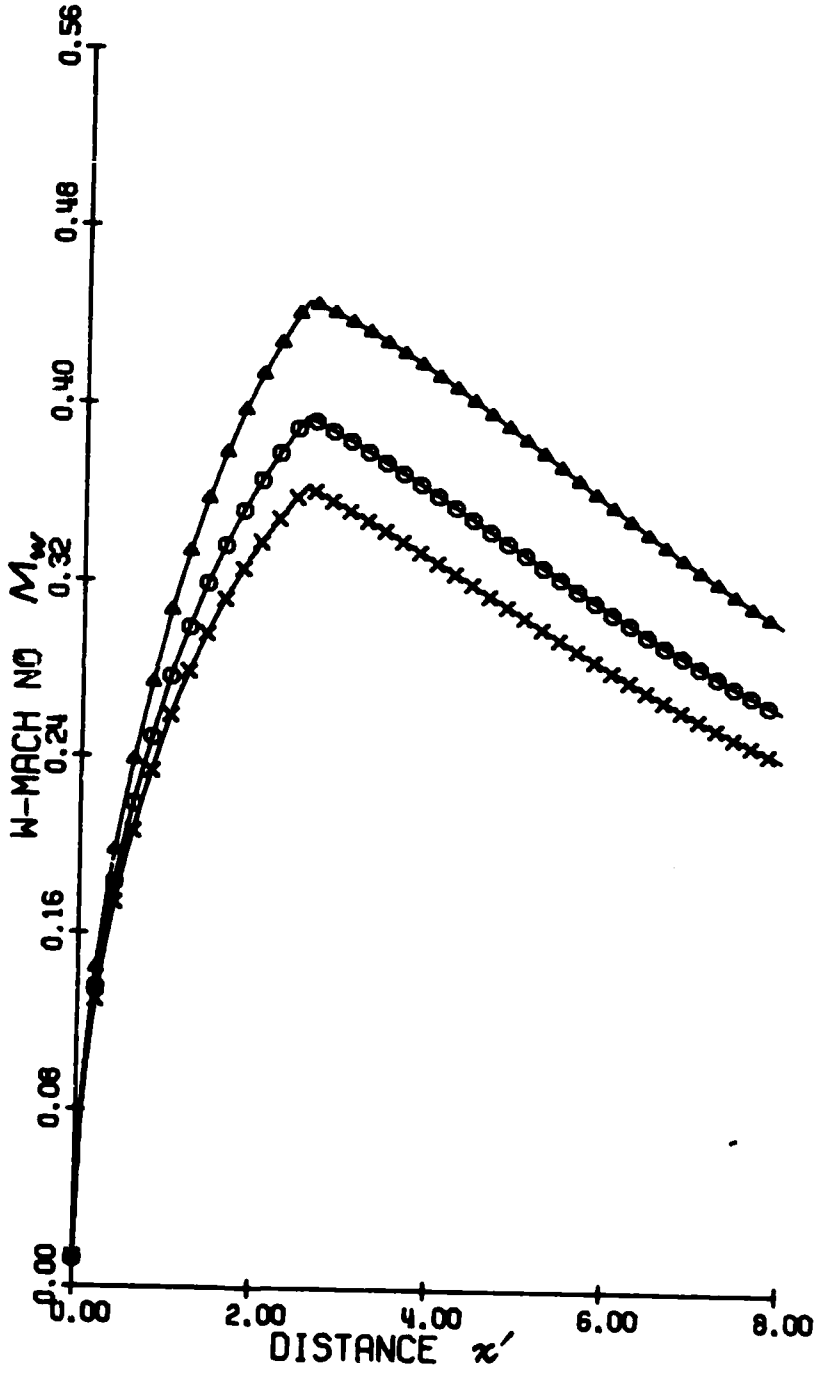
0.56
0.48
0.40
0.32
0.24
0.16
0.08
0.00
W-MACH NO M_w
0.00
2.00
4.00
6.00
8.00
DISTANCE x'

Fig. 4.17

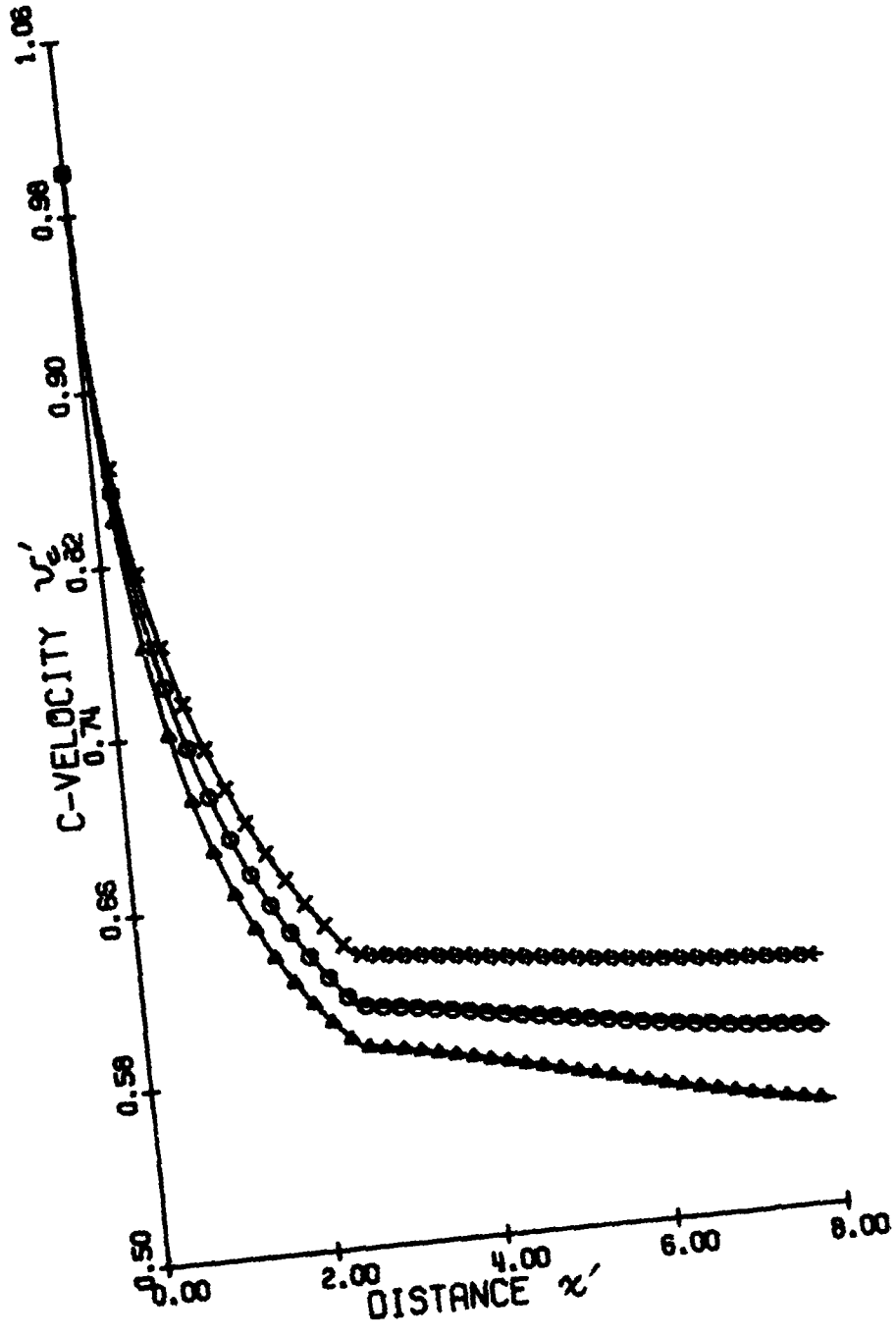
1.08
0.98
0.90
0.82
0.74
0.66
0.58
0.50
C-VELOCITY
0.00
2.00
4.00
6.00
8.00
DISTANCE x'

Fig. 4.18

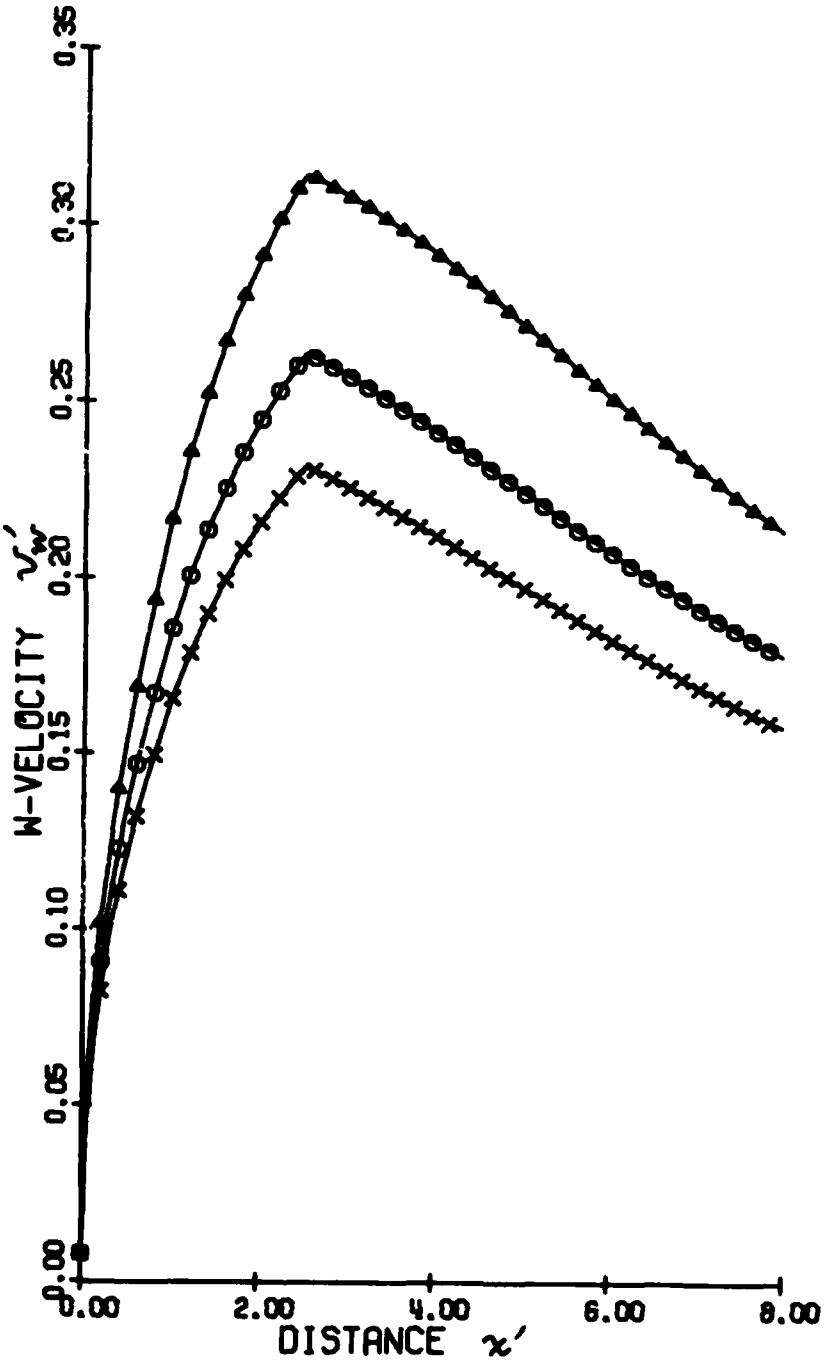
W-VELOCITY v_w'
0.00
0.05
0.10
0.15
0.20
0.25
0.30
0.35
0.00
2.00
4.00
6.00
8.00
DISTANCE x'

Fig. 4.19

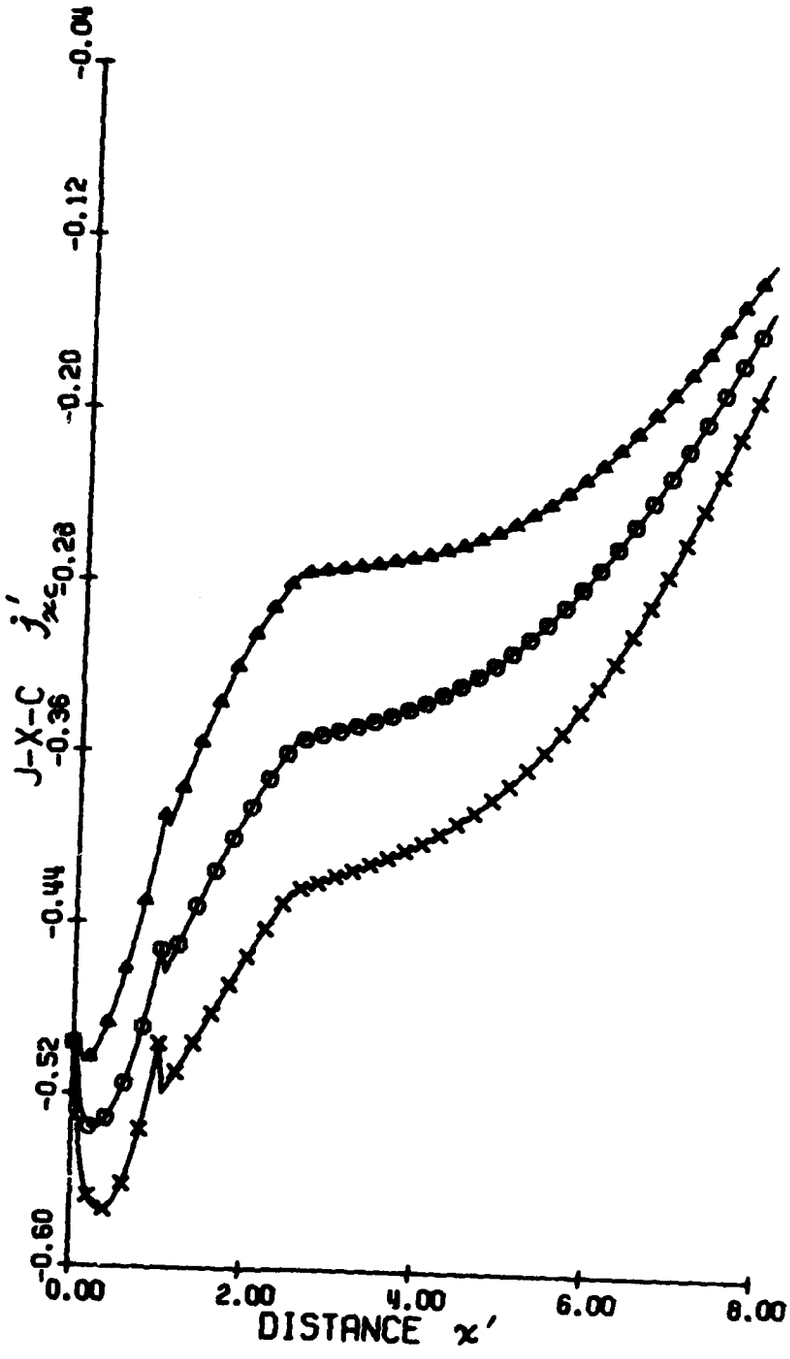
J-X-C
-0.04
-0.12
-0.20
-0.28
-0.36
-0.44
-0.52
-0.60
0.00
2.00
4.00
6.00
8.00
DISTANCE x'

Fig. 4.20

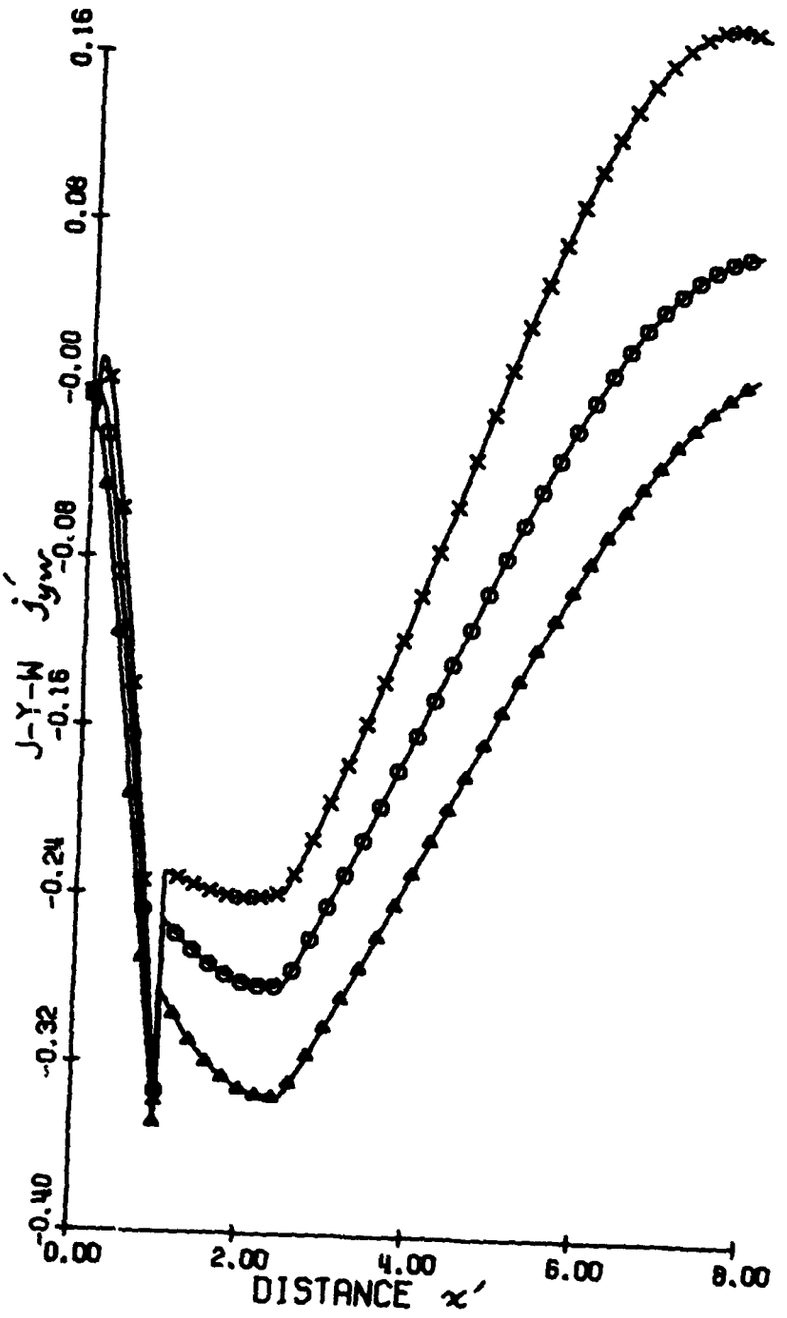
0.16
0.08
-0.00
-0.08
-0.16
-0.24
-0.32
-0.40
J-Y-W j'_{yw}
0.00
2.00
4.00
6.00
8.00
DISTANCE x'

Fig. 4.21

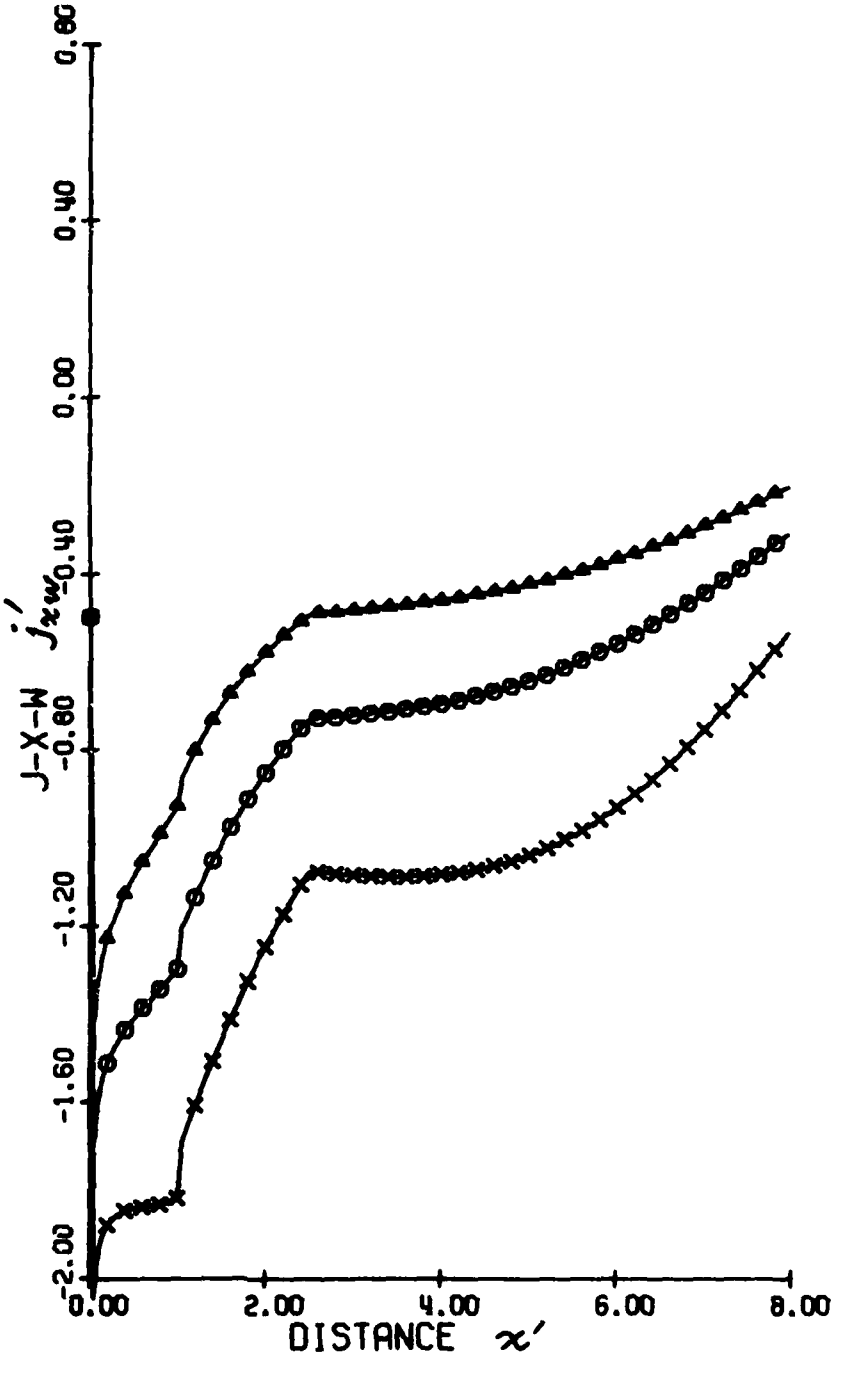
0.80
0.40
0.00
-0.40
-0.80
-1.20
-1.60
-2.00
J-X-W j'_{xw}
0.00
2.00
4.00
6.00
8.00
DISTANCE x'

Fig. 4.22

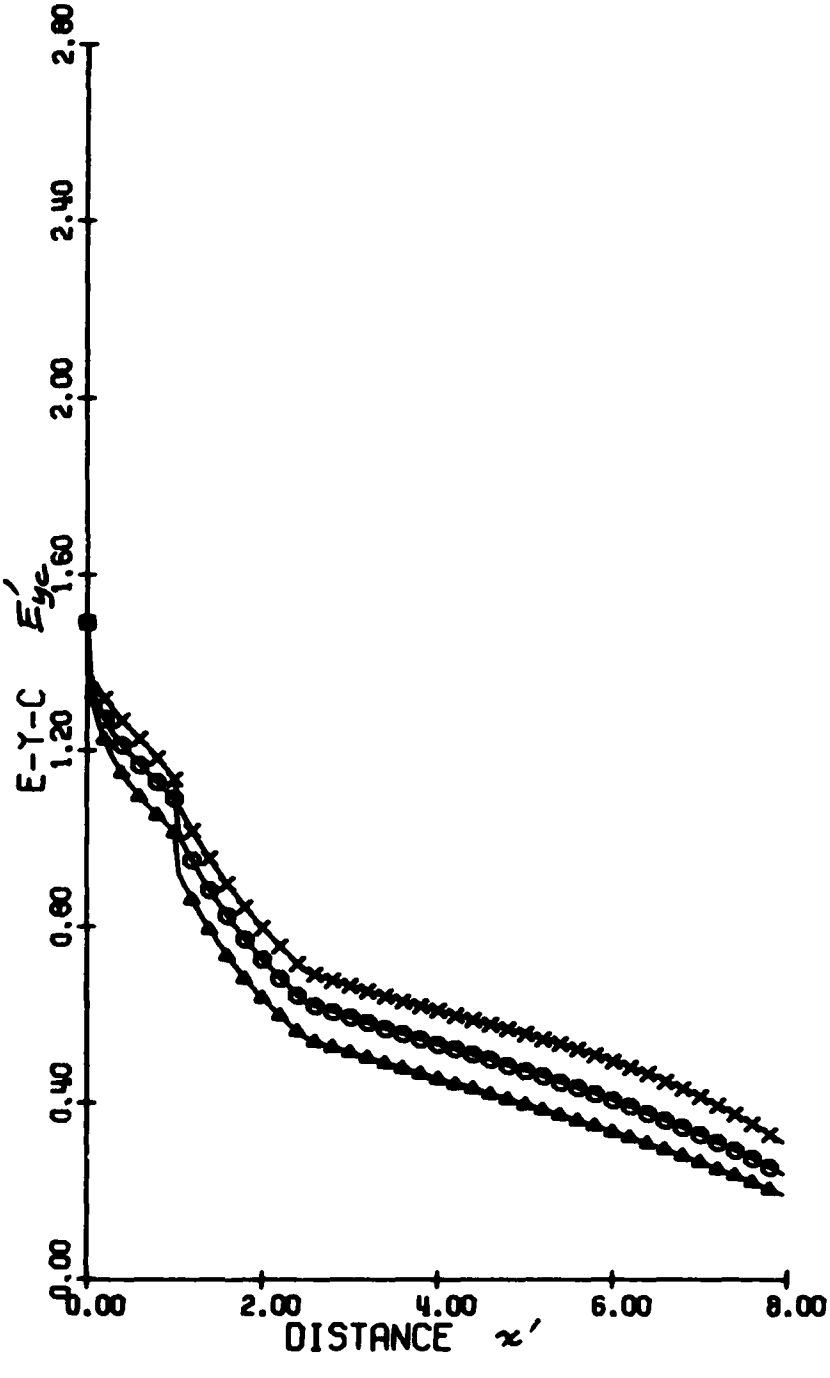
E-Y-C
E'_{yc}
2.80
2.40
2.00
1.60
1.20
0.80
0.40
0.00
0.00
2.00
4.00
6.00
8.00
DISTANCE x'

Fig. 4.23

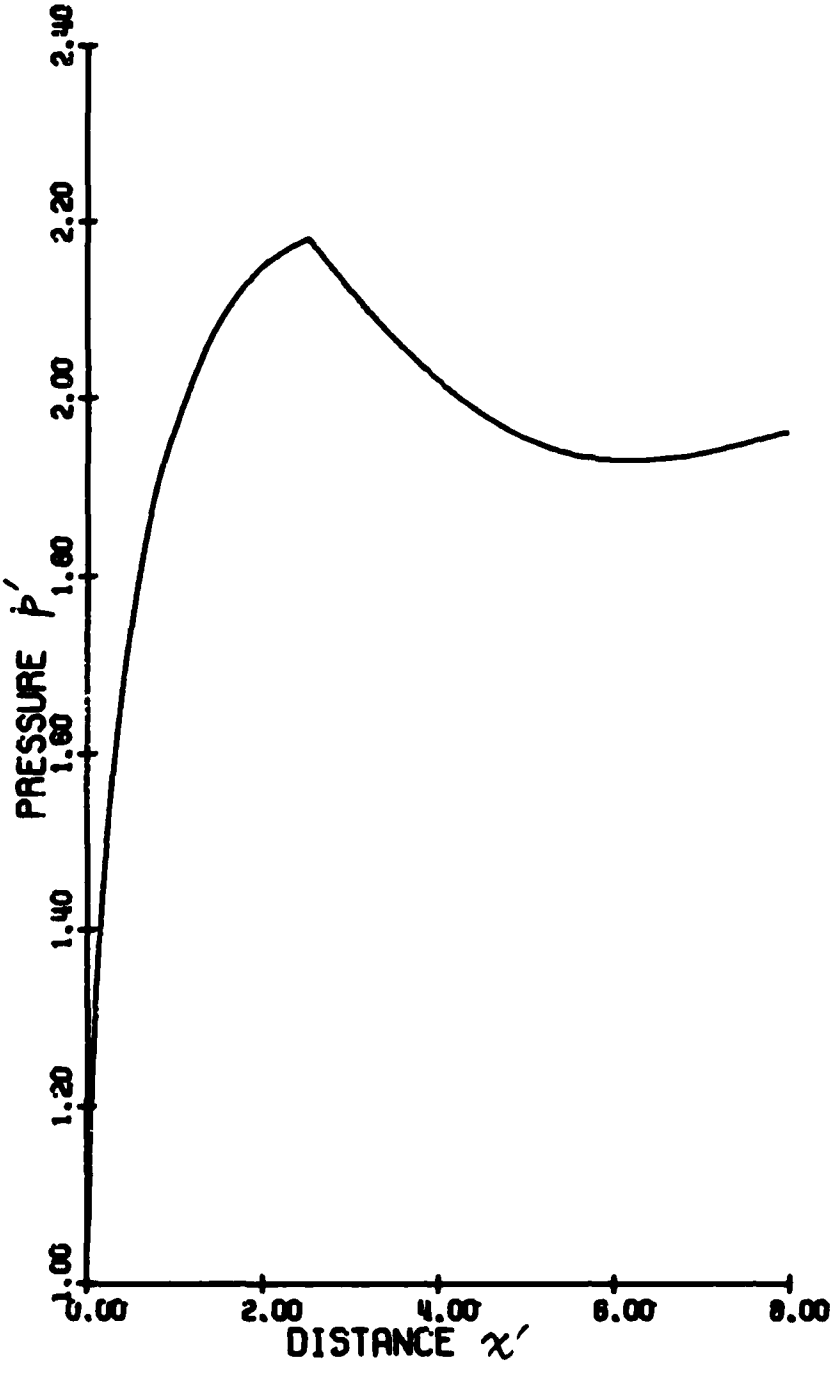
PRESSURE p'
1.00
1.20
1.40
1.60
1.80
2.00
2.20
2.40
0.00
2.00
4.00
6.00
8.00
DISTANCE x'

Fig. 4.24

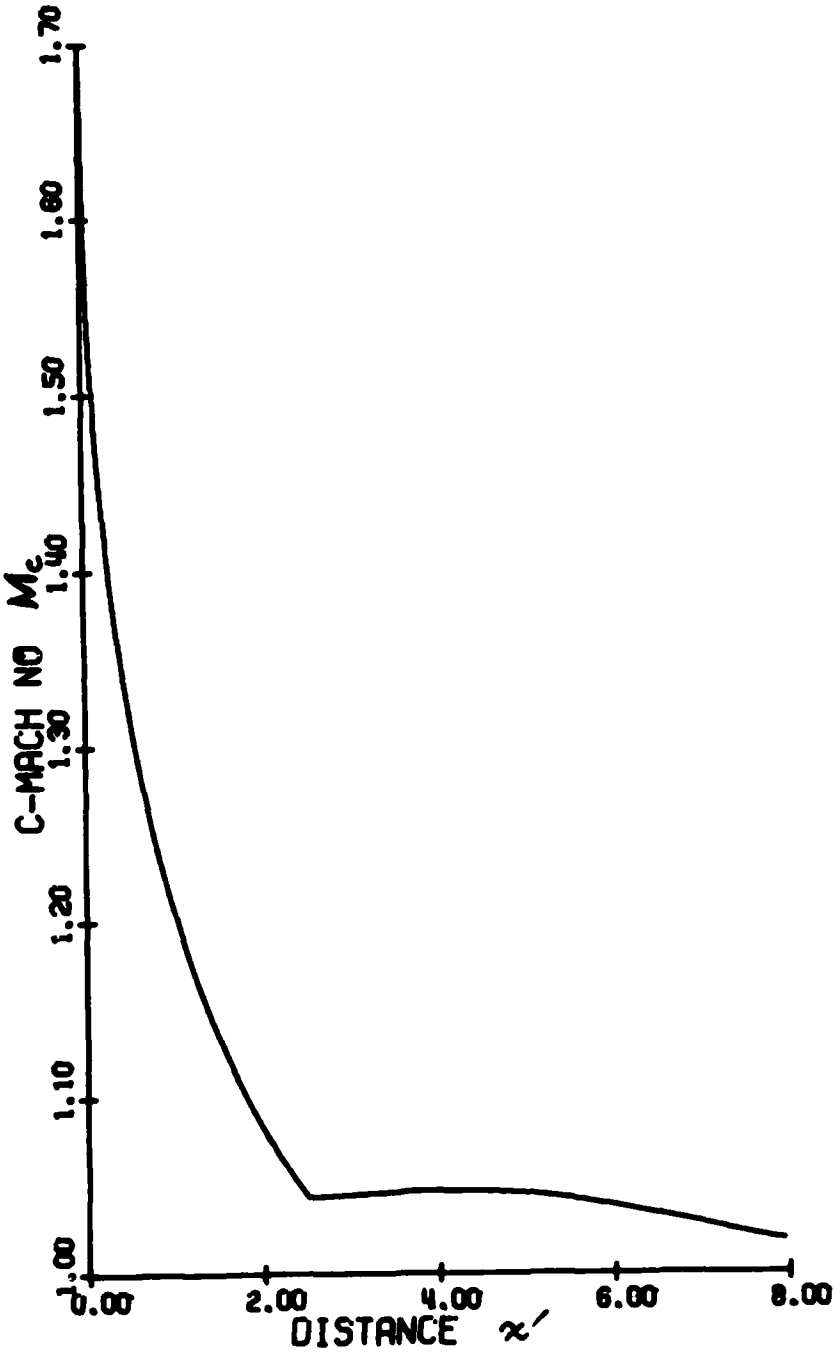
C-MACH NO M_e
1.70
1.60
1.50
1.40
1.30
1.20
1.10
1.00
0.00
2.00
4.00
6.00
8.00
DISTANCE x'

Fig. 4.25

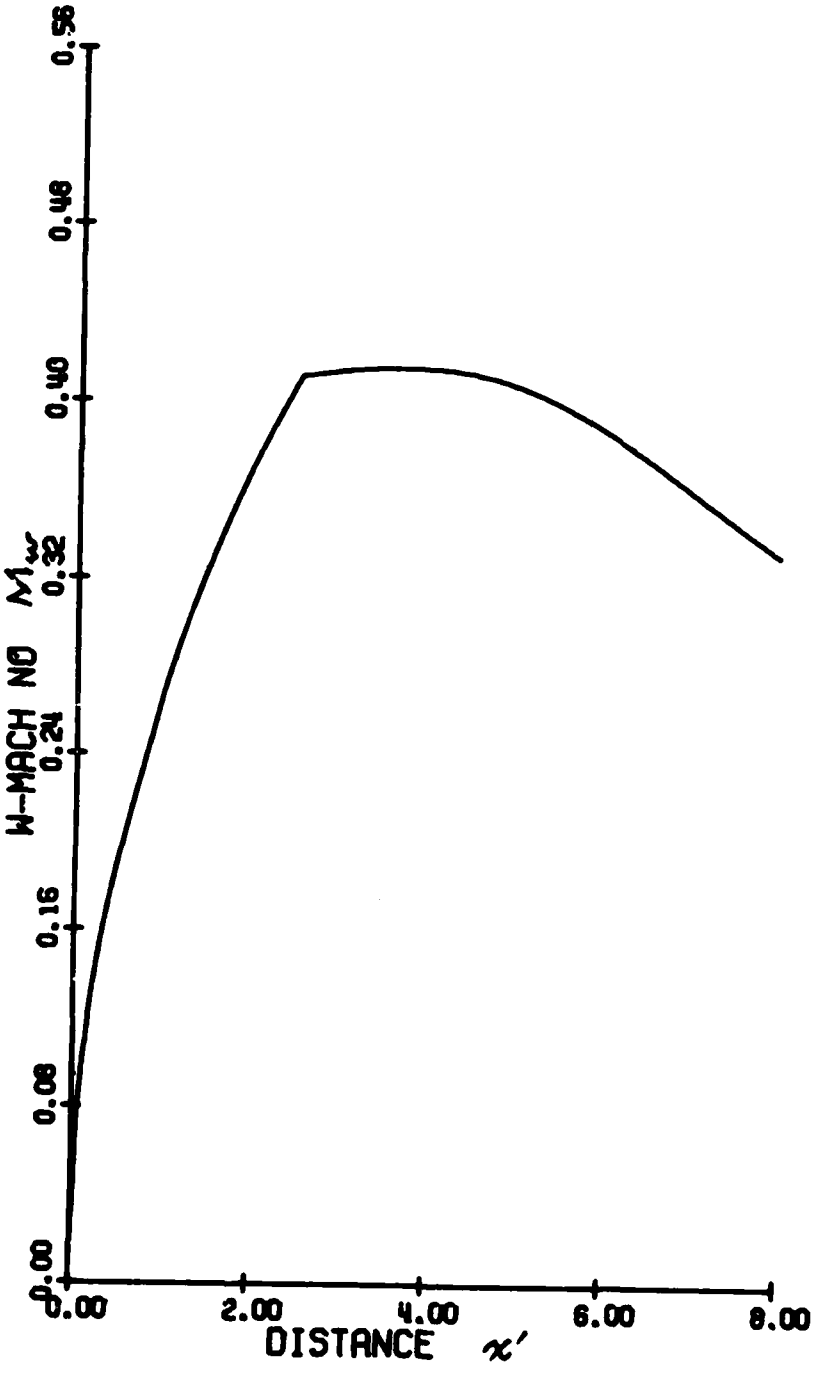
0.56
0.48
0.40
0.32
0.24
0.16
0.08
0.00
W-MACH NO M_w
0.00
2.00
4.00
6.00
8.00
DISTANCE x'

Fig. 4.25

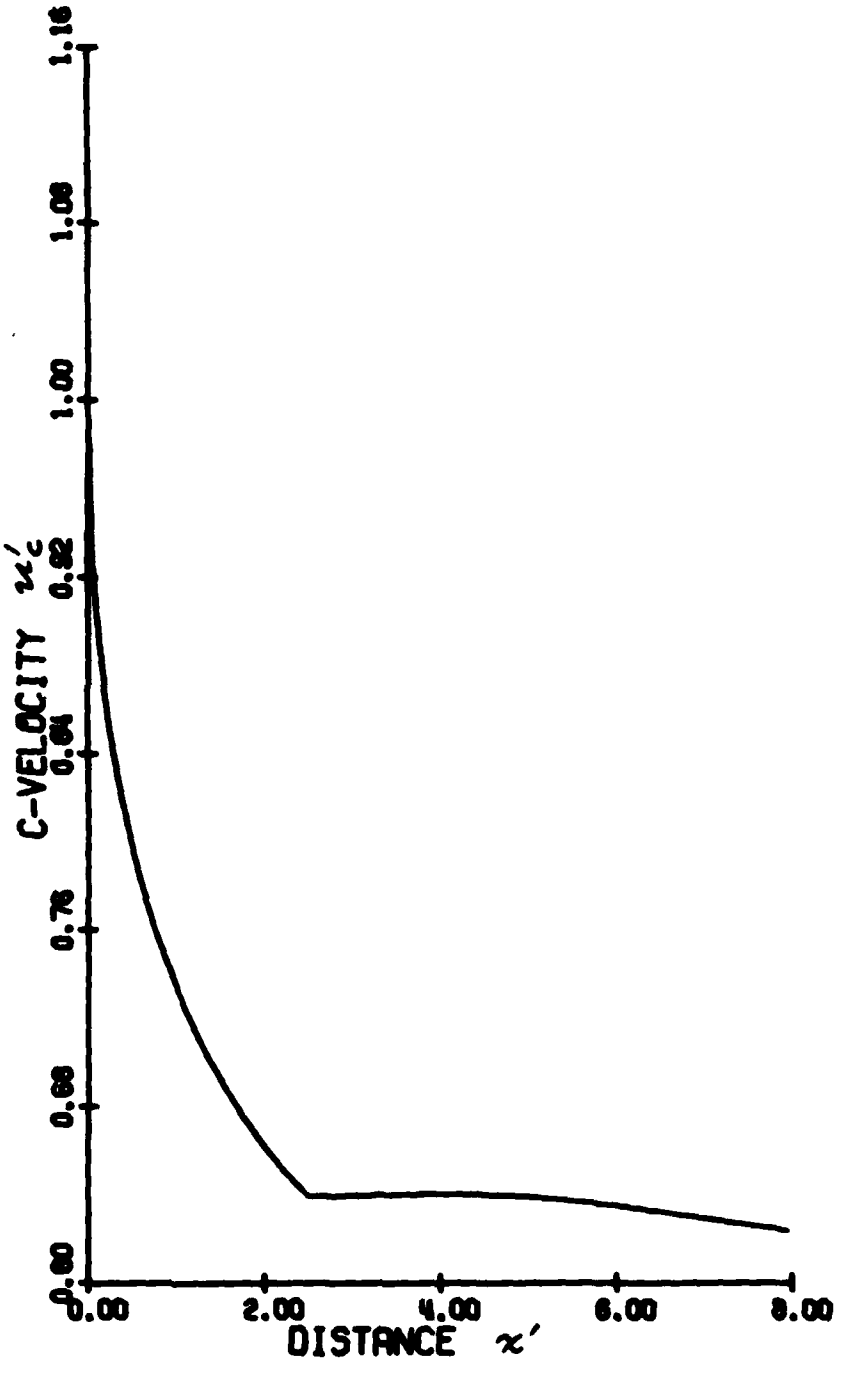
C-VELOCITY u'c
1.16
1.08
1.00
0.92
0.84
0.76
0.68
0.60
0.00
2.00
4.00
6.00
8.00
DISTANCE x'

Fig. 4.26

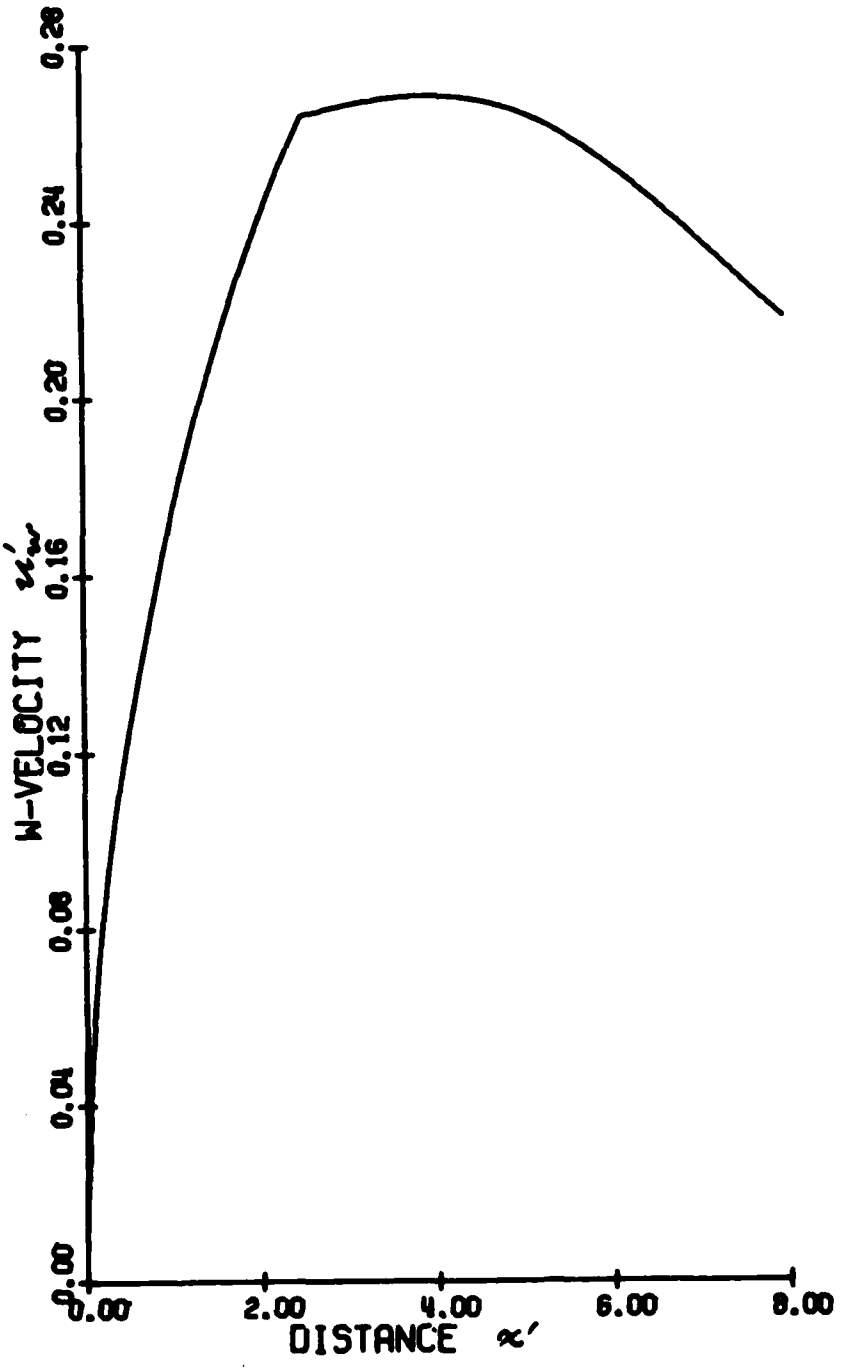
W-VELOCITY u'w
0.00
0.04
0.08
0.12
0.16
0.20
0.24
0.28
0.00
2.00
4.00
6.00
8.00
DISTANCE x'

Fig. 4.27

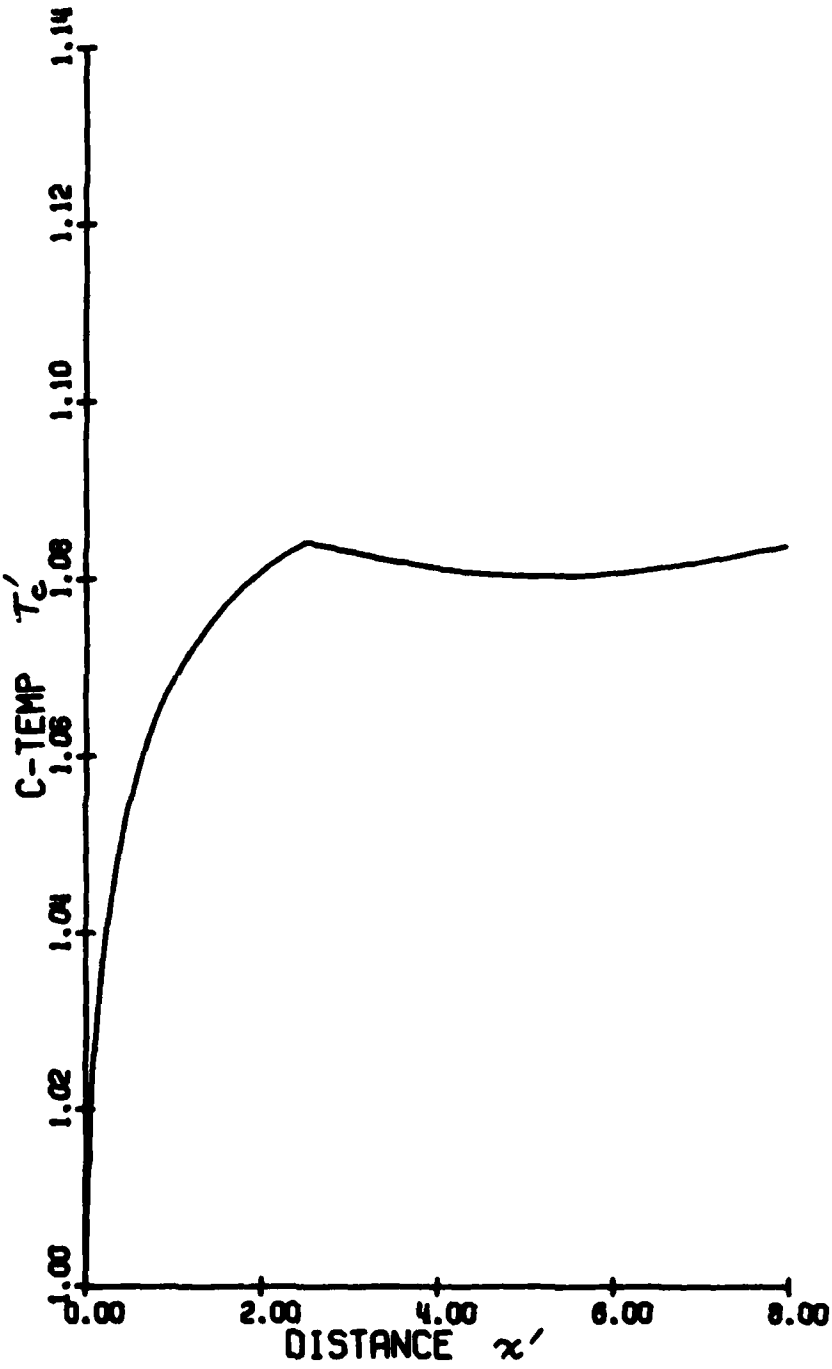
C-TEMP T_e'
1.00
1.02
1.04
1.06
1.08
1.10
1.12
1.14
0.00
2.00
4.00
6.00
8.00
DISTANCE x'

Fig. 4.28

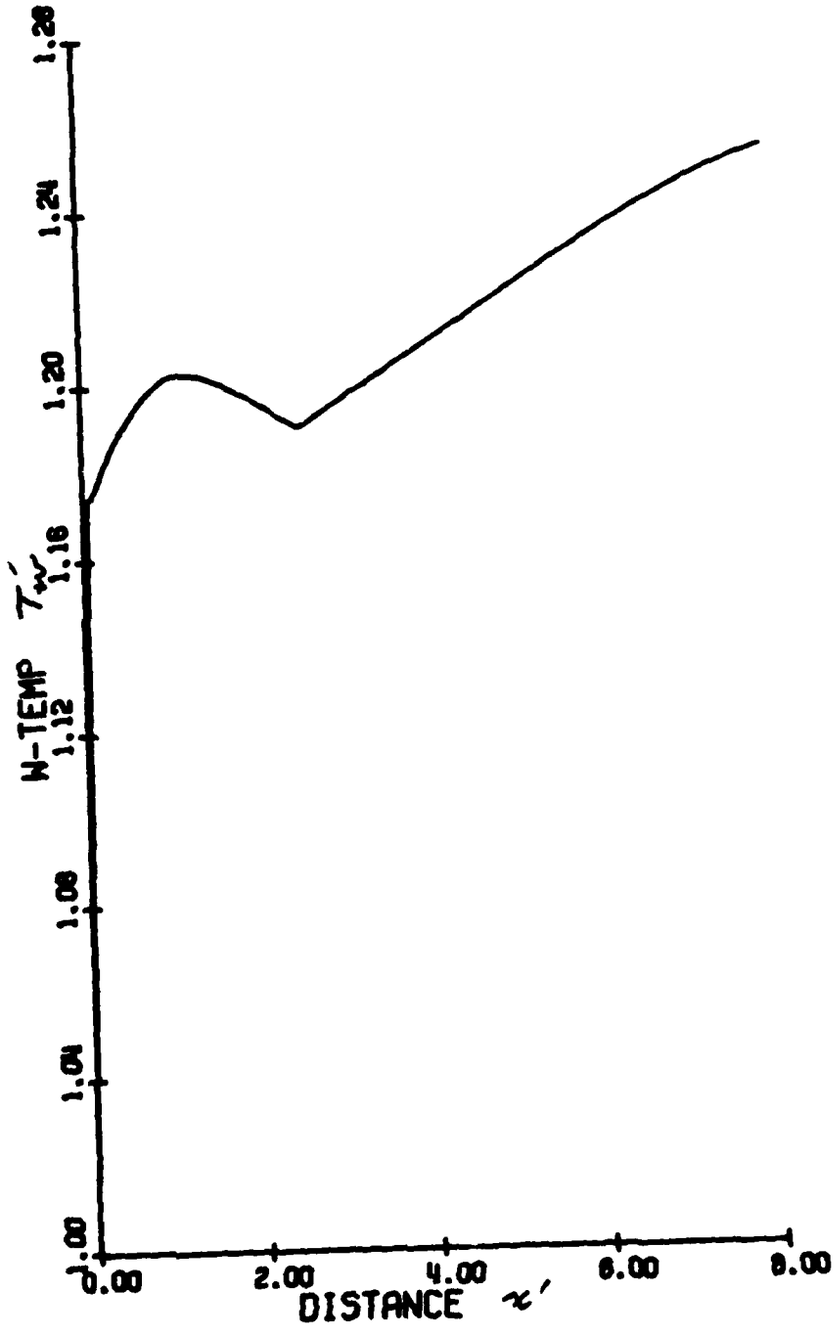
1.28
1.24
1.20
1.16
1.12
1.08
1.04
1.00
W-TEMP T_w'
0.00
2.00
4.00
6.00
8.00
DISTANCE x'

Fig. 4.29

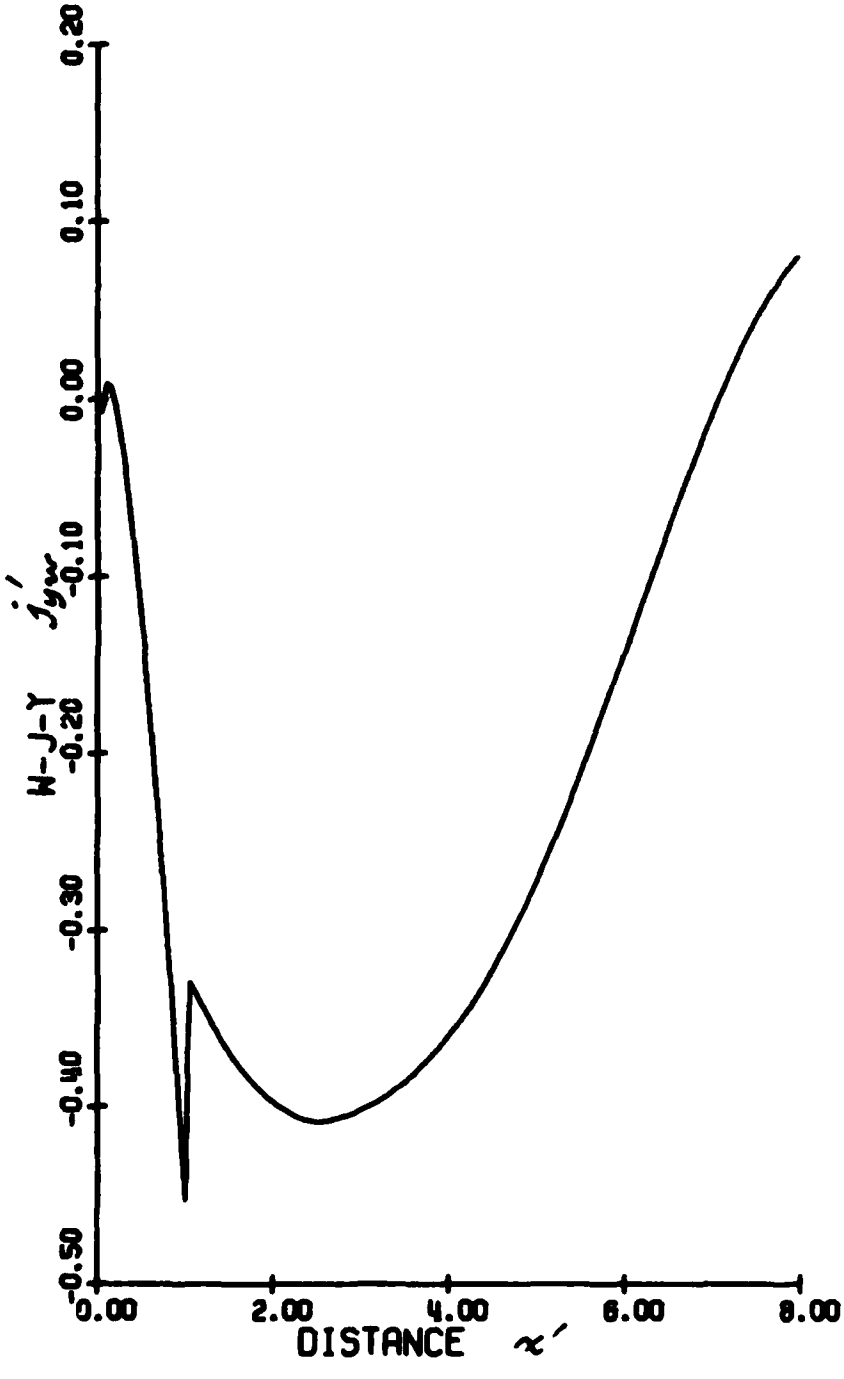
0.20
0.10
0.00
-0.10
-0.20
-0.30
-0.40
-0.50
W-J-Y j'_{yw}
0.00
2.00
4.00
6.00
8.00
DISTANCE x'

Fig. 4.30

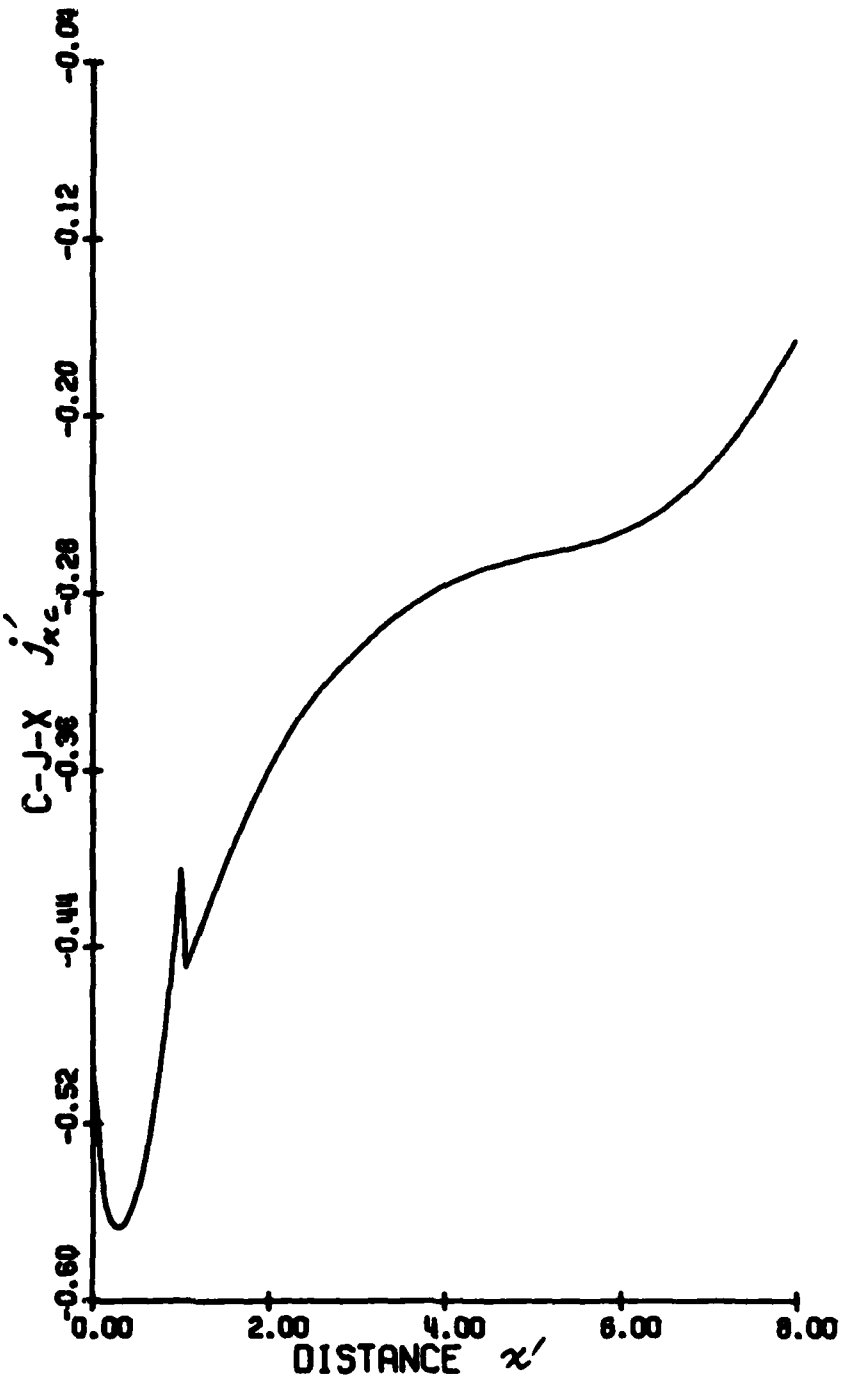
C-J-X j'_{xc}
-0.04
-0.12
-0.20
-0.28
-0.36
-0.44
-0.52
-0.60
0.00
2.00
4.00
6.00
8.00
DISTANCE x'

Fig. 4.31

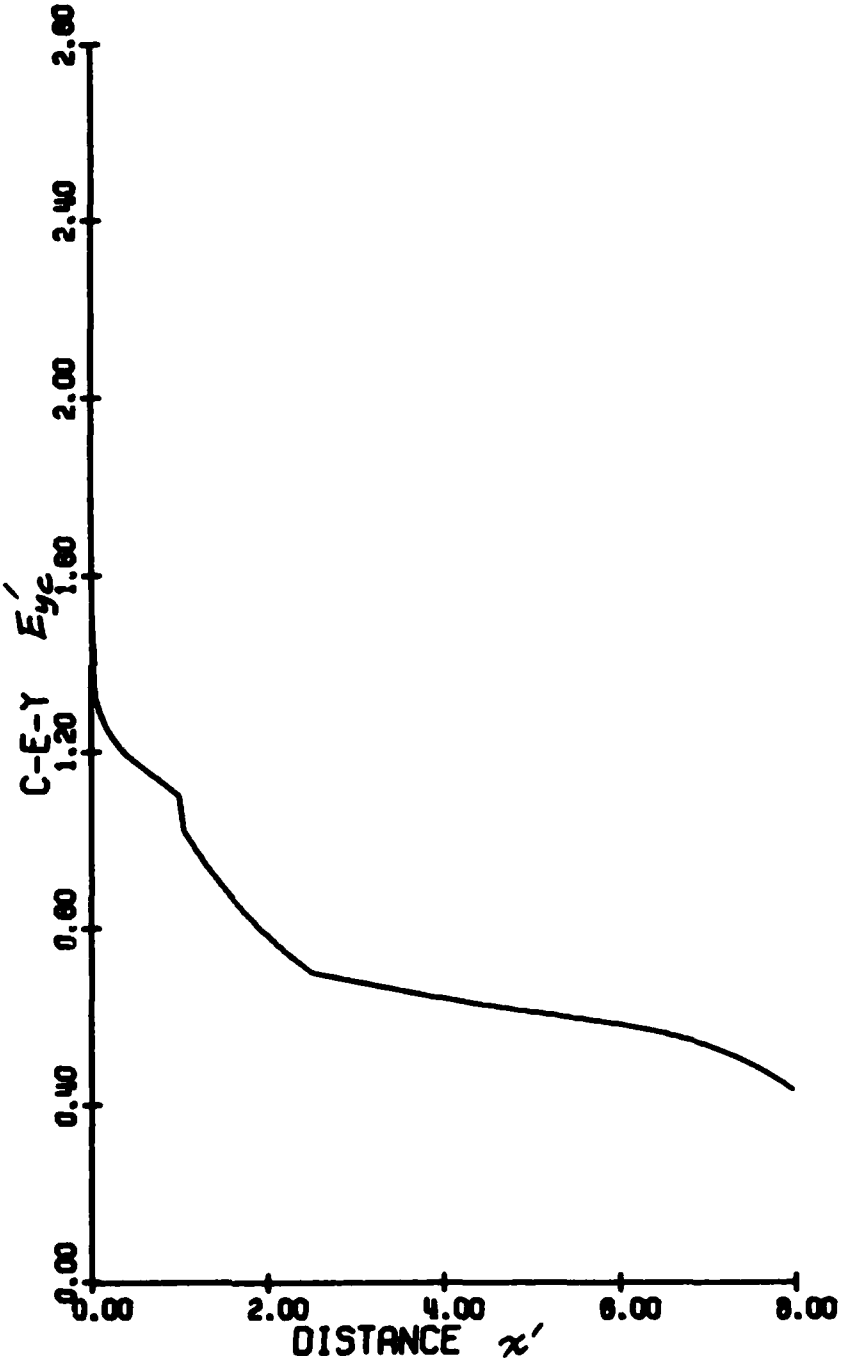
C-E-Y E'_{yc}
2.80
2.40
2.00
1.60
1.20
0.80
0.40
0.00
0.00
2.00
4.00
6.00
8.00
DISTANCE x'

Fig. 4.32

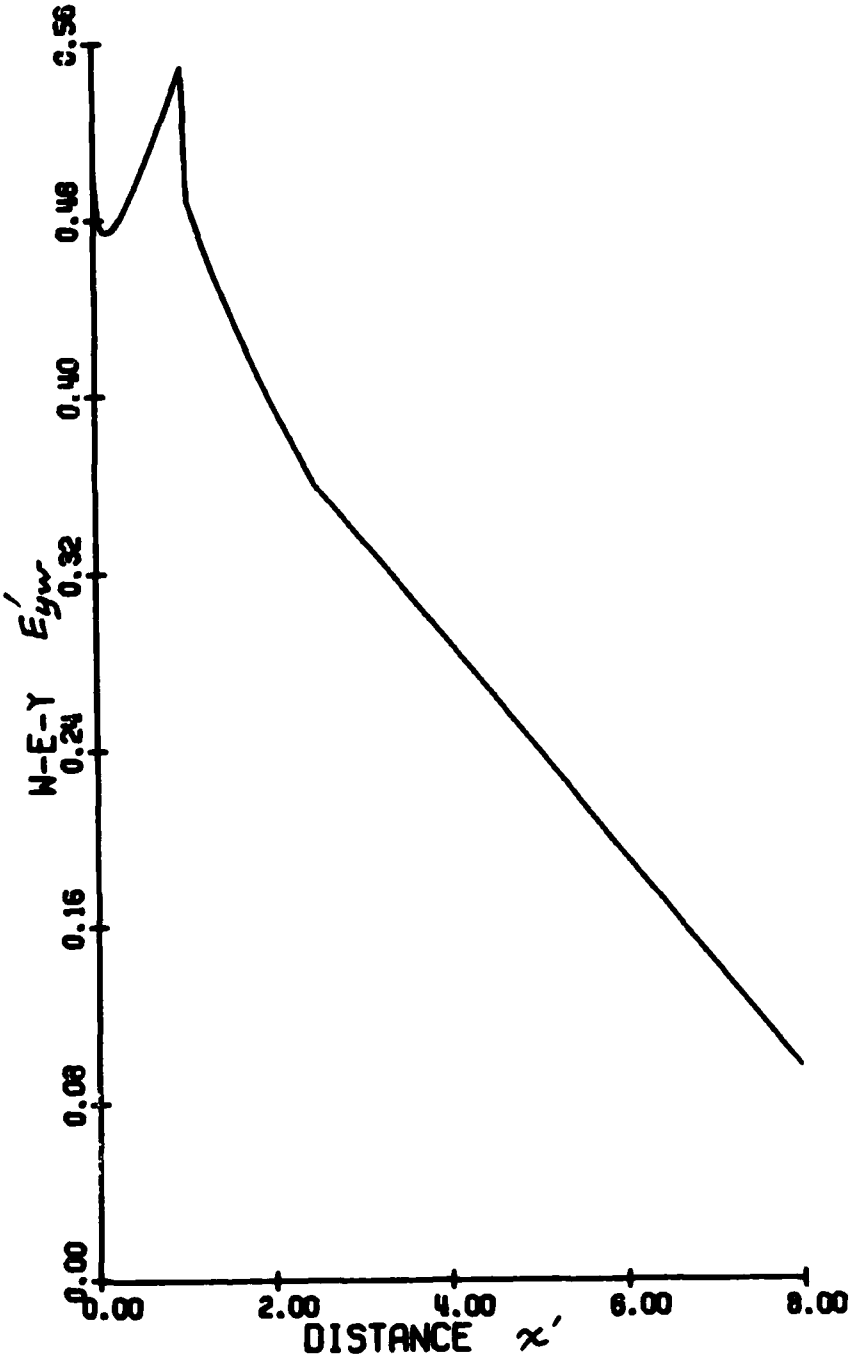
0.56
0.48
0.40
0.32
0.24
0.16
0.08
0.00
W-E-Y E'_{yw}
0.00
2.00
4.00
6.00
8.00
DISTANCE x'

Fig. 4.33

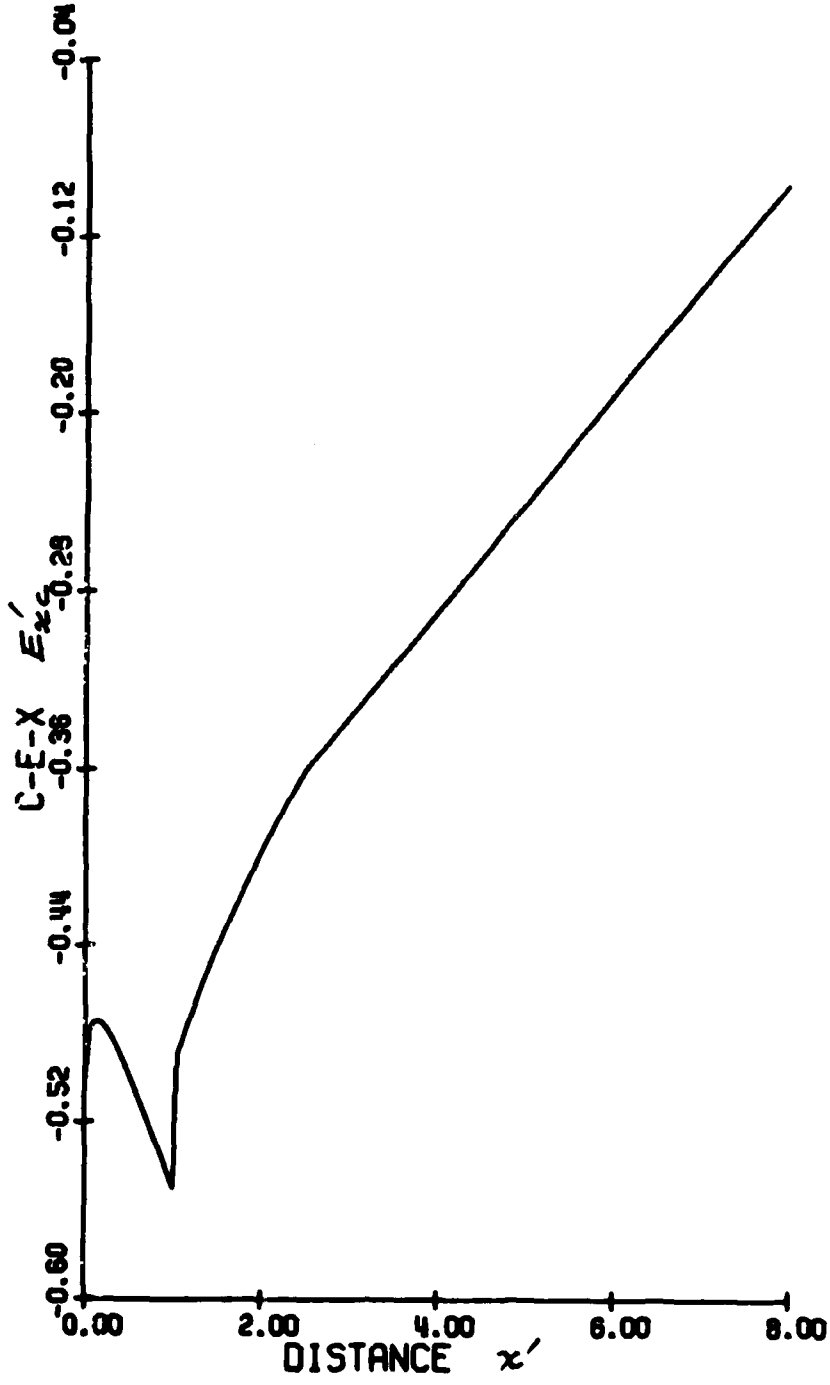
-0.04
-0.12
-0.20
-0.28
-0.36
-0.44
-0.52
-0.60
C-E-X E'_{xc}
0.00
2.00
4.00
6.00
8.00
DISTANCE x'

Fig. 4.34

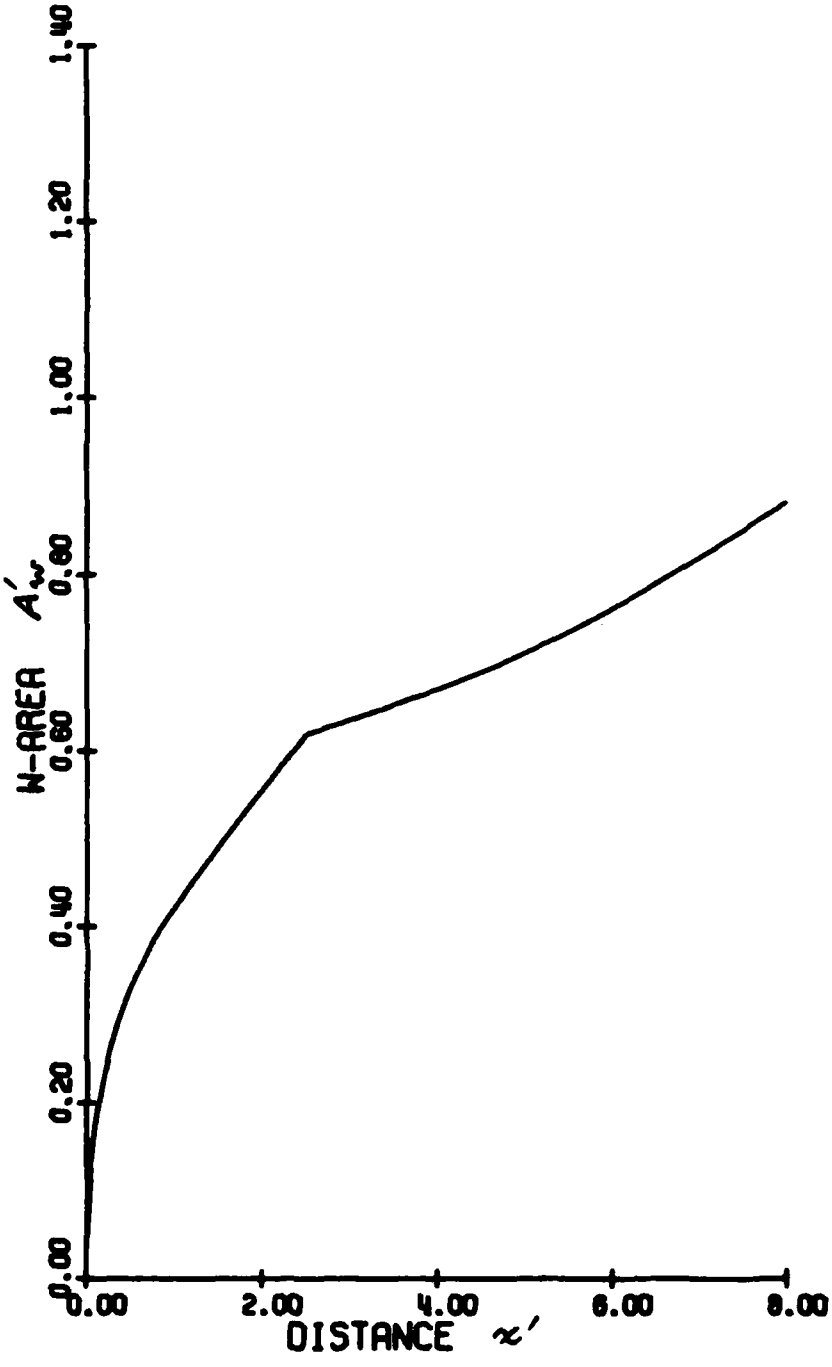
W-AREA A'_w
1.40
1.20
1.00
0.80
0.60
0.40
0.20
0.00
0.00
2.00
4.00
6.00
8.00
DISTANCE x'

Fig. 4.35

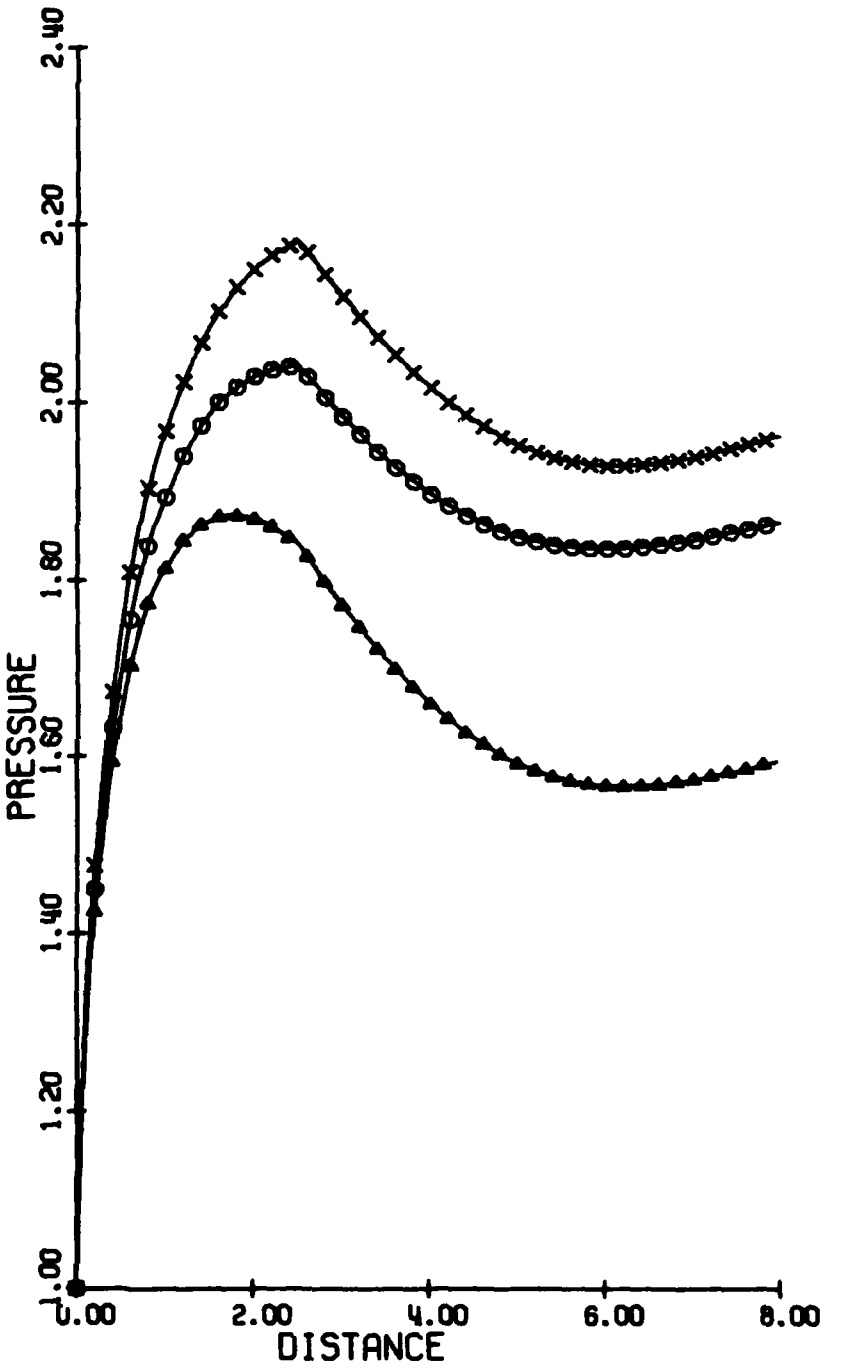
PRESSURE
2.40
2.20
2.00
1.80
1.60
1.40
1.20
1.00
0.00
2.00
4.00
6.00
8.00
DISTANCE

Fig. 4.36

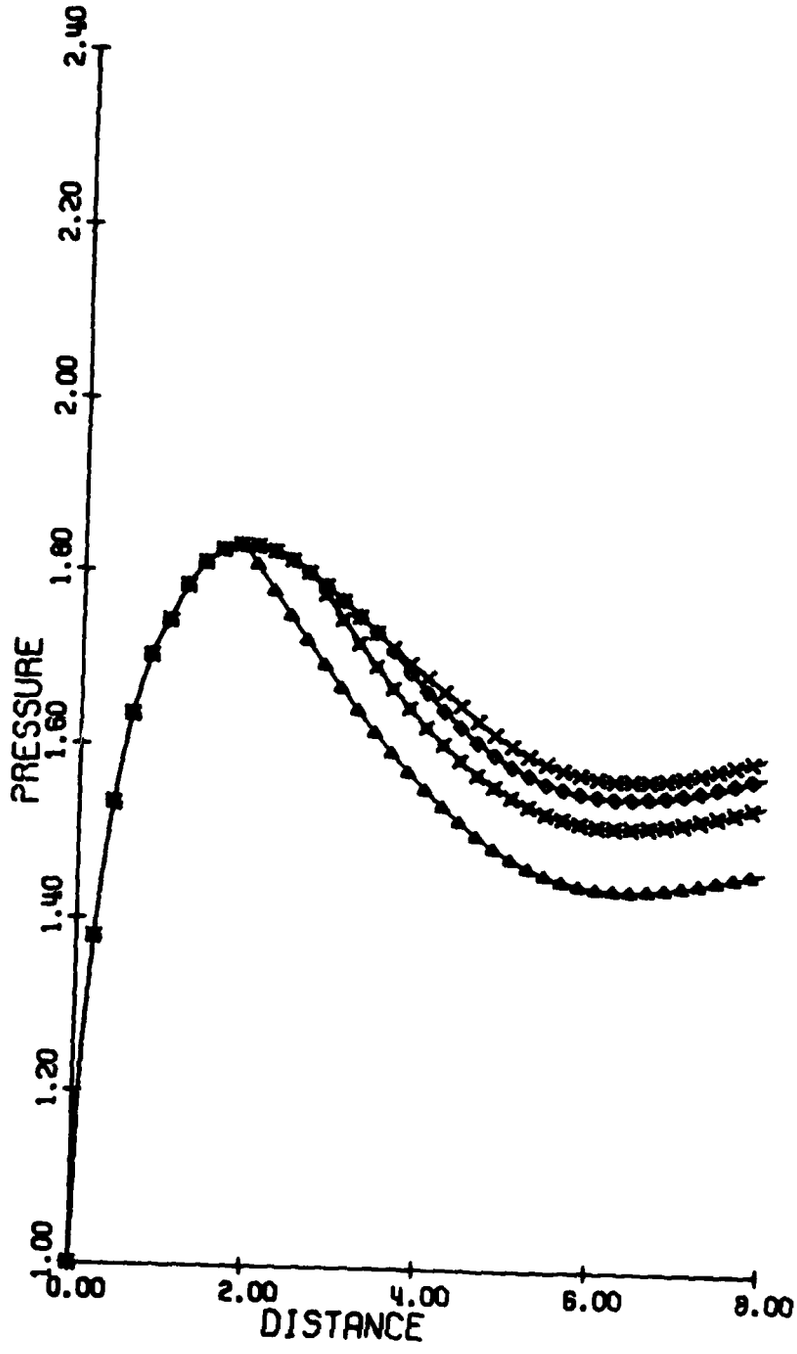
PRESSURE
2.40
2.20
2.00
1.80
1.60
1.40
1.20
1.00
0.00
2.00
4.00
6.00
8.00
DISTANCE

Fig. 4.37

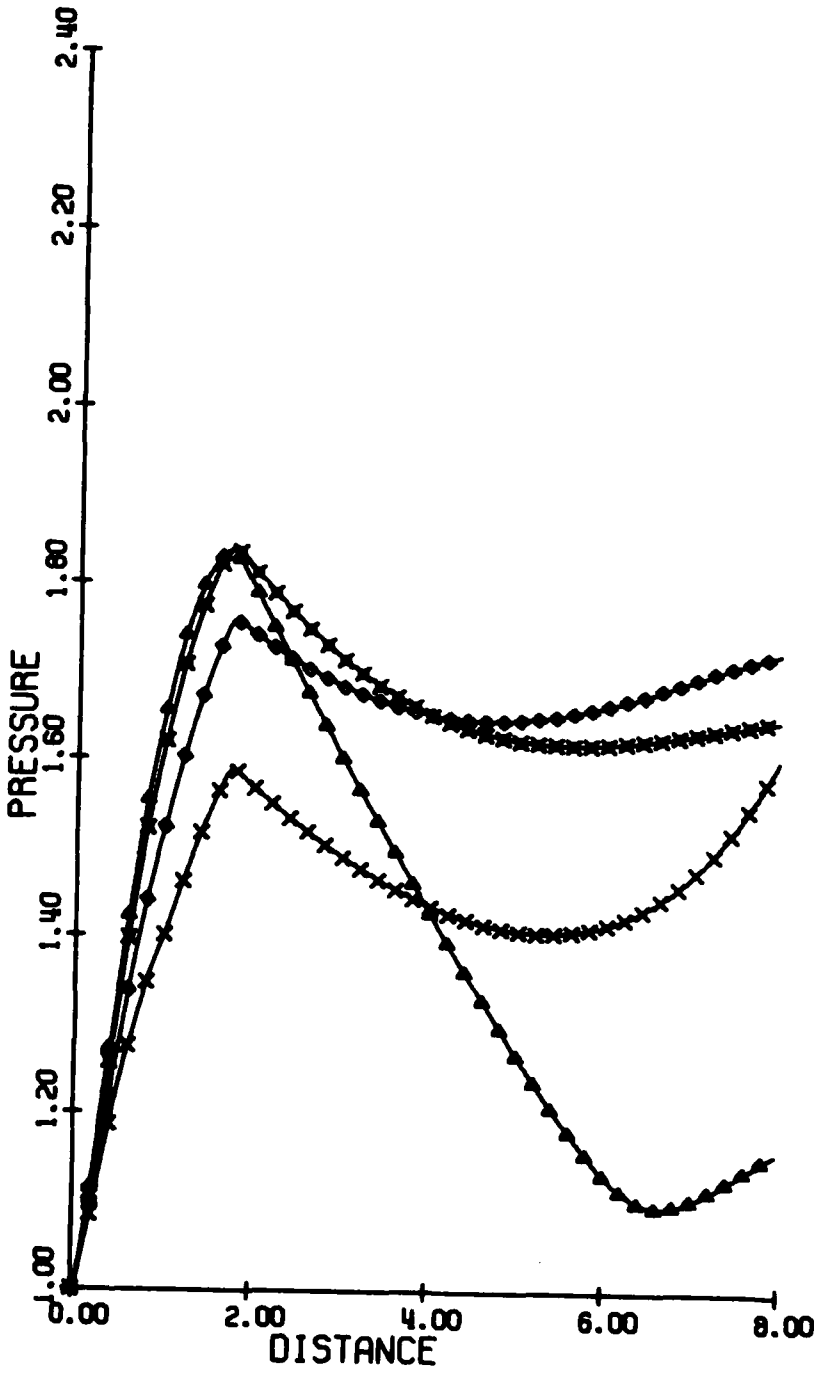
PRESSURE
2.40
2.20
2.00
1.80
1.60
1.40
1.20
1.00
0.00
2.00
4.00
6.00
8.00
DISTANCE

Fig. 4.38

APPENDIX -- COMPUTER PROGRAM

```
C THIS PROGROM IS TO CALCULATE THE DEPENDENT VARIABLES OF TWO-REGION MHD
C CHANNEL FLOW . TWO SUBROUTINES ARE USED , NAMELY FCT AND CAC INDIVIDU-
C ALLY . THE FORMER USES THE MODIFIED GAUSS-JORDON METHOD TO SOLVE FIVE
C DIFFERENTIAL EQUATIONS TO GET THE GRADIENT OF DEPENDENT VARIABLES .
C THE LATTER DEFINES ALL AUXILLIARY QUANTITIES AND ELEMENTS OF THE MATR-
C IX WHICH IS GOING TO BE USED IN SUBROUTINE FCT .
C THE PARAMETERS BEING USED IN THIS PROGRAM ARE DEFINED AS FOLLOWS :
C Y(1)----VELOCITY OF CORE-REGION
C Y(2)----VELOCITY OF WALL LAYER REGION
C Y(3)----TEMPERATURE OF CORE-REGION
C Y(4)----TEMPERATURE RATIO OF WALL LAYER REGION
C Y(5)----PRESSURE RATIO
C X-------DISTANCE RATIO ALONG THE X-DIRECTION
C AM------MACH NUMBER AT ENTRANCE
C CK------LOADING FACTOR
C S-------INTERACTION PARAMETER
C AR------RATIO OF HALL FIELD TO FARADAY FIELD
C XP------INTERVAL SIZE FOR PRINTING OUT
C DERY(I)----DERIVATIVESOF DEPENDENT VARIABLES
C GC-----RATIO OF SPECIFIC HEAT CAPACITIES
      IMPLICIT REAL*8 (A-H,P-Z)
      DIMENSION Y(5),DERY(5)
      COMMON GC,AR,CK,AM,S
C DEFINE CONSTANTS :
      GC=1.10D00
      AR=-1.00D00
      CK=0.50D00
      AM=1.50D00
C DEFINE INITIAL VALUES OF VARIABLES :
      Y(1)=1.00D00
      Y(2)=0.80D-2
      Y(3)=1.00D00
      Y(4)=1.00D00
      Y(5)=1.00D00
      S=0.40D00/1.50D00
      X=0.00D00
      WRITE(6,300)
  300 FORMAT('1',12X,'X',19X,'Y(1)',16X,'Y(2)',16X,'Y(3)',16X,'Y(4)',16X
     1       ,'Y(5)')
      XP=0.00D00
      H=0.50D-2
   10 CALL FCT(X,Y,DERY)
      IF(DABS(X-XP)-0.1D-6)50,50,60
   50 WRITE(6,100)X,Y(1),Y(2),Y(3),Y(4),Y(5)
  100 FORMAT(1X,6D20.6)
      XP=XP+0.05D00
   60 DO 20 I=1,5
   20 Y(I)=Y(I)+H*DERY(I)
      X=X+H
      IF(X.GT.8.00D00)GO TO 30
      GO TO 10
   30 STOP
      END
```

```
C
      SUBROUTINE CAC(X,Y,Z)
      IMPLICIT REAL*8 (A-H,P-Z)
      DIMENSION Y(5),Z(5,6)
      COMMON GC,AR,CK,AM,S
C
C
      IF(X.GT.1.00D00) GO TO 11
      B=1.00D00+0.50D00*X
      GO TO 12
   11 B=1.50D00*(1.00D00-0.10D00*X)
C
C
C
   12 A=0.20D00*X+1.00D00
      DA=0.20D00
C
C
C
      U=0.12D00*X+0.30D-3
      DU=0.12D00
C
C
C
      IF(U.LT.0.30D00) GO TO 31
      U=0.30D00
      DU=0.00D00
C
   31 DSP=DSQRT(Y(5))
      SIW=(Y(4)**10)/DSP
      SIC=(Y(3)**10)/DSP
      STW=DSQRT(Y(4))
      STC=DSQRT(Y(3))
      BETAW=B*STW/Y(5)
      BETAC=B*STC/Y(5)
      ARK=AR*CK
C
      AA1=SIW/(1.00D00+BETAW*BETAW)
      AA2=SIC/(1.00D00+BETAC*BETAC)
      AKC=AA1*(CK*Y(1)-Y(2)+ARK*BETAW*Y(1))/Y(1)/AA2+1.00D00-ARK*BETAC
      AA3=ARK*ARK+(AKC-1.00D00)*(AKC-1.00D00)
      AA=Y(1)*B*B
      GG=GC/(GC-1.00D00)
      CC=GC*AM*AM
      Z(1,1)=0.00D00
      Z(1,2)=0.00D00
      Z(1,3)=GG*Y(5)/Y(3)
      Z(1,4)=0.00D00
      Z(1,5)=-1.00D00
      Z(1,6)=S*AA2*AA3*AA
C
C
      AA4=ARK*BETAC+AKC-1.00D00
      Z(2,1)=CC*Y(5)*Y(1)/Y(3)
      Z(2,2)=0.00D00
      Z(2,3)=0.00D00
      Z(2,4)=0.00D00
      Z(2,5)=1.00D00
```

```
      Z(2,6)=S*AA2*AA4*AA
C
C
      AA5=CC*(Y(1)-Y(2))*(Y(1)-Y(2))*0.50D00-GG*(Y(4)-Y(3))
      AA6=ARK*ARK*Y(1)*Y(1)+(CK*Y(1)-Y(2))*(CK*Y(1)-Y(2))
      BB=B*B
      Z(3,1)=0.00D00
      Z(3,2)=0.00D00
      Z(3,3)=0.00D00
      Z(3,4)=U*GG*Y(5)*Y(2)/Y(4)
      Z(3,5)=-U*Y(2)
      Z(3,6)=Y(5)*AA5*DU*Y(2)/Y(4)+U*S*AA1*AA6*BB
C
C
      AA7=CK*Y(1)*(AR*BETAW+1.00D00)-Y(2)
      PP=Y(5)*Y(2)/Y(4)
      Z(4,1)=0.00D00
      Z(4,2)=U*CC*PP
      Z(4,3)=0.00D00
      Z(4,4)=0.00D00
      Z(4,5)=U
      Z(4,6)=CC*PP*DU*(Y(1)-Y(2))+U*S*AA1*AA7*BB
C
C
      AA8=(Y(1)*Y(4)-Y(2)*Y(3))
      AA9=Y(2)*Y(3)+U*AA8
      Z(5,1)=(AA9-U*Y(1)*Y(4))/(Y(1)*AA9)
      Z(5,2)=(AA9-Y(2)*Y(3)*(1.00D00-U))/(Y(2)*AA9)
      Z(5,3)=-Y(2)*(1.00D00-U)/AA9
      Z(5,4)=-Y(1)*U/AA9
      Z(5,5)=1.00D00/Y(5)
      Z(5,6)=AA8*DU/AA9-DA/A
      RETURN
      END
```

```
C
C
      SUBROUTINE FCT(X,Y,DERY)
      IMPLICIT REAL*8 (A-H,P-Z)
      DIMENSION Y(5),DERY(5),A(5,6)
      COMMON GC,AR,CK,AM,S
C
C
      CALL CAC(X,Y,A)
      N=5
      M=N+1
C
C
      DO 30 K=1,N
      KP1=K+1
      IF(K.EQ.N)GO TO 11
      JJ=K
      BIG=DABS(A(K,K))
      DO 7 I=KP1,N
      AB=DABS(A(I,K))
      IF(BIG-AB)3,7,7
    3 BIG=AB
      JJ=I
    7 CONTINUE
      IF(JJ-K)8,11,8
    8 DO 9 J=K,M
      TEMP=A(JJ,J)
      A(JJ,J)=A(K,J)
    9 A(K,J)=TEMP
   11 DO 20 J=KP1,M
   20 A(K,J)=A(K,J)/A(K,K)
      DO 30 I=1,N
      IF(I.EQ.K)GO TO 30
      DO 25 J=KP1,M
   25 A(I,J)=A(I,J)-A(I,K)*A(K,J)
   30 CONTINUE
      DO 40 I=1,N
   40 DERY(I)=A(I,M)
      RETURN
      END
```

REFERENCES

1. Rosa, R. J., Magnetohydrodynamic Energy Conversion, McGraw-Hill Book Co., New York, 1968.

2. Sutton, G. W. and A. Sherman, Engineering Magnetohydrodynamics, McGraw-Hill Book Co., New York, 1965.

3. Crocco, L., "One-dimensional Treatment of Gas Dynamics," Fundamentals of Gas Dynamics, ed., H. W. Emmons, Princeton University Press, 1958.

4. Roberts, P. H., An Introduction to Magnetohydrodynamics, American Elsevier Publishing Co., Inc., New York, 1967.

5. Maxwell Laboratories, Inc., "High Power Study Final Briefing Presentation Material," for the Air Force Aero Propulsion Laboratory, Wright-Patterson Air Force Base, Ohio, 12 January 1976.

6. Shapiro, A. H., The Dynamics and Thermodynamics of Compressible Fluid Flow, vol. 1, John Wiley & Sons, Inc., New York, 1953.

7. Lu, P. C., "Preliminary Design Procedure for High Power Density MHD Generators," (unpublished) Final Report, USAF-ASEE Summer Faculty Research Program, Air Force Aero Propulsion Laboratory, August 1978.

8. Crocco, L., "Considerations on the Shock-Boundary Layer Interaction, Proc. Conf. High-Speed Aeronautics, Polytechnic Institute of Brooklyn, 1955.

9. Holt, James F., Cutting, John C., and Robert A. Nimmo, "Experiments with KIVA-I Open Cycle MHD Generator System," Proceedings of the 13th Symposium on Engineering Aspects of MHD, Stanford University, 1973.

10. Sonju, O. K., et al., "Experimental Research on a 400 kW High Power Density MHD Generator," AFAPL-TR-71-5, Air Force Aero Propulsion Laboratory, May 1971.

11. Sonju, O. K., and J. Teno, "Experimental and Analytical Research on a Two Megawatt, High Performance MHD Generator," AFAPL-TR-74-47, Air Force Aero Propulsion Laboratory, June 1974.

12. Roy, G. D., and Y. C. L. Wu, "Study of Pressure Distribution along Supersonic Magnetohydrodynamic Generator Channels," AIAA 7th Fluid and Plasma Dynamics Conference Paper #74-508, Palo Alto, June 17-19, 1974.

13. Ikeda, S., Masuda, T., Kusaka, Y., Honda, T., and Y. Aiyama, "Experiment on MHD Generator with a Large-scale Superconducting Magnet (ETL MARK V)," AIAA J., vol. 11, pp. 1655-1656, 1976.

14. Crocco, L., and L. Lees, "A Mixing Theory for the Interaction between Dissipative Flows and Nearly Isentropic Streams," J. Aero. Sciences, vol. 19, pp. 649-676, 1952.

15. Crocco, L., and R. F. Probstein, "The Peak Pressure Rise across an Oblique Shock Emerging from Turbulent Boundary Layer over a Plane Surface," Princeton University Aeronautical Engineering Report 254, March 1954.

LIST OF SYMBOLS
(except Section 1.2)

A	Cross-sectional area of channel, m^2
A_c	Cross-sectional area of core region, m^2
A_w	Cross-sectional area of wall layer, m^2
B	Magnetic field strength, T(esla)
b	Width of generator duct, m
c_p	Specific heat capacity, J/(kg·K)
E	Electric field strength, N/C
H	$c_pT + u^2/2$, J/kg
h	Specific enthalpy, J/kg
j	Electric current density, $C/(m^2 \cdot s)$
K	Loading factor (E_{yw}/u_cB)
K_c	E_{yc}/u_cB
K_w	E_{yw}/u_wB
M	Mach number
m	Total mass flow rate through generator, kg/s
m_c	Mass flow rate in core region, kg/s
m_w	Mass flow rate in wall layer, kg/s
$\hat{n}$	Unit normal vector
p	Pressure, N/m^2
R	Gas constant, J/(kg·K)
S	MHD interaction parameter
s	Specific entropy, J/kg·K
T	Temperature, K

U	Specific internal energy, J/kg
u	Flow velocity, m/s
V	Specific volume, m^3/kg
x	Cartesian coordinate along the duct axis, in the flow direction, measured from the entrance, m
α	Ratio of Hall field to Faraday field (E_x/E_y)
β	Hall-current parameter
γ	Ratio of specific heat capacities (c_p/c_v)
ϕ	Angle of inclination of segments (= $\tan^{-1}\alpha_w$, Figs. 2.1 to 2.2), rad.
μ	Ratio of mass flow rate in wall layer to the total mass flow rate through the generator
ν	Ratio of cross-sectional area of wall layer to that of entire duct
ρ	Density, kg/m^3
σ	Electric conductivity, Ω^{-1}/m^3

Superscripts

$( )'$	Dimensionless quantities (see Section 3.2 and beginning of Section 3.1)
$\vec{( )}$	Vectorial quantities
$\hat{( )}$	Unit vectors

Subscripts

c	Of core region
i	At entrance
w	Of wall layer
x	Component in the x-direction
y	Component in the y-direction (see Fig. 2.1)


DATE
FILME
8